TYING ROCK PROPERTIES FROM CORE TO DEPOSITIONAL PROCESSES AND EXAMINING THE RELATIONSHIP THROUGH FORWARD SEISMIC REFLECTION MODELING IN THE KAIPAROWITS PLATEAU, UTAH

by

Karenth Dworsky

A thesis submitted to the faculty of
The University of Utah
in partial fulfillment of the requirements for the degree of

Master of Science

in

Geology

Department of Geology and Geophysics

The University of Utah

August 2015

The University of Utah Graduate School

STATEMENT OF THESIS APPROVAL

The thesis of **Karenth Dworsky**

has been approved by the following supervisory committee members:

Lisa Stright	, Chair	**3/25/2015** Date Approved
Cari Johnson	, Member	**3/25/2015** Date Approved
Tiziana Vanorio	, Member	Date Approved

and by **John Bartley**, Chair/Dean of

the Department/College/School of **Geology and Geophysics**

and by David B. Kieda, Dean of The Graduate School.

ABSTRACT

Nearshore fluvial to tidal transitional depositional systems are becoming increasingly important due to the large number of global hydrocarbon reserves held in such deposits. These deposits are inherently complex due to their heterolithic nature and therefore, interpreting facies and facies relationships in seismic reflection profiles is problematic. The fluvial and tidally influenced nearshore deposits of the late Cretaceous John Henry Member (JHM) of the Straight Cliffs Formation, located in the Kaiparowits Plateau of southern Utah, offers an excellent opportunity to improve our understanding of how the fluvial to tidal transition impacts subsurface petroleum reservoirs and their expression in seismic reflection profiles.

The focus of the first chapter is to investigate the impact of heterogeneous depositional environments and their rock properties to model amplitude versus offset (AVO) using a single core. Core EP-25 exhibits lithofacies from a progradational succession, from shoreface through tidal to fluvial. In order to model the most likely lithofacies stacking patterns present in the core, Markov Chain analysis was conducted. Benchtop measurements performed on 1 inch core plugs obtained rock properties (*Vp*, *Vs*, density, permeability, and porosity) for each lithofacies. Average rock properties for each lithofacies were used to generate synthetic seismic reflection models of the different upward fining facies associations documented directly from the core, in order to model variations in amplitude versus offset responses as a function of variable tidal influence.

The focus of the second chapter is to capture probable 3-dimensional geobody distributions with a particular focus on coal geobody distribution using previously studied cores and outcrops on the plateau. Three different seismic forward models were created ranging in

complexity, using cores EP-25, EP-07, density logs, and the nearby outcrop study Left Hand Collet. The rock properties obtained from the benchtop measurements were used to populate the three models based on different depositional environments at the separate depth slices capturing multiple geomorphic rather than stratigraphic models. A seismic survey was acquired on the plateau using 80 Hz frequency; this produced a high-resolution seismic profile. Comparing the forward seismic model to the acquired seismic profile allows for a conceptual understanding between predictive models of what is expected and what is captured in seismic reflection profiles.

TABLE OF CONTENTS

LIST OF FIGURES

LIST OF TABLES

ACKNOWLEDGEMENTS

I would first like to thank my advisor, Lisa Stright. Not only did she believe in me from the very beginning, but he has provided so many fantastic opportunities that have enabled a more than successful graduate school experience, in addition to helping build the foundation for a successful future. I would also like to thank my committee members, Cari Johnson and Tiziana Vanorio; Cari for being a solid foundation of geologic knowledge concerning not only the Kaiparowits Plateau, but sedimentary geology in its entirety, and Tiziana and the rest of the Stanford Rock Physics Laboratory for support and donated time to making sure I understood the equipment I worked with and the theory and concepts behind them. The Rocks to Models consortium have also provided invaluable discussion and ideas throughout the course of my work, including William Gallin, Patrick Dooling, Brenton Chetnik, Julia Mulhern, Wassim Bellinham, Alexandre Turner, and Tyler Szwarc. I would also like to acknowledge the companies who support the consortium without whose support the work could not have been accomplished.

I would also like to express gratitude towards the helped I received from undergraduate students from the University of Utah, Utah Valley University, and Brigham Young University during the seismic acquisition. I would like to especially thank Pier Paolo Bruno for designing the seismic acquisition survey and the INGV for providing processing facilities.

I would like to thank the UGS, in particular Peter Nielsen, for all the technical

help digitizing logs, and being incredibly helpful when it came to the core description and core plug extraction process. I am appreciative to the BLM for allowing me to conduct fieldwork in the beautiful Kaiparowits Plateau. Lastly I would like to personally thank my partner Gavin Dixon for his comfort, patience and unwavering support throughout my entire graduate school experience.

CORE DESCRIPTION, MARKOV CHAIN ANALYSIS AND AVO MODELING OF A TIDAL TO FLUVIAL TRANSITION ZONE IN THE CRETACEOUS STRAIGHT CLIFFS FORMATION, SOUTHERN UTAH, USA

Abstract

Deposits within tidal successions are generated by a complex mixture of processes from fluvial input to tidal reworking, both impacted by shoreline transgressions and regressions. The resulting subtle changes at the bed scale in the transition from tidal to fluvial deposits make lithofacies differentiation from subsurface wireline log and seismic reflection data problematic. Because reservoirs comprised of tidally influenced deposits account for a significant portion of petroleum reserves, forward seismic reflection modeling coupled with a predictive facies model framework derived from core and outcrops can lead to invaluable insights for interpreting subsurface data. The goal of this research is to assess to what extent the fluvial and tidal facies associations can be distinguished in amplitude versus offset (AVO) forward models using lithofacies stacking patterns, depositional interpretations, and direct rock properties.

The Cretaceous John Henry Member (JHM) is exposed along the edges of the Kaiparowits Plateau in southern Utah, revealing excellent outcrop exposures of fluvial and tidally influenced deposits. These exposures, coupled with core and wireline log data

in the center of the plateau, present an exceptional opportunity to improve our understanding of wireline log interpretation and seismic imaging in similar subsurface petroleum reservoirs. The focus of this study is centered on core EP-25 (240 m), located in the north-central Kaiparowits Plateau. The core captures a progradational succession from shoreface through tidally influenced lagoon to fluvial. Transition probabilities between lithofacies observed in the core were quantified with a Markov Chain analysis, resulting in seven complete upward fining packages (facies associations), and 34 incomplete packages. These facies associations represent end members from tidally influenced to fluvially influenced deposits and transitional packages between the two end members. Benchtop measurements were performed on 1 inch core plugs to obtain rock properties (*Vp*, *Vs*, density, permeability, and porosity) for each lithofacies. The resulting rock property exhibits a wide range of values as a direct result of the highly heterolithic nature of these deposits. As expected, significant overlap between fluvial and tidal rock properties is observed due to the transitional nature of the depositional environments. However, there is a distinguishable difference between clusters of the tidal and fluvial groups. Average rock properties were assigned to lithofacies comprising the seven facies associations and 1-dimensional amplitude versus offset (AVO) predictions were generated to elucidate near- to far-offset amplitude changes as a function of variable tidal influence. A near-offset amplitude decrease is observed in the transition from more fluvial- to tidally influenced depositional environments. 1-dimensional AVO model was then performed on the full length of the core using velocities and densities from the core plug measurements. Not only does the core also distinguish between reflectors in tidal and fluvial in the offset plot, but exhibits offset in the far angle based on increasing

marine influence with depth.

Introduction

A number of studies have recognized the importance of understanding the impact of the fluvial-marine depsitional processes and their intricate link to reservoir quality amidst increasing tidal influence (Shanmugam et al., 1993; Nordahl et al., 2005; Longhitano et al., 2012). Core studies can not only be used to capture vertical stacking patterns (Powers and Easterling, 1982; Ahmad et al., 2012), but they also aid in the recognition of heterolithic lithofacies as a key indicator for interpreting depositional environment and stratigraphic architecture (Yoshida et al., 1999; Martinius et al., 2001). A significant amount of work has been done on describing tidal depositional environments and the direct link between repeating stacking patterns of lithofacies (termed parasequence by some authors) and their seismic-reflectivity character in both modern (Fenies et al., 1998; Yoshida et al., 2001; Chakrabarti, 2005) and ancient environments (Tanavsuu-Milkeviciene and Plink-Bjorklund, 2009; Feldman et al., 2014). These studies have focused primarily on the 1- and 2-dimensional seismic expression of geobodies. Although these studies are useful in interpreting geobody distribution, what they lack is the ability to identify the impact of depositional processes on the deposits within the fluvial to tidal transition zone, and their effect on seismic reflectivity, and more specifically, amplitude response with offset (AVO).

Forward seismic-reflectivity modeling is a valuable tool, particularly when used to predict seismic-reflectivity responses as a function of lithofacies changes in varying depositional environments. There have been a number of forward seismic-reflectivity

modeling studies that focus on offshore sedimentary rocks (Christensen and Szymanski, 1991; Vernik and Nur, 1992; Falivene et al., 2010; Tetyukhina et al., 2010; Howell et al., 2014; Stright et al., 2014), as well as tidal sedimentary rocks (Wen et al., 1998; Yoshida et al., 1999; Hodgetts and Howell, 2000; Yoshida et al., 2001; Tetyukhina et al., 2014), although very few have concentrated on the fluvial to tidal transition zone (Martinius and Gowland, 2011). A majority of these studies have used seismic rock properties either from analog core plug measurements, wireline logs from analogs, or theoretical rock property modeling.

The first rock property models were derived from empirical relationships between acoustic and elastic wave velocities as a function of pressure, clay content, and porosity, and calibrated to benchtop measurements (Han, 1986; Eberhart-Phillips et al., 1989). Following the anaysis of empirical rock property relationships, a number of studies investigated the rock properties from specific environments of deposition using either direct or modeled rock properties (Biddle et al., 1992; Falivene et al., 2010). Although these studies have characterized and modeled rock properties based on instrinsic properties (pressure, clay content, porosity, and acoustic and elastic wave velocities), there are few studies that couple the rock properties tightly with bed-scale depositional processes and none specifically in the fluvial to tidal transition zone.

The goal of this research is to assess to what extent the fluvial and tidal facies associations can be distinguished in bed- to log-scale AVO forward models using rock properties measured directly from core, lithofacies stacking patterns, and depositional environment interpretations. In order to accomplish this, core description within the John Henry Member of the Straight Cliffs, Utah is presented within a hierarchical framework.

Stacking patterns of fundamental bed-scale observations (lithofacies) are quantified using Markov Chain Analysis to calculate transition probabilities and characterize lithofacies stacking patterns (facies associations) to aid in characterization of depositional environments. The resulting facies associations represent deposits from tidal and fluvial end members and the intermediate transitional packages. AVO forward modeling was generated to reveal near- to far-offset amplitude changes as a function of variable tidal influence by employing direct rock property measurements. Coupling geological observations from core to their seismic response, by placing them within a hierarchical framework, enables core plug rock property measurements to be tied to depositional processes and upscaled in order to analyze the seismic amplitude in fluvial to tidal transition zones.

Geologic Background

Regional Geology

Sediments preserved in the Upper Cretaceous Straight Cliffs Formation of the Kaiparowits Plateau were deposited in an asymmetrical foreland basin formed by loading from the Sevier fold and thrust belt to the west (Kauffman and Caldwell, 1993; Allen and Johnson, 2010a) (Fig. 1.1). The siliciclastic sediments that form the Kaiparowits Plateau were sourced from three locations: the Sevier fold and thrust belt to the west, the Mongollon Highlands to the south, and the Cordilleran Volcanic Arc to the southwest (Peterson, 1969a; Eaton and Nations, 1991; Hettinger, 1995a; Szwarc et al., 2014). Paleoshorelines were oriented northwest-southeast (Peterson, 1969a; Shanley and McCabe, 1991; Shanley et al., 1992; Hettinger, 1995a; Allen and Johnson, 2010a). The

easternmost outcrop exposures along the plateau comprise offshore through intertidal facies and represent the paleoshoreline of the Western Interior Seaway in southern Utah (Shanley and McCabe, 1991).

Stratigraphy

Peterson (1969) divided the Straight Cliffs Formation in the Kaiparowits Plateau into four members: the lower cliff-forming Tibbet Canyon Member, the slope and ledge forming Smoky Hollow Member and John Henry Member (JHM), and the upper cliff-forming Drip Tank Member. The JHM, the focus of this study, is the thickest (200-500 meters) and early Coniacian to late Santonian in age (~88 to 83.5 Ma) (Fig. 1.2) (Peterson, 1969a; Eaton, 1991; Hettinger et al., 1993; Szwarc, 2014). The base of the JHM is marked by a landward shift in facies recording a transgression that occurred after deposition of the Smoky Hollow Member (Shanley and McCabe, 1991). In the southern, western, and northeastern Kaiparowits Plateau, the upper JHM consists primarily of multi-story and single-story fluvial channel belts interbedded with carbonaceous floodplain mudstones and coal (Gooley, 2010; Pettinga, 2012). The center of the plateau contains paludal deposits with thick coal beds and are interstratified with tidal deposits (Vaninetti, 1979). Seven shoreface sandstone packages were identified at Left Hand Collet in the central part of the plateau along the paleoshoreline, ranging from wave dominated lagoon to tide dominated barrier island system (Peterson, 1969a; Dooling, 2012). There are three coal zones present in the JHM: Lower Christensen, Rees, and Alvey coal zones (Fig. 1.2). These zones were interpreted by Shanley and McCabe (1992) as being deposited in steep raised mires. The preservation of transgressive lagoon

and complete progradation (regressive) shoreface successions indicate that accommodation and sedimentation rates were moderately high throughout deposition of the entire JHM (Allen and Johnson, 2010b).

The northeastern part of the plateau has been examined to a lesser degree than the southern part of the plateau. Left Hand Collet and highway 12 outcrops are the only outcrop exposures that have been studied thus far (Shanley et al., 1992; Dooling, 2012; Chentnik et al., 2014). In the northern-central section of the plateau, data are limited to 23 core that were extracted by Utah Power and Light (UP&L) in the early 1970s in order to investigate coal in the region. One particular core intersects the entire JHM, core EP-25. Gallin (2010) logged and interpreted this core to provide valuable information regarding the extent of depositional environments across the central Kaiparowits Plateau. Gallin's (2010) core analysis offered a benchmark on which to support further work in the northeastern part of the plateau.

Core Description

Core EP-25 is a 240 m thick cored interval, logged in the northeastern Kaiparowits Plateau, Utah that intersects the entire John Henry Member (Table 1.1). The smallest scale of observation, lithofacies, was subsequently used to interpret the different depositional environments and their associated architectural elements. Within core EP-25, eight different lithofacies were identified and described at a core plug scale (1-20 cm) (Gallin, 2010) (Fig. 1.3). The lithofacies are defined by grainsize, bed features, bioturbation, laminations, and organic content. Gallin also noted an overall trend that reveals a transition from marine to fluvial influence moving up in the core. Based on

fossils assemblages, coal, amount of bioturbation, and lithofacies distribution, three depositional environments were identified: coastal plain (fluvial), tidal, and shoreface (Hettinger, 1995a; Gallin, 2010). The lithofacies are described below by Gallin's observation, categorized into their interpreted architectural elements, and then grouped into depositional environments (Fig. 1.4).

Core Description: Lithofacies, Architectural Elements, and Depositional Environments

Carbonaceous Shale

This lithofacies is dark gray to black colored shale. It is often laminated but can be structureless. Abundance of organic material is present, comprised primarily of plant fragments; however, brackish water *corbulids* and other small gastropods are also present. Vertically, carbonaceous shale often grades into coal. This lithofacies is interpreted as being low energy lagoonal mudstone within a tidal depositional environment.

Bioturbated Mudstone

This lithofacies consists of horizontally laminated mud or mud with no laminations and varying degrees of bioturbation. The bioturbation index used to quantify the amount of bioturbation uses a scale which ranges in amount of disturbance to original bedding structures from 0-100%, with 100% being complete obliteration of original sedimentary structures (Droser and Bottjer, 1988). The bioturbation in the tidal mudstone tends to be filled with very fine to fine grained sandstone. Organic material in this

lithofacies consists of plant fragments, leaf imprints, bivalve, and gastropod shells. Vertically, this lithofacies often grades into carbonaceous shale and coal. This lithofacies is interpreted as being low energy, represented in both the tidal and coastal plain depositional environments. In the tidal depositional environment, bioturbation is heaviest and there is an abundance of tidal environment trace fossils (*Teichichnus, Thalassinoides, Ophiomorpha, Asterosoma*). This lithofacies represents the architectural elements tidal mudstone and overbank fines in the respective depositional environments.

Flaser/Wavy/Lenticular Bedded Sandstone

This lithofacies reveals alternating laminations of sandstone and mudstone. Grainsize ranges from very fine to medium, while the mud fraction consists of siltstone, shale, or carbonaceous shale. Flaser mud drapes sometimes occur as accumulations of carbonaceous material. This bedding style is indicative of bi-directional flow and tidal influence (Finzel et al., 2009). Intervals comprised of flaser/wavy/lenticular bedforms are interpreted as deposits from tidal and coastal plain depositional environments. Although this lithofacies is associated mainly with tidal influence, it can be found seen in the fluvial environment as likely being located on the edge of the transition zone between fluvial and tidal environments. The architectural elements include tidal mudstone and overbank fines.

Planar Bedded Sandstone

This lithofacies is composed of fine to medium grained sandstone. Laminations observed in the sandstone dip $< 5°$. This lithofacies is associated with high-energy flow

regimes and is present in all three depositional environments. In the fluvial depositional environment, this lithofacies represents part of upward fining, fluvial channel architectural element. In the tidal depositional environment, this lithofacies represents highly sinuous distributary tidal channel architectural elements. In the shoreface depositional environment, this lithofacies represents well-sorted shoreface sheet sandstone clean on mud draping and may constitute hummocks or swales. In this environment, large robust bivalve fragments are preserved including *Granocardium*.

Trough Cross-bedded Sandstone

This lithofacies is comprised of fine to coarse grained sandstone. The trough and planar tabular sets range between 1– 5 mm thickness and the foresets dip between ~5-40°. This lithofacies represents unidirectional flow and is present in all three depositional environments. In the fluvial depositional environment, this lithofacies represents part of upward fining, low sinuosity fluvial channel architectural element. In the tidal depositional environment, this lithofacies represents the landward end of a highly sinuous distributary tidal channel architectural element. In the shoreface depositional environment, this lithofacies represents well-sorted shoreface clean sheet sandstone ripples and hummocks with no mud draping as the shoreface architectural element. The trough cross-stratification may constitute hummocks and swales in the shoreface environment.

Structureless Sandstone

This lithofacies is composed of very fine to coarse grained sandstone. Sedimentary structures are not apparent. Occasional bivalve shell fragments are present. This lithofacies is present in all three depositional environments. In the fluvial depositional environment, this lithofacies represents part of the fluvial channel architectural element. In the tidal depositional environment, this lithofacies represents the tidal channel architectural elements. In the shoreface depositional environment, this lithofacies represents well sorted clean shoreface architectural element.

Mud Rip-up Sandstone

This lithofacies reveals grainsizes that range from very fine to coarse. Within the sandstone matrix, angular to subangular, flat to moderately rounded mud rip-up clasts are present. The clasts are thin (< 1 cm) flakes. Vertically, the grainsize in this lithofacies coarsens upward over 10's of cm. This lithofacies is interpreted as high energy channel lag deposits within a fluvial depositional environment. More specifically, mud rip-up clasts are interpreted as being located at the base of the fluvial channel architectural element that cut through the overbank fines and tidal mudstone.

Coal

This lithofacies is black with dull vitreous reflectance and lacking distinct laminations. It is often accompanied by surficial and interstitial sulfur precipitates. Typically, this lithofacies is underlain by bioturbated mudstone or carbonaceous shale. The coal seams are < 1 m thick. This lithofacies is interpreted as being present

exclusively in the tidal depositional environment. Although the coal is associated with the tidal depositional environment, it is believed to have formed in raised coal mires that persisted for long periods of time with limited input from either fluvial or marine realms (Hettinger, 1995). Vertically, the coal tends to become thinner and less frequent upward. This decreasing frequency of the coal and increase in grainsize of sandstone lithofacies upward in the core is tied to an overall decrease in marine influence from the base of the core to the top.

Detailed core description and observations at the lithofacies core plug scale provide a hierarchical framework which can be subsequently upscaled and tied to depositional processes. The upscaled lithofacies and their rock property measurements are analyzed in order to gain a better understanding of the seismic amplitude in fluvial to tidal transition zones.

Methods

Prediction between scales, from lithofacies to stacked geobodies (core to reservoir scale), is accomplished by placing the observations within a hierarchical framework. A Markov Chain Analysis (MCA) is used to determine the 1-dimensional transition probabilities of lithofacies to quantify larger scale stacking patterns as facies associations. Rock property measurements from core plugs are used to generate AVO forward models of the facies associations to test if there is a near- to far-offset amplitude signature that can aid in predicting the amount of tidal influence, and therefore, reservoir quality from seismic reflectivity.

Facies Associations Stacking Patterns

In order to determine whether the lithofacies making up the facies association show a preferred stacking or regular vertical arrangement, a MCA was performed on the core observations. The MCA quantified the probability of transitioning from one lithofacies into another and therefore captures probable stacking patterns (Ahmad et al., 2012). The rationale of calculating transition probabilities is that an unbiased analysis of the repeatable stacking patterns can be captured from the core. The MCA was performed over the entire core with a transition count matrix where all possible vertical lithological transitions were tabulated at a 0.1 ft. sample rate (Table 1.2). These were converted to transition probabilities by normalizing the counts for each of the lithofacies by the total counts.

To characterize fully preserved depositional packages, only complete facies associations were extracted from the core based on three criteria. The three criteria of a full facies package were:

1) The facies associations had to include at least three consecutive, statistically related lithofacies. No facies association was selected if it contained only two lithofacies, for example, only carbonaceous shale and coal. The rejection of packages that did not have at least three stacked lithofacies takes into account the fact that the association may not be directly penetrating full architectural elements. This eliminates the packages that occur in the marginal position of the architectural elements and therefore do not represent a full depositional sequence.
2) Each of the lithofacies had to be at least as thick as the average bed thickness

for each lithofacies. For example, if a facies association was comprised of trough cross-bedded sandstone, planar bedded sandstone, bioturbated mudstone, carbonaceous shale, and coal, but all or one of the thicknesses was less than the lowest standard deviation, the association was disregarded.

3) The bases of each facies association were assumed to be comprised of either mud rip-up sandstone or trough cross-bedded sandstone.

Using the three criteria for building the facies association, in conjunction with the MCA results, seven facies associations were ultimately selected to conduct AVO modeling.

Rock Properties

To investigate the rock properties of the eight lithofacies 60, 1 inch diameter by 1 inch vertical, perpendicular to bedding core plugs were collected from the EP-25 core. The only lithofacies not represented by core plugs was the coal. Measurements for rock properties of coal were not attempted due to its friability and many of the coal intervals were missing from the core as a result of sampling from historical coal exploration work. Core plug benchtop measurements (at room temperature (68°F) and atmospheric pressure) were conducted for porosity, density, compressional wave (*Vp*), and shear wave velocities (*Vs*). The samples were prepared by first sanding the top and base to get a flat surface to ensure 1) good contact with the electrodes, which uses piezoelectric crystals to generate a high voltage electric pulse into the core plug to measure velocity and 2) accurate length measurements for bulk volume calculations. Prior to testing the samples were dried for 72 hours to remove all moisture. Dry rock density was calculated from

bulk volume and mass measurements. Porosity was measured using a porosimeter. *Vp* and *Vs* velocities were measured using an ultrasonic velocimeter.

Laboratory-derived measurements of *Vp*, *Vs*, and density were used to generate average P-impedance (*Ip*) and S-impedance (*Is*) for each lithofacies. These relationships were interrogated to elucidate the relationship between lithofacies and the measured rock properties. Clay content was calculated by estimating a percentage of shale (VShale) from the preexisting gamma ray log. Average values for each lithofacies within each depositional environment were used for the forward modeling to compare the impact of packaging of the lithofacies (facies associations) without introducing variability (noise) from rock property measurements. Cross plots of *Ip* versus *Vp/Vs* colored by lithofacies, architectural elements, and depositional environments were used to elucidate the impact of depositional processes and environment controls on the seismic response. In order to analyze net-to-gross (NTG) and grainsize, the core plugs were visually examined with a hand lens. The core plug values were then plotted on the *Ip* versus *Vp/Vs* cross plot to identify possible patterns and ties to lithofacies, architectural elements, and depositional environments.

1-Dimensional Synthetic Seismic Modeling

1-dimensional synthetic seismic models were generated using the seven facies association columns obtained from the MCA and populated with the average rock property values of lithofacies from the different environments of deposition (Table 1.2). The background rock property used was the overall average values for the bioturbated mudstone in the respective depositional environments (7022 Ns/m^3 for coastal plain and

7600 Ns/m^3 for tidal). Angle-dependent reflectivities were then calculated for each facies association column using the Zoeppritz equation (Zoeppritz, 1919) to capture seismic reflectivity as a function of incidence angle (Castanga, 1992). The reflectivity series was subsequently convolved with a 25-Hz, zero phase, + 90° rotated, Ricker wavelet with an offset range from 0 to 30 degrees.

To better understand the imaging of the stacked facies association packages at the well log to seismic scale, a 1-dimensional synthetic trace was generated of the full core EP-25. All 60 measurements of *Vp* and *Vs* were used for this modeling instead of the average values. The only logs associated with core EP-25 available were gamma gamma density and gamma ray logs. *Vp* and *Vs* logs were generated using sequential Gaussian simulation (*sGs*) for each lithofacies leveraging values measured from core plugs as hard data. The coal lithofacies used a single value for the *Vp* (2000 m/s) and *Vs* (1200 m/s) rather than a simulation (Morcote et al., 2010). Once the seven different lithofacies logs were combined using values extracted from each lithofacies simulation at their exact locations in the core at 0.5 ft. steps. The logs were spliced together to create full 1D logs that represents the eight different lithofacies throughout the core. A pre-existing density log from when the core was originally drilled was corrected to match the density values of sandstone bodies from the rock property measurements because the logs were initially calibrated to the coal values when originally cored; however, since the rock property measurements demonstrate the accurate density values, the log was recalibrated to the sandstone bodies. Using the velocities (*Vp* and *Vs*), and density log, *Ip*, and *Is* were calculated. The reflectivity series was convolved with a 25-Hz zero phase +90 rotated Ricker wavelet with an offset range from 0 to 30 degrees.

Results

Facies Association Stacking Pattern

The combination of the MCA with the cutoff criteria produces seven complete facies associations based on the three criteria of containing at least three lithofacies, lithofacies thickness that falls within the standard deviation and underlain by mud rip-up and trough cross bedded sandstone. These facies associations were subsequently categorized as either tidal or fluvial. One key indicator of depositional environment was the capping lithofacies of the packages. The facies associations that are capped by carbonaceous shale and coal are typical of tidal depositional environment, whereas facies associations that are capped by bioturbated mudstone exclusively, without carbonaceous shale or coal present, is indicative of the overbank fine architectural element, pointing to a fluvial depositional environment. Another indicator of depositional environment is the base lithofacies of each package, where, when present, mud rip-up sandstone is interpreted to be associated with fluvial channels (Table 1.2). These interpretations corroborate Gallin's (2010) interpreted depositional environments.

The lithofacies stacking patterns observed within the facies associations indicate that there is a range of distinct stacking patterns in both the fluvial and tidal environments of deposition (Fig. 1.5). The MCA results illustrate which lithofacies are most likely to stack on top of one another in a statistically significant pattern. These stacking patterns and their measured bed thicknesses (Fig. 1.6) comprise the facies associations that were observed within interpreted environments of deposition both of complete and incomplete packages (Fig. 1.7).

The results for one of the fluvial facies association (fluvial 1) is comprised of a

base of mud rip-up sandstone to trough cross-bedded sandstone (55 %), capped by bioturbated mudstone (14%). The most likely fluvial facies association based on (fluvial 2) stacking pattern that was extracted from the core is a mud rip-up base followed by trough cross-bedded sandstone (55%) followed by planar bedded sandstone (50%), flaser/wavy/lenticular bedded sandstone (52 %), capped by bioturbated mudstone (84 %).

There are five MCA results for the tidal facies association likely due to the fact that it is a much thicker depositional environment in the core. The tidal facies associations do not exhibit mud rip-up sandstone in this environment; the base in each of the five facies associations is trough cross-bedded. Tidal 1 has a base of trough cross-bedded sandstone transitioning to planar bedded sandstone (45 %), carbonaceous shale (12 %), and capped by coal (100 %). Tidal 2 has a base of trough cross-bedded sandstone transitioning to planar bedded sandstone, bioturbated mudstone (42 %), and capped by coal (22 %). Tidal 3 has a base of trough cross-bedded sandstone transitioning to flaser/wavy/lenticular bedded sandstone (36 %), bioturbated mudstone (84 %), carbonaceous shale (34 %), and capped by coal (100 %). Tidal 4 has a base of trough cross-bedded sandstone transitioning to planar bedded sandstone (50 %), flaser/wavy/lenticular bedded sandstone (46 %), carbonaceous shale (16 %), and capped by coal (100 %). Tidal 5 has a base of trough cross-bedded sandstone transitioning to planar bedded sandstone (50 %), flaser/wavy/lenticular bedded sandstone (46 %), bioturbated mudstone (84 %), carbonaceous shale (38 %), and capped by coal (100 %). Tidal 5 facies association is comprised of lithofacies that represent the most likely stacking based on percentages. This association is assumed to represent the most representative end member in a tidal environment. Based on the most likely stacking

pattern in the fluvial environment, the representative end member would be something in between fluvial 1 and fluvial 2.

The facies associations capture not only likely statistical transition between lithofacies, but also show distinct patterns linking each package to depositional processes. All of the facies associations contain the trough cross-bedded sandstone lithofacies, which indicates the presences of either fluvial or tidal channels. The planar bedded sandstone points to a high velocity flow, the flaser/wavy/lenticular bedded sandstone illustrates bi-directional flow which suggests tidal influence, bioturbated mudstone indicates a quiet environment with little disturbance from flow, and both coal and carbonaceous shale represent organic input and stagnant depositional conditions representative of paludal depositional environments.

Between all the facies association, the columns can be differentiated by the absence or inclusion of the following lithofacies; 1) facies associations containing planar bedded sandstone (in 5 of 7 facies associations, both in tidal and fluvial); 2) facies associations with flaser/wavy/lenticular bedded sandstone (in 4 of 7 facies associations, both in tidal and fluvial) and; 3) facies associations capped by carbonaceous shale and coal (in all tidal facies associations).

Rock Properties

The rock properties show a wide range of values as a direct result of the highly heterolithic nature of these deposits. The distribution of rock property data for each lithofacies sorted by depositional environment is presented in Table 1.3. The values derived from laboratory measurements including *Vp*, *Vs*, density, and porosity, are

cataloged into the three depositional environments. Three samples with a *Vp* values less than 1500 m/s were removed from further calculations because they were believed to be bad samples due to these unrealistically low values. The error in the remainder of the measurements is less than 1% for all tests.

The standard deviation for *Vp*, *Vs*, and density is low for the mud rip-up clast sandstone. Although there are not enough data to calculate a standard deviation for the planar bedded sandstone, values for this lithofacies has the largest range the maximum and minimum values for *Vp* and *Vs*. The trough cross-bedded sandstone in both fluvial and tidal depositional environments exhibit similar values. In the tidal environment, the highest standard deviation for *Vp* and *Vs* is the planar bedded sandstone 940 m/s and 618 m/s, respectively. The lowest standard deviation for *Vp* is flaser/wavy/lenticular bedded sandstone; however, it also has the highest standard deviation for porosity (275 m/s and 6.2 %, respectively). The lowest standard deviation for *Vs* and porosity is carbonaceous shale (185 m/s and 2.7 %, respectively). The other lithofacies all have similar standard deviations in the middle for both velocities. The wide range in values emphasizes the complexity in interpreting the seismic expression of these highly heterolithic depositional environments.

It is difficult to identify velocity and density as separate variables from seismic profiles; however, *Ip* and *Is* can be easily obtained. Therefore, a common way to identify velocity and density is to plot *Ip* and *Is* as a ratio to derive *Vp/Vs*. The general trends observed in the rock properties cross plot of *Ip* versus *Vp/Vs* is increasing *Ip* and decreasing *Vp/Vs* as a function of decreasing grainsize, decreasing net-to-gross, and decreasing porosity (Fig. 1.8D, 1.8E, and 1.8F, respectively). Although there is an inverse

relationship between grainsize and *Ip*, the siltstone, and mudstone are difficult to distinguish from one another (Fig. 1.8D). A general trend between decreasing net-to-gross and increasing *Ip* is clear; however, there is a considerable amount of overlap in the high *Ip* with some higher net-to-gross exhibiting higher *Ip* (Fig.1.8E). In addition, there is a clear inverse relationship between porosity and *Ip* (Fig. 1.8F); however, where the porosity values have values of less than < 5 %, the porosity plots show a distinct positive slope. The inverse trend is also evident in the percentage of clay illustrating an increase in Ip with an increase in clay content (Fig. 1.8G). Poorly-sorted samples tended to have a high *Ip*, while the well-sorted tended to have a lower *Ip* (Fig. 1.8H). Furthermore, sandstone lithofacies in general are characterized as high net-to-gross, high porosity, large grainsize, and low *Ip* (Fig 1.8A). One lithofacies in particular that is an outlier to these general trends is planar bedded sandstone which exhibit larger grainsize and net-to-gross, but high *Ip* and low porosity. Bioturbated mudstone and carbonaceous shale have low net-to-gross, low porosity, small grainsize, and high *Ip*. Tidal and coastal plain environments are clearly differentiated with the tidal elements having higher average values of *Vp/Vs* and *Ip* (Fig. 1.8B).

There is a v-shape apparent in the plots showing low *Ip* from fluvial and tidal channels, demonstrating a poorly correlated negative slope, and high *Ip* architectural elements which correspond to the tidal and fluvial mudstones and exhibit a distinct positive slope (Fig. 1.8B). The positive slope, high *Ip* trend in the rock properties plot represents the tidal mudstone and overbank fines. Tidal mudstone and the fluvial overbank fines are distinguishable as shown by an offset in the averages which indicates that the tidal mudstone has a higher *Vp/Vs* and *Ip* compared to the overbank fines at, 0.08

and 11100 (Ns/m^3), respectively (Fig. 1.9). Although the tidal mudstone and overbank fine elements have low porosity, grainsize, and net-to-gross, the tidal mudstone in particular have varying amounts of bioturbation while the circled points (overbank fine), illustrate no bioturbation (Fig. 1.8C).

The plot colored by architectural elements illustrates a strong distinction between the different types of sandstone beds (interpreted as channels) in the *Vp/Vs*, where the tidal mudstone and overbank fines are more easily distinguished by the *Ip* spread (Fig. 1.9). In the channel sandstone, the tidal *Vp/Vs* is 0.04 and the *Ip* is 2000 (Ns/m^3) which is greater than the fluvial sandstone which has a *Vp/Vs* of 0.35 and *Ip* of 5000.

In order to investigate different ways to distinguish the channel sandstone elements, the lithofacies that comprise the sandstone elements were plot as *Ip* versus porosity (Fig. 1.10). The lithofacies that comprise channel sandstone are planar bedded sandstone (D, Fig. 1.3), trough cross-bedded sandstone (E, Fig. 1.3), structureless sandstone (F, Fig. 1.3) and mud rip-up sandstone (G, Fig. 1.3). The core plugs are separated into two groups based on marine influence moving up in the core: tidally influenced channels, and fluvial channel sandstone at the top of the core. Employing tidal and fluvial channel sandstone lithofacies investigates the differences in the channels based on the channel architectural elements and core depth (Fig. 1.10). The end member, fluvial channel sandstone has high porosity values and low *Ip* while the tidally influenced channel sandstone demonstrates low porosity and high *Ip* values (Fig. 1.10a). Based on the depth plot, the tidal channel samples that are clustered in the low porosity zone correlate to the upper most section of the tidal environment (310-340 m). The mid-range porosity and *Ip* samples in the tidal environment correlate to the middle section of the

tidal environment (340-370 m), while the base of the tidal environment correlates to high *Ip* and low porosity channels (370-400 m) (Fig. 1.10B). Recalling that core EP-25 displays increasing marine influence moving down in depth the plot *Ip* versus porosity aids in highlighting the distinction between the more marine influenced channelized sandstone and the fluvial influenced channel sandstone (Fig. 1.10C).

Forward Seismic Modeling

The maximum positive amplitude at zero-phase was used as the location across which to analyze offset amplitudes (Fig. 1.11). In the near-far amplitude versus offset plot, fluvial facies associations have higher amplitude for the full range of offsets in comparison to the tidal facies associations which have lower amplitudes. The key difference between the tidal and fluvial facies associations is the presence of coal and carbonaceous shale in the tidal facies association and the mud rip-up clast sandstone at the base of the fluvial.

In contrast to the modeling of single facies association packages with a mudstone background, AVO modeling of the full core EP-25 represents multiple facies associations stacked on top of one another with the measured and interpolated rock properties rather than averages (Fig. 1.12). The AVO model of the entire core illustrates some similarities and differences to the facies association AVO models. In the offset plot, the maximum amplitude fluvial coastal plain amplitude reflection is also larger than the tidal zone amplitude reflection. Facies associations containing planar bedded sandstone are observed in both fluvial and tidal facies associations, and have a large spread in values which is muted in the individual facies association modeling due to the use of average

values. The impact is a large range of resulting AVO responses. The Drip Tank Member, at the top of the core, is a gravelly sheet comprised of high *Ip* sandstone. When juxtaposed against the low *Ip* overbank fines and fluvial channels in the upper JHM, an amplitude reflection is generated that is unique compared to the other wavelets in the core; this wavelet has a more significant decrease in amplitude in the far offset.

The second pattern that emerges from the AVO analysis of the facies associations is observed in the amplitude reflection coefficient versus offset plot (Fig. 1.12). The fluvial facies associations have higher amplitude reflections compared to the tidal facies association in the near and the far angles. However, there is more obvious distinction between the fluvial and tidal facies associations in the near angle; the distinction is much less apparent in the far angle. The difference between the tidal and fluvial is due to the fluvial associations having a base of low *Ip* and capped by bioturbated mudstone that has a lower *Ip* than the tidal association bioturbated mudstone. The inclusion of the high *Ip* carbonaceous shale and low *Ip* coal is also a significant distinguishing feature between the tidal and fluvial associations that is revealed in both the rock properties and subsequently the AVO analysis.

Discussion

Interpreting Degree of Tidal Influence from Lithofacies Stacking Patterns

Predictive, probabilistic stacking patterns at the lithofacies scale using MCA is an advantageous way of recognizing repeatable and statistically significant stacking patterns in vertical successions. Due to the complexity of tidally influenced deposits, stacking patterns predicted from a MCA indicate nuances which help better constrain

interpretations and place measured rock properties within an architectural framework. The fluvial and tidal facies associations illustrate variable terrestrial versus marine influence evident in both the stacking patterns and patterns in the rock properties. These trends can be used as a basis to improve seismic interpretation in tidal environments.

All seven of the resulting facies association columns have a slightly different stacking pattern. These variations in stacking patterns signify small but important differences in the depositional processes. The most likely stacking pattern in the fluvial succession is a basal mud rip-up sandstone, trough cross bedded sandstone, planar bedded sandstone, and capped by bioturbated mudstone. This is interpreted as an erosional fluvial channel transitioning to overbank fines in a coastal plain depositional setting with no marine influence. However, the second facies association located within what has been interpreted as a fluvial package (fluvial facies association 2) includes flaser/wavy/lenticular bedded sandstone. This section is likely located within a coastal plain because of the lack of a carbonaceous shale and coal cap. However, this package sits above a tidal package and contains bedforms consistent with tidal influence (carbonaceous shale and coal). This section could be exhibiting some transitional properties associated with a conformable change from tidally influenced to coastal plain, more seaward than fluvial 1, but still more inward than the tidal facies associations.

The five different tidal facies associations show even more variation. The most likely stacking pattern for a tidal facies association is a basal trough cross-bedded sandstone, planar bedded sandstone, flaser/wavy/lenticular bedded sandstone, bioturbated mudstone, carbonaceous shale, capped by a coal. However, there is only one facies association column that represents these statistics and is interpreted as an end member

representation of the furthest seaward tidal package (tidal 5). This full stacking pattern is characterized by a high flow regime tidal channel transitioning to low energy tidal mudstone and capped by coal. Tidal associations 1 and 2 do not contain flaser/wavy/lenticular bedded sandstone which points to a lack of direct tidal influence. However, the inclusion of coal indicates these two facies associations as being deposited in a more paludal setting transitioning from coal mires to channels more inland compared to the other tidal facies associations. Because tidal 2 contains bioturbated mudstone rather than carbonaceous shale, it is likely that this package was deposited the furthest from the coast line, possibly in the transition between paludal and coastal plain depositional environments. Tidal 1 and 2 may also correspond to a more lateral transition or deposition off axis from the tidal and fluvial channels. In tidal associations 3 through 5, flaser/wavy/lenticular bedded sandstone is present, thus placing them closer to the shoreline. The variations in AVO in these three associations are linked to the inclusion and exclusion of bioturbated mudstone and planar bedded sandstone. Those facies association that include bioturbated mudstone correlate to a longer period of quiescence with low energy and tied more closely with a paludal depositional environment. The facies associations with planar bedded sandstone are related to a high energy flow regime. This can be interpreted as tidal channels that have an increased flow compared to those tidal facies associations that lack the planar bedded sandstone lithofacies which represent a lower flow regime. While the stacking patterns reveal the type of processes and location within the depositional environments, the rock property characteristics indicate how the lithofacies properties are expressed collectively as a depositional package and revealed in AVO modeling.

Interpreting Degree of Tidal Influence in Rock Properties

The relationship between *Vp/Vs* and *Ip* show the anticipated trend of an increase in *Ip* with increasing mudstone and decreasing porosity (Fig. 1.8 C, D, E, G). Although the v-shape appears to correlate to clay content, when separating the trends by architectural elements, several additional patterns begin to emerge. For example, fluvial and tidal mudstone can be distinguished in the cross plot clusters; however, the acoustic responses within the tidal mudstone exhibit a much larger spread in properties (Fig. 1.8). This spread is possible due to a larger range of bioturbation, and a wider range of organic material. Fluvial overbank mudstone is often homogeneous and does not exhibit bioturbation compared to its fine-grained tidally influenced counterpart (Fig. 1.8C).

The second major trend that appears is the distinction between tidal and fluvial channel elements (Fig. 1.8 B). There is a significant amount of overlap in rock properties across these two channel sandstone types; however, the averages illustrate there is a small amount of offset between the two architectural elements (Fig. 1.9). When examining the relationship between *Ip* and porosity for the sandstone beds within these channelized architectural elements (Fig. 1.10). The fluvial end member channel sandstone exhibits the lowest *Ip* of all the channel sandstone. The tidal facies association end member is comprised of channel sandstone with the most marine influence which exhibits the highest *Ip* values. The low fluvial channel *Ip* juxtaposed against the mid-range overbank fines *Ip* should produce a high amplitude reflection. Although the tidal mudstone can be variable in *Ip*, it is generally high; the high *Ip* channel sandstone juxtaposed against high *Ip* tidal mudstone are expected to produce lower amplitude reflection.

AVO Analysis

The AVO analysis clearly shows the impact of lithofacies associated with tidal influence, the consequence of averaging rock properties rather than using exact property results, and a discrete difference between the fluvial and tidal facies association. The individual facies associations reveal a distinction between the tidal and fluvial associations in the AVO plot. There is not a clear trend within the tidal associations but the implication of the offset between the fluvial and tidal in the amplitude versus offset plot is a useful predictor to distinguish between the better reservoir channel sandstone in the fluvial environment and tidal channel sandstone which exhibit lower quality reservoir sands.

The full EP-25 core AVO illustrates, on a much larger scale, the increase in marine influence with increasing depth of the core and the ability to discern the tidal fluvial packages from tidal in the AVO response (Fig. 1.12). There are two trends when examining the full EP-25 core AVO modeling results. The first trend is based on the rock properties within the JHM, and the link to overall increase in rock properties values of both channels and mudstone with increasing marine influence (Fig. 1.10). Similar to the individual facies association models, the amplitude of reflectivity in the near and far angles decreases with increasing marine influence (Fig. 1.12). This decrease is caused by the increase in *Ip* with increasing marine influence in the channel sandstone, but also the increase in coal with increasing marine influence. The AVO modeling suggests that the relatively high *Ip* channel sandstone contrasting with the frequent alternation between coal and carbonaceous shales produces lower amplitude than the facies associations with more fluvial input. The fluvial and tidal channel sandstone with little marine influence

has much lower relative *Is* in contrast to the overbank fines and the tidal mudstone. The decrease in the amplitude reflection coefficient steadily downward in the core is inextricably linked to increase in marine influence. In addition, it is more difficult to distinguish between the tidal and shoreface reflectors in the near angle as they are clustered around the 0.2 amplitude reflection coefficient; however, with increasing marine influence moving downward in the core the reflectors appear to separate in the far angles, with the far offset amplitude of the shoreface approaching zero. Although there is a more noteworthy offset between the fluvial and tidal amplitude reflections in the near angle, the offset decreases in the far angles, making it more difficult to distinguish between the fluvial and tidal amplitude reflections. This indicates that the AVO modeling of the *Ip* and *Is* does not significantly improve interpretation between fluvial and tidal, and in order to distinguish the tidal and fluvial reflectors, only *Ip* is necessary; however, it can be used to potentially differentiate tidal and shoreface.

One caveat is the first fluvial package shows a dramatically different AVO character than the other packages, with a much higher amplitude reflection coefficient in the near offset angle and lower in the far offset angle. This variation is tied to the difference between using average rock property values and true rock property values for the lithofacies. Those lithofacies that exhibit a large standard deviation in the rock properties have a much more significant impact on the full model. The gradient difference between the fluvial 1 facies association and the fluvial 2 facies association in the AVO plot may be tied to the difference between the high *Ip* Drip Tank Member juxtaposed against the JHM (Fig. 1.12). This gradient difference between fluvial 1 and fluvial 2 illustrates the difference between the sheet gravel Drip Tank Member and the

paralic JHM.

Therefore, the AVO modeling appears to be useful not only when distinguishing between tidal and shoreface environments and the association with increasing marine influence, it may also be useful when detecting sharp changes due to unconformities. Similar to the AVO modeling of the individual facies associations, the full EP-25 core forward model highlights in a more comprehensive way the importance of location in the depositional system by the variations in the near- to far- offsets in the AVO plot by the distinction in the fluvial and tidal amplitude reflections.

Interpreting the Proximity to Shoreline from Seismic Reflectivity

Based on the MCA and rock properties results, a landward shift upward in the core is corroborated. Marine influence in the lower portion of the core is shown in the lithofacies stacking patterns by the inclusion of different lithofacies that represent tidal influence (flaser/wavy/lenticular bedded sandstone, carbonaceous shale, and coal) (Fig. 1.9). A decreasing marine influence upward in the core is shown by higher *Ip* and lower porosity in more marine influenced channels and lower *Ip* and higher porosity with less marine influence (Fig. 1.10). The overlap in the high *Ip* as a function of net-to-gross supports the interpretation of high impedance tidally influenced channel sandstone (Fig.1.8E).

Stacking patterns predicted from a MCA help better constrain interpretations and illustrate the impact of variable terrestrial and marine influence. The implication of variable marine influence and proximity to shoreline is inherently linked to reservoir quality. Based on the results from the rock properties, the high porosity channel

sandstone is located in the environments with the least amount of marine influence, while the channel sandstone that are located in the tidal depositional environment and more seaward have much lower porosity. Consequently, the channel sandstone that has the least amount of tidal influence correlates to the highest reservoir quality. The impedance contrasts between the different channels and the overbank fines and tidal mudstone facilitate in distinguishing the high quality reservoir sandstones from the poor quality reservoir sandstone. The facies associations that contain little to no tidal influence exhibit a stronger *Ip* contrast and therefore likely a higher amplitude reflection. The effect of reservoir quality due to the variability of marine influence is best understood by modeling how these variations in seismic reflection.

Not only do the rock properties show a wide range of values as a direct result of the highly heterolithic nature of the deposits, the overlap and the fluctuating marine influence demonstrates the heterogeneity of tidal zones. Although AVO modeling did not show a strong impact on differentiating the tidal influence, it did show a strong difference between tidal and shoreface deposits. The forward seismic modeling did, however, show a strong difference in the zero-incidence amplitudes that would help to differentiate coastal plain from tidal, and a clear gradational change between the two end members.

Conclusion

Tidally influenced reservoirs are significant global sources of petroleum reserves. The complex nature of coastal depositional processes results in highly heterolithic deposits which make reservoir prediction difficult. A Markov Chain Analysis performed

on lithofacies observations, based on bedforms generated by different depositional processes, from core revealed statistically significant stacking patterns which were interpreted as either tidally influenced or fluvial packages. These stacking patterns corroborate previous depositional environment interpretations and help to clarify where there was ambiguity by simple core observation alone. In particular, the MCA analysis assisted in interpreting facies associations located in the system based on the depositional processes that the stacking patterns signified. Stacking patterns and the inclusion of tidally influenced lithofacies such as flaser/wavy/lenticular bedded sandstone, carbonaceous shale, and coal enables an interpretation of where the package was deposited relative to the shoreline.

Analysis of rock properties measured from core further aided in distinguishing tidal and coastal plain depositional environments as well as their related architectural elements. By examining rock properties cross plots, channel sandstone lithofacies show an increase in *Ip* for both tidal channel sandstone and mudstone which made these deposits distinguishable from coastal plain overbank fines and fluvial channels. In particular, the two resulting patterns emerged from the MCA and rock property analyses. These were clear indications of proximity to shoreline from the MCA stacking pattern results including flaser/wavy/lenticular bedded sandstone, carbonaceous shale, and coal which point to a more seaward depositional environment. The impact that proximity to the shoreline has on the resulting tidal channel sandstone is a decrease in porosity with increasing tidal influence. Using the MCA facies association results and the rock properties, the tidal and fluvial facies associations were differentiated in the AVO plot. The AVO, however, did not add any additional information. The zero-incidence

reflectivities are enough to differentiate fluvial and tidal end member. The implication of this discovery is the ability to denote high porosity fluvial packages from low porosity tidal packages in seismic reflection profiles for improved understanding of reservoirs.

The full EP-25 core AVO and rock property results also indicate that the increase in marine influence of being closer to shoreline results in a higher the *Ip* in the tidally influenced channel sandstone lithofacies. The direct impact on the seismic response is a lower amplitude reflection than the low *Ip* fluvial channels and overbank fines. Higher fluvial input suggests high porosity and low *Ip* in both the mudstone and the channels compared to the tidal environments. The information from the rock properties and AVO modeling demonstrates the extent that the depositional environment geology impacts the seismic expression. Small seaward or landward shifts of the tidal environment have significant effects of the rock properties including porosity of the channel sandstone porosity.

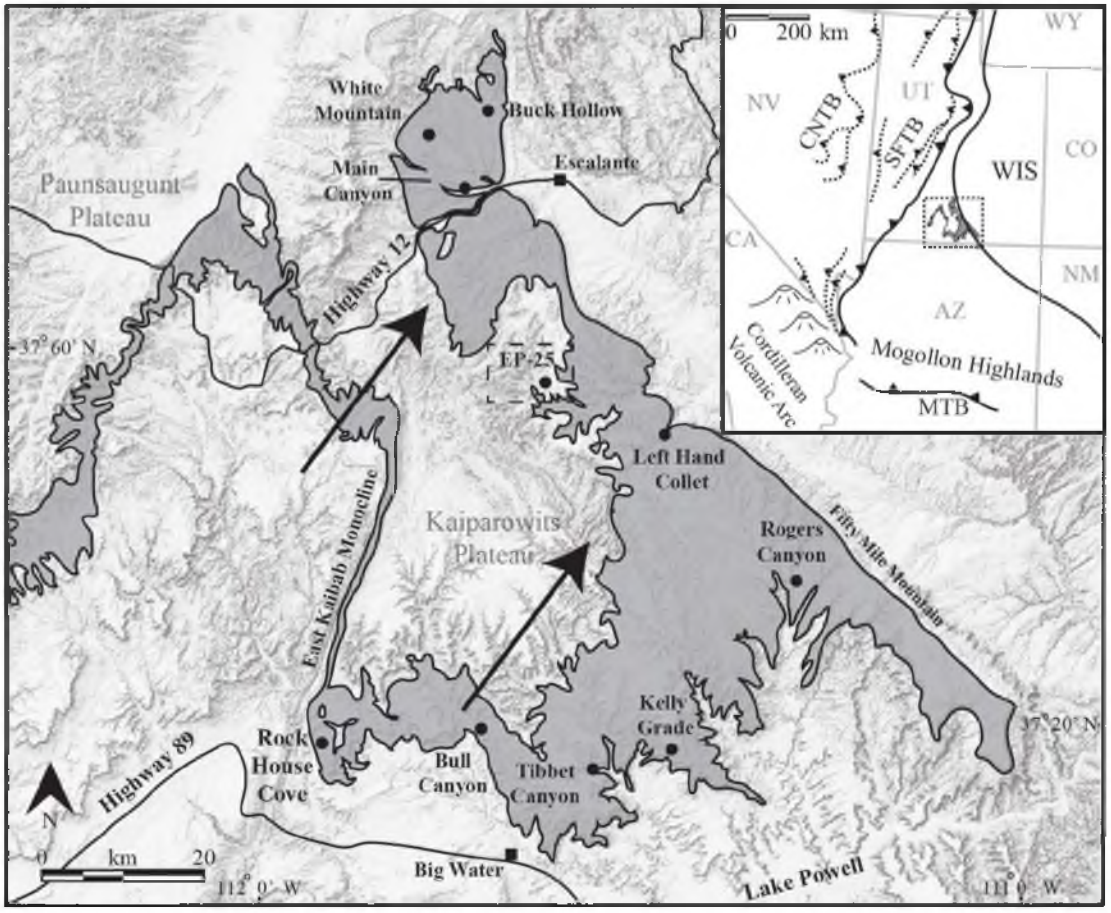

Figure 1.1. Map of Kaiparowits Plateau and previous studies modified from Chentnik (2014). The black dots indicate the location of previous studies throughout the plateau. The main focus of this study is on core EP-25 located in the north central portion of the plateau. The western edge of the plateau is dominated by fluvial deposits, the arrows are indicative of fluvial paleocurrent flow direction. The center of the plateau is tidally influenced deposits, and the western edge along Fifty Mile Mountain is the paleoshoreline extent of the western Cretaceous seaway.

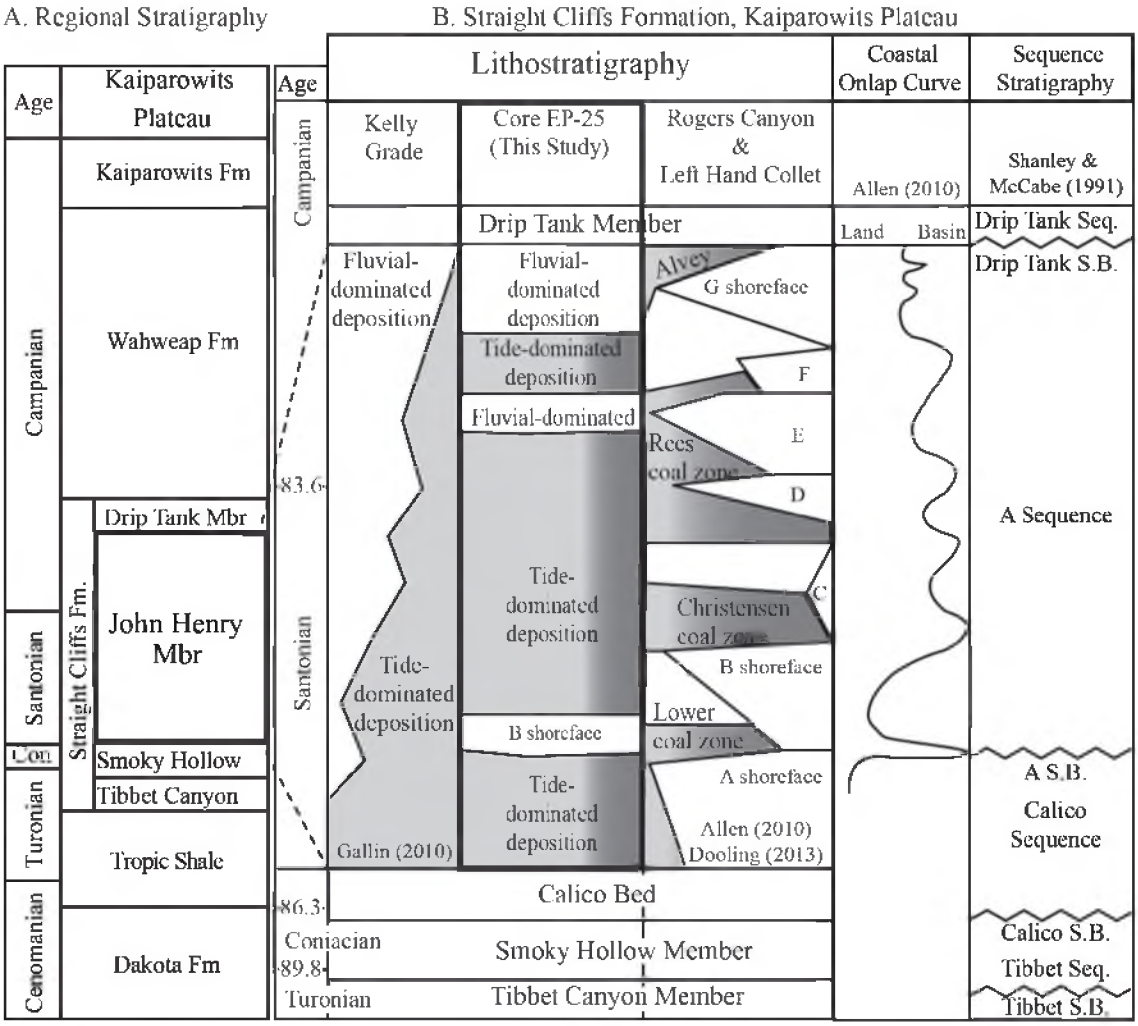

Figure 1.2. Regional stratigraphy and stratigraphic columns of study area. (A) Stratigraphic column of the Coniacian to Santorian deposits throughout Kaiparowits Plateau, and (B) the study area. Kelly Grade to Left Hand Collet to EP-25 represents the south to north deposits of the John Henry Member. Seven marine sandstone packages were named "A-G" by Peterson (1969a). The packages pinch out landward into coal zones and coastal plain facies. Core EP-25 intersects the three coal zones through the B sandstone. The coastal onlap curve is derived from the Rogers canyon study on the southwestern part of the plateau (Allen and Johnson, 2011).

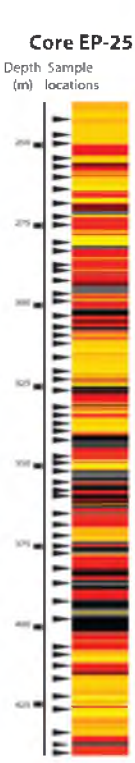

	Lithofacies	Description	Number of samples	Interpretation	Core plugs
A	Carbonaceous shale	Dark gray to black colored shale, often laminated but sometimes structureless; abundant organic material; often grades in and out of coal facies	10	Low energy paludal and lagoonal deposits	
B	Bioturbated mudstone	Horizontally laminated mud or mud with no apparent laminations, heavy bioturbation	12	Low energy lagoonal and fluvial overbank muds	
C	Flaser/wavy/lenticular bedded sandstone	Alternating laminations of sandstone and mudstone; sand grain size ranges from very fine to medium sandstone	12	Bi-directional flow associated with tidal deposits	
D	Planar bedded sandstone	Laminations dip at < 5°; grain size ranges from fine to medium sandstone	4	High flow regime, proximal shoreface, tidal and fluvial channels	
E	Trough cross-bedded sandstone	Trough and planar foresets dip between 5-40°; grain size ranges from fine to coarse sandstone	11	Unidirectional flow associated with fluvial and tidal channels	
F	Structureless sandstone	Sedimentary structures are apparent; grain size ranges from very fine to coarse sandstone	4	Rapid deposition from high energy suspension in proximal shoreface deposits	
G	Mud rip-up clast sandstone	Angular to subangular mud rip-up clasts in a sandstone matrix; matrix grain size ranges from very fine to coarse sandstone	4	High energy fluvial channel lag deposits	
H	Coal	Black with dull vitreous reflectance and lacking distinct laminations; coal beds are < 1 m thick	0	Low energy paludal and lagoonal deposits	

Figure 1.3. Lithofacies and core plugs. Lithofacies observed in core EP-25 with a representative core plug photograph. The number of core plug samples from each lithofacies is a statistical representation of the proportion of that lithofacies present in the core.

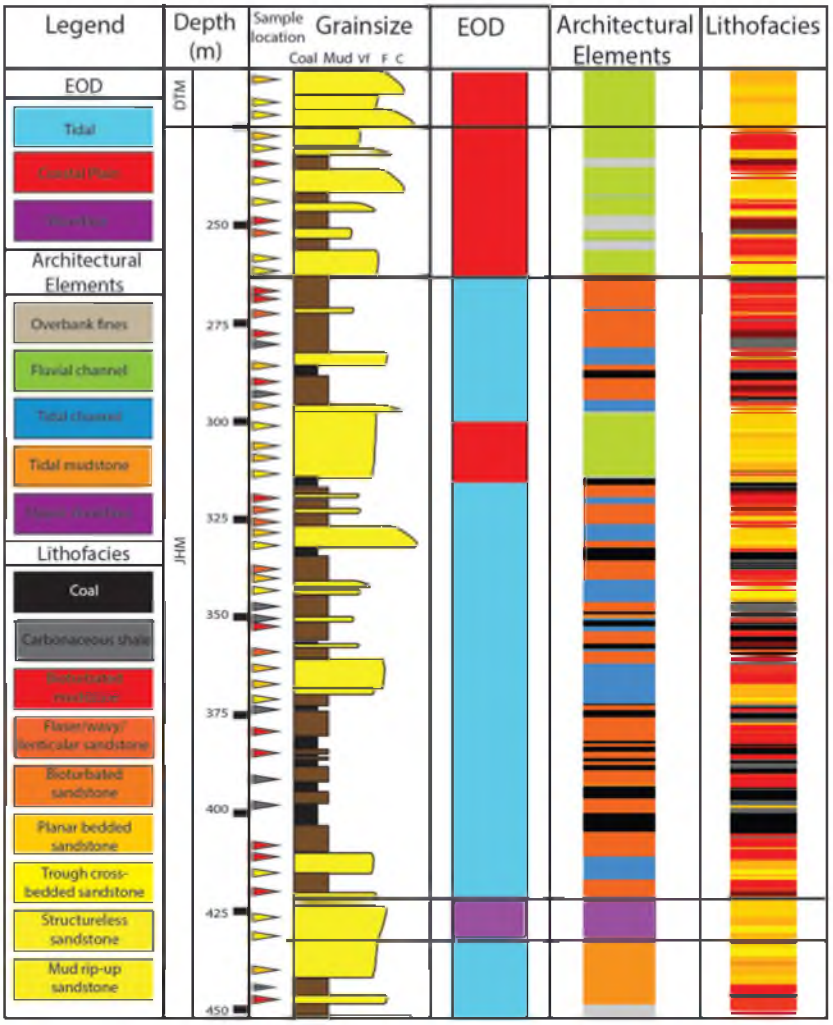

Figure 1.4. Core EP-25 logs including depositional environments, architectural elements, and lithofacies. Gallin (2010) logged core EP-25 producing a grainsize log, identifying the three different environments of deposition and eight lithofacies. The environment of deposition was further broken down into architectural elements.

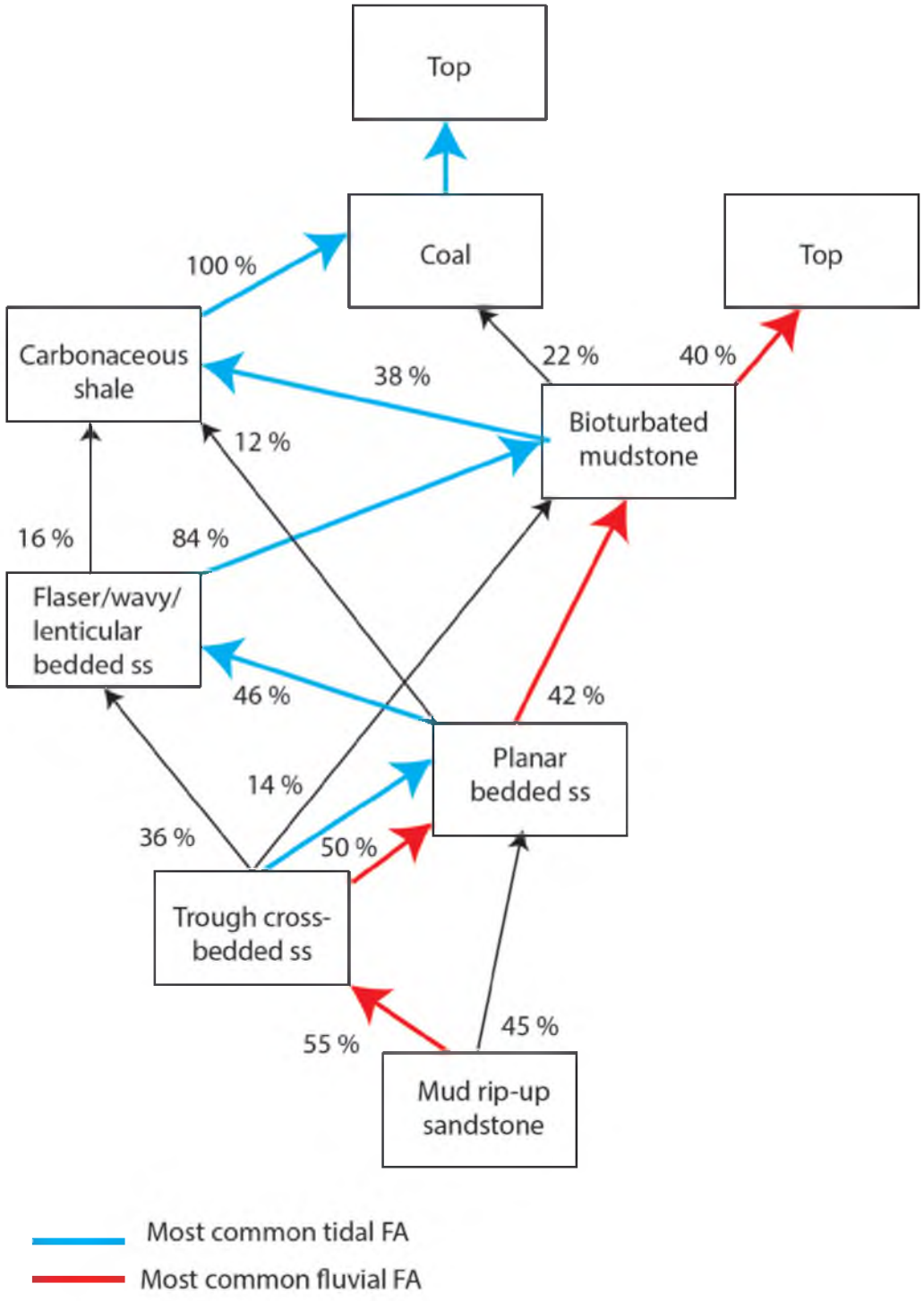

Figure 1.5. Markov Chain transitional statistics. Transition probability tree showing frequency and probability (%) with which lithofacies are overlain by other lithofacies. Arrows point towards the lithofacies, and boxed numbers indicate the probability of occurrences of the lithofacies that are succeeded directly by another lithofacies. The blue arrows indicate the most likely stacking.

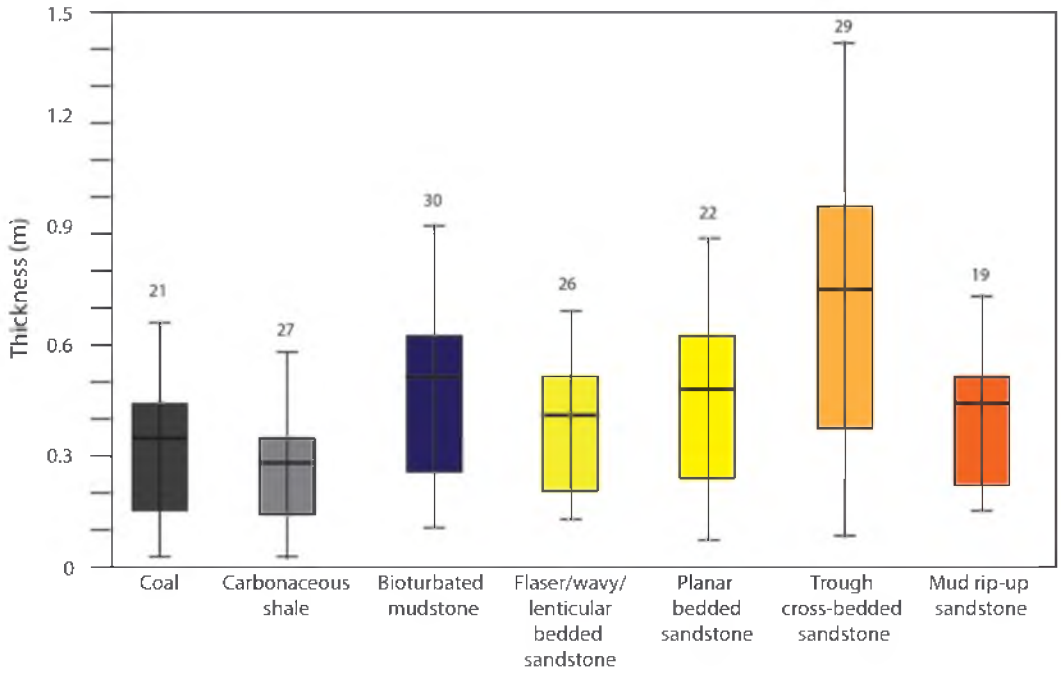

Figure 1.6. Lithofacies thickness box and whiskers plot. The graph illustrates the average thickness in meters of each of the lithofacies. The bar shows the standard deviation in thickness. The number on top of each bar represents the number of beds of each of the lithofacies.

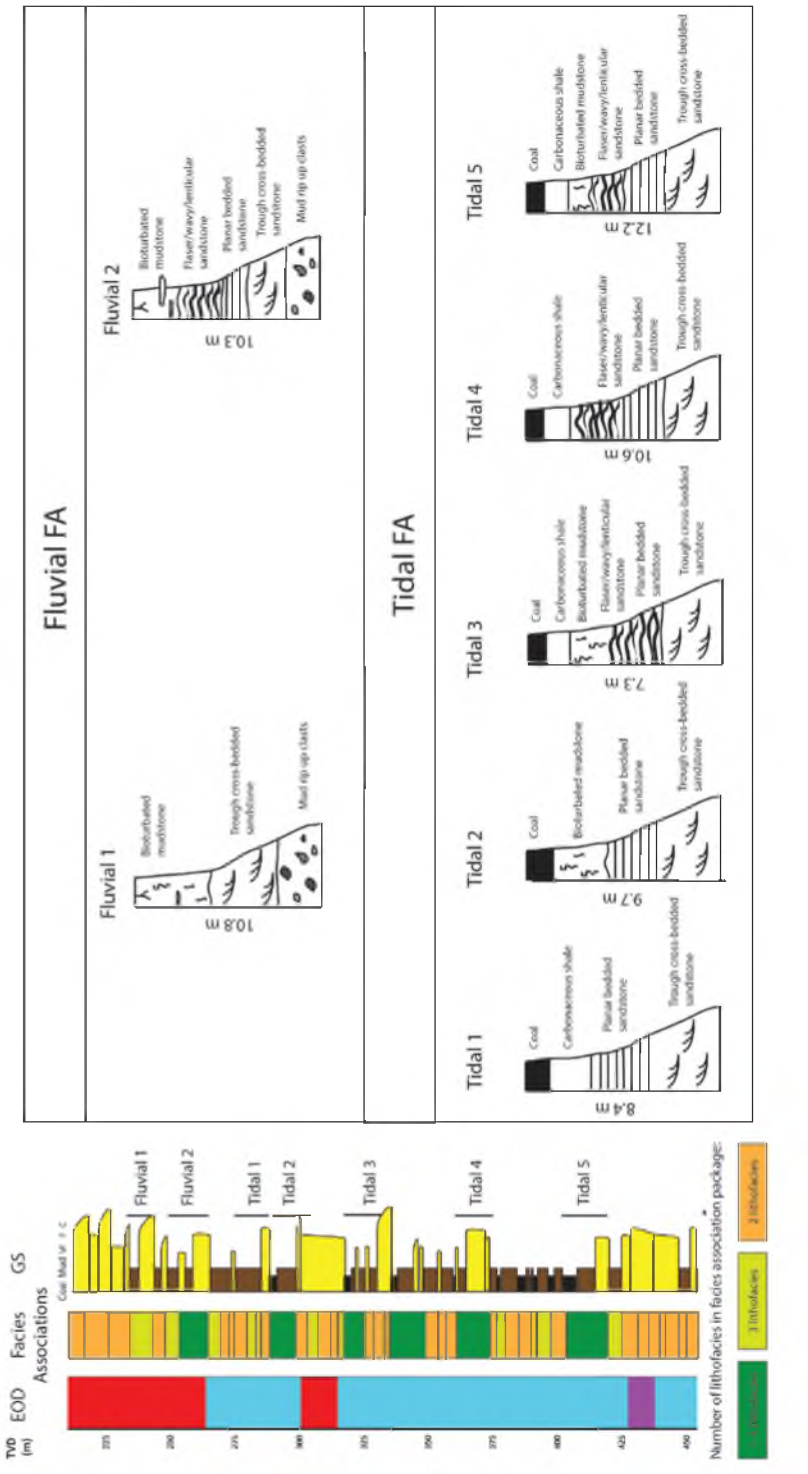

Figure 1.7. Facies associations columns. Facies associations extracted directly from core EP-25. There are two fluvial facies associations and five tidal facies associations. Each of the facies associations represents different lithofacies stacking patterns. The facies associations also exemplify different thickness present in the core.

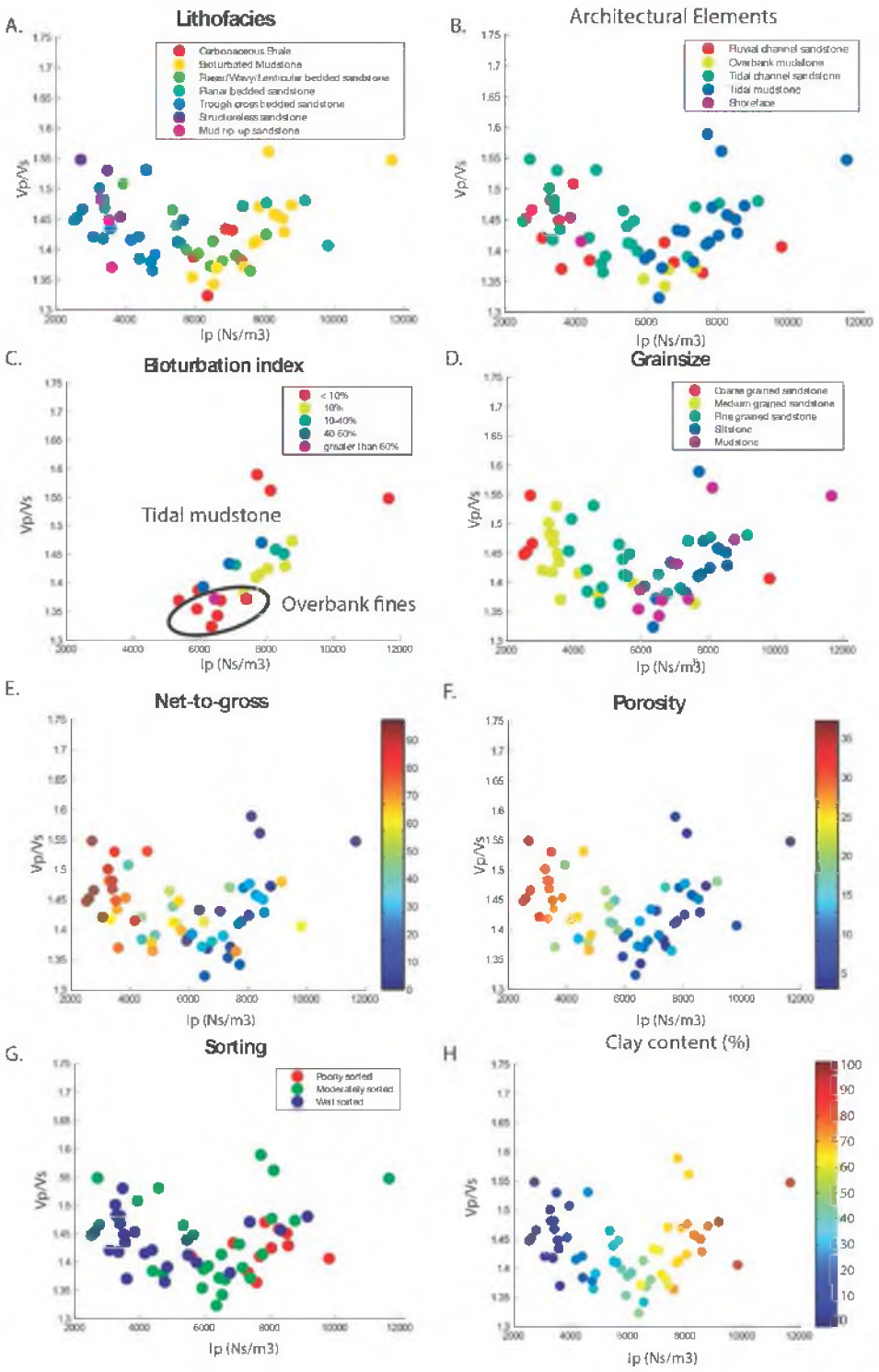

Figure 1.8. Rock plots. *Vp/Vs* versus *Ip* cross plots showing the relationship between measured rock properties and core plug attributes: A) lithofacies, B) architectural elements, C) bioturbation index of tidal mudstone and overbank fines, D) grainsize, E) net-to-gross, and F) porosity. The black circle in the bioturbation plot corresponds to the overbank fines. The remaining points in the bioturbation plot correspond to the tidal mudstone.

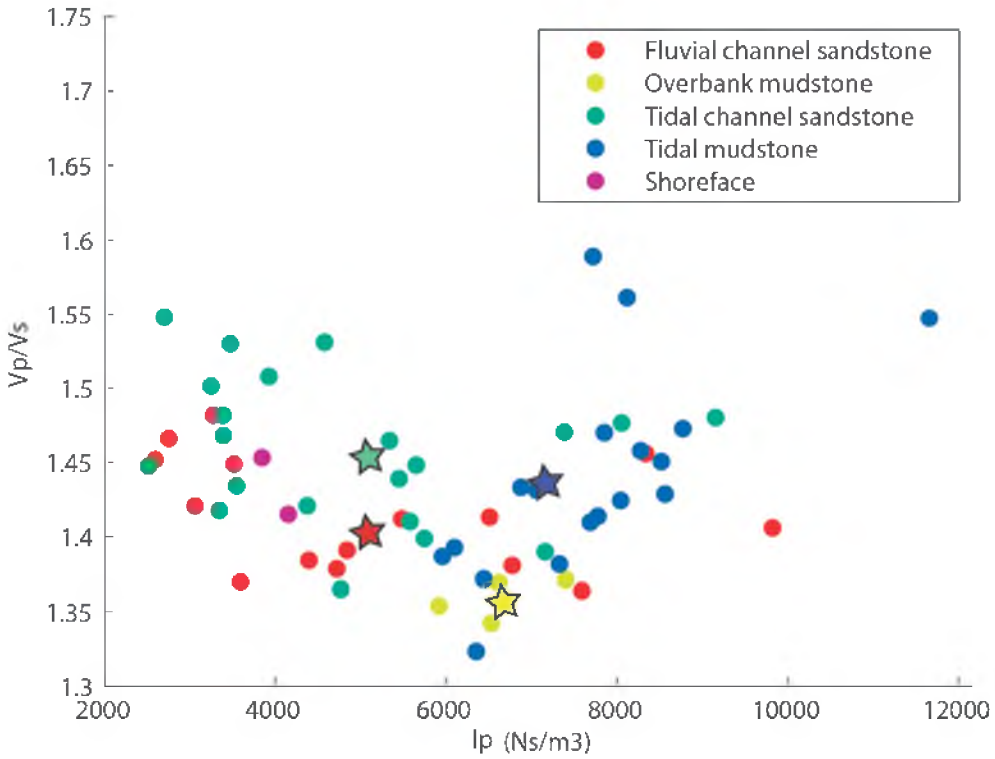

Figure 1.9. Architectural element plot with averages. Plots of *Vp/Vs* versus *Ip* directly from core plug measurements and colored by architectural elements. The stars represent the averages for each of the architectural elements, highlighting the distinction between the sandier elements and the finer grained elements. Both the tidal elements have higher *Vp/Vs* and *Ip* compared to the fluvial elements.

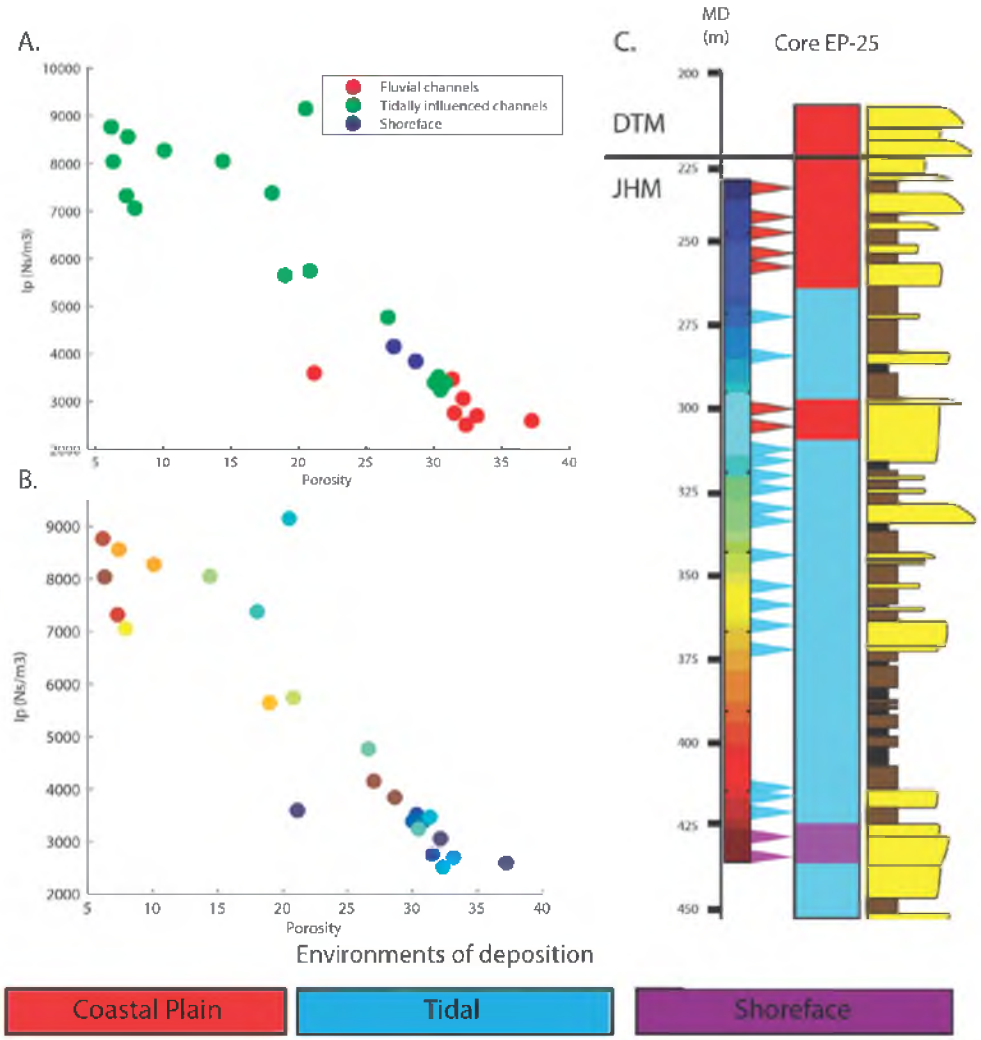

Figure 1.10. Channel sandstone porosity versus Ip plot and the relationship to marine influence. *Ip* versus porosity of channel sandstone only from the core plugs to illustrate the effect of reservoir quality (e.g., porosity) as a function of either fluvial to tidal processes on impedance. A) *Ip* versus porosity divides the plugs into tidally influenced channels and fluvial channels. B) *Ip* versus porosity plots the plugs based on core depth, illustrating the lower channels in the core have higher *Ip* and lower porosity. C) Core EP-25 shows the core plug with depth correlating to the colored points in plot B.

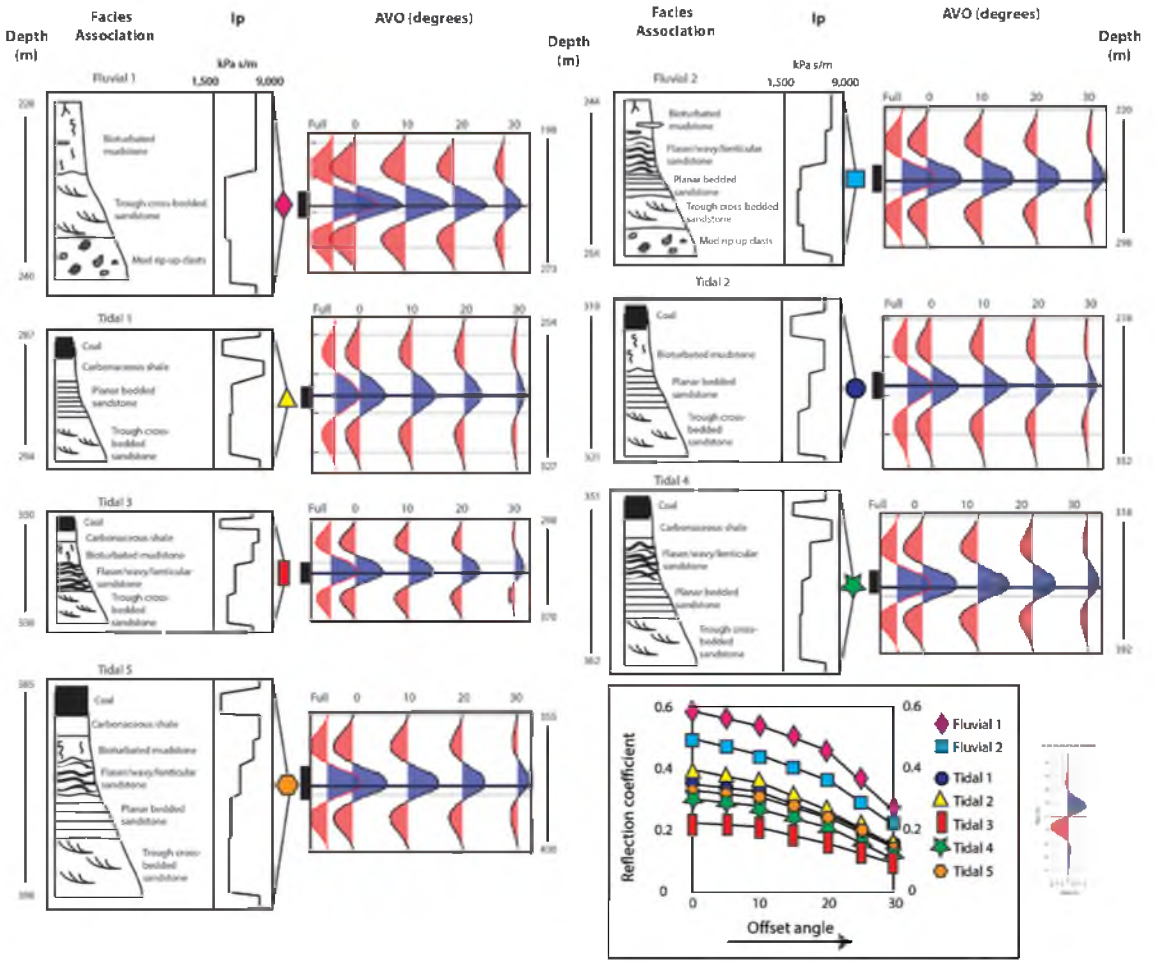

Figure 1.11. Facies associations AVO modeling. Modeled AVO responses for tidal and fluvial facies associations using Zoeppritz equation and a 25 Hz rotated + 90° Ricker wavelet from 0 to 30 degrees. Each lithofacies *Ip* average was used as the input for the AVO modeling. The background lithofacies used is the average *Ip* of bioturbated mudstone. The AVO plot is analyzed at the maximum amplitude of the full stack. The reflection coefficient along the line at the maximum amplitude in the full stack at zero degrees is plotted at the 0, 5, 10, 15, 20, 25, and 30 degree.

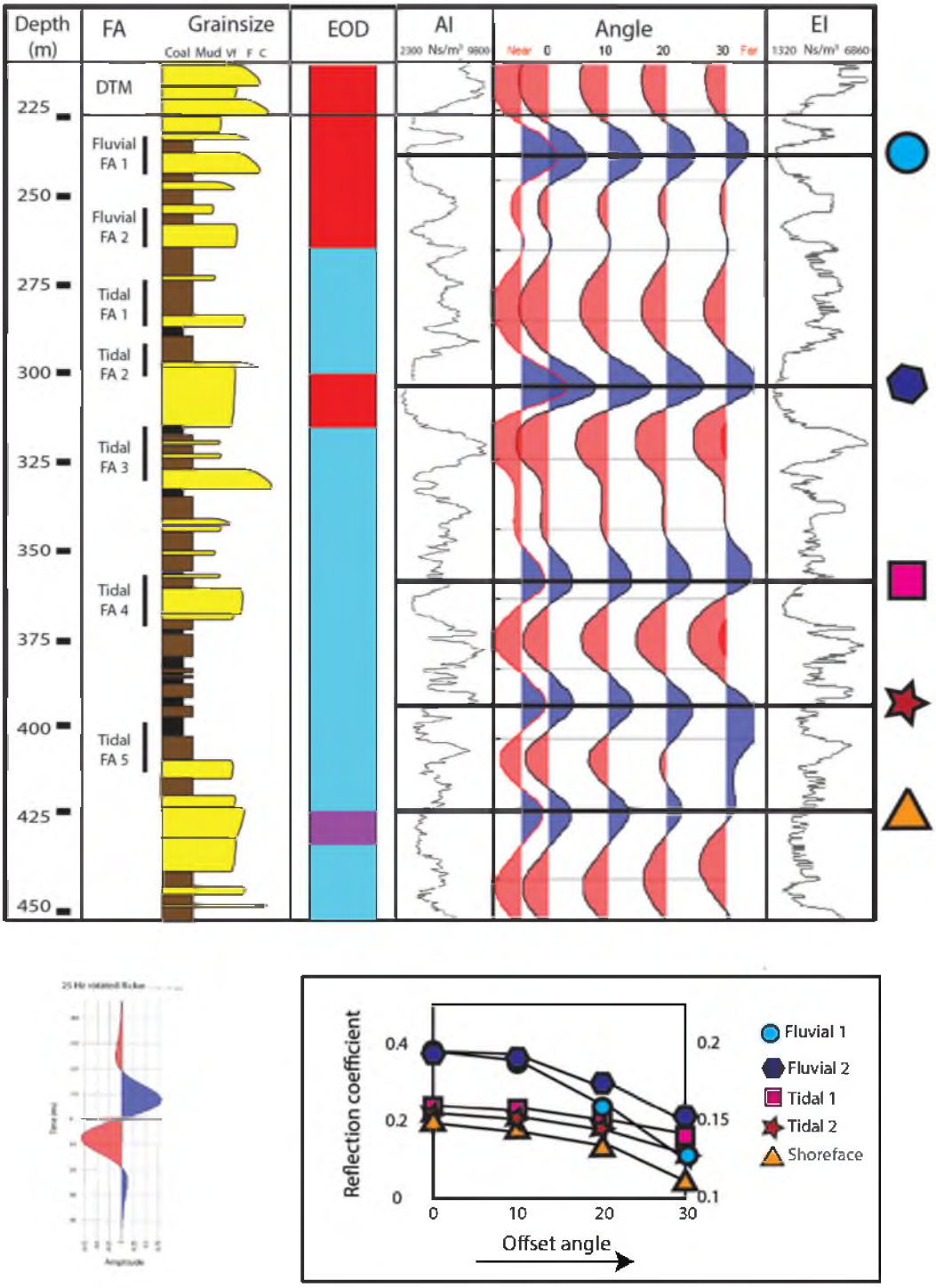

Figure 1.12. 1-dimensional AVO modeling of core EP-25. The full core EP-25 is presented by the grainsize log which shows the location of the seven facies association and the environment of deposition log. *Vp* and V_s logs were calculated from a sequential Gaussian simulation based on core plug values and combined with a density log to obtain *I*p and *Is*. The wavelet used for AVO modeling was a 25 Hz +90 rotated Ricker wavelet.

Table 1.1

Facies associations, environmental description, architectural elements and lithofacies

Environment of deposition	Description	Architectural elements	Lithofacies
Facies Association 1 - Coastal Plain			
1.1 - Laterally extensive channel belts	Fine to coarse grained sandstone. Channel sandstone fines upward. Vertical increase of channel belt amalgamation. Low sinuosity fluvial channels. Individual channels 0.5 - 3 m thick. Channel complexes 10 m thick. Overall lack of fossils present.	**Fluvial channels**	D, E, F, G
1.2 - Mudstone floodplain and overbank fines	Floodplain mudstone are silt and shale rich with lack of carbonaceous shale and coal. weakly bioturbated with some visible laminations.	**Fluvial overbank fines**	B, C
Facies Association 2 - Tidal			
2.1 - Highly sinuous tidal channels, isolated distributary channels	Very fine to medium grained sandstone. Grain size coarsens upward in the core along with an increase in marine influence. Tidal rythmites present. Individual channels 1 - 5 m thick. Channel complexes 15 m thick. Prevalence of brackish water and marine bivalves.	**Tidal channels**	C, D, E
2.2 - Lagoonal and estuarine mires with heavy bioturbation	Grainsize ranging from silt to mudstone. Bioturbated mudstone often grades into carbonaceous shale and terrestrial coals. Heavy bioturbation with some orginal sedimentary structures completely obliterated. Abundance of tidal environment trace fossils.	**Tidal mudstone**	A, B, H
Facies Association 3 - Shoreface			
3.1 - Shoreface sheet sandstone	Fine- to coarse grained well-sorted sandstone. Hummocky cross-stratified sandstone. Large robust marine bivalves are present.	**Proximal shoreface**	D, E, F

Lithofacies rock properties averages in the three depositional environments. The descriptions are by grainsize, stacking patterns, bedform, geometry, and fossils. The descriptions represent the smallest scale of observation of lithofacies. Each of the architectural elements exhibits multiple different lithofacies. Within each environment of deposition are architectural elements. There are three different environment of deposition interpreted in core EP-25.

Table 1.2

Markov chain analysis of lithofacies

lower lithofacies \ upper lithofacies	Coal	Carbonaceous shale	Bioturbated mudstone	Flaser/wavy/ lenticular bedded sandstone	Planar bedded sandstone	Trough cross-bedded sandstone	Mud rip-up sandstone
Coal	X	0.41	0.09	0.04	0.03	0.43	
Carbonaceous shale	0.72	X	0.08	0.01	0.04	0.05	
Bioturbated mudstone	0.18	0.30	X	0.02	0.06	0.32	0.12
Flaser/wavy/ lenticular bedded sandstone		0.15	0.78	X	0.05	0.02	
Planar bedded sandstone		0.12	0.39	0.44	X	0.04	0.01
Trough cross-bedded sandstone			0.35	0.13	0.5	X	0.02
Mud rip-up sandstone					0.45	0.55	X

Table 1.3

Rock properties table

EOD	Lithofacies	core plugs (#)	Vp (m/s)				Vs (m/s)				Density (g/cm3)				Porosity			
			max	min	average	std. dev.	max	min	average	std. dev.	max	min	average	std. dev.	max	min	average	std. dev.
COASTAL PLAIN	*Bioturbated mudstone*	3	3531	2738	3053	296.7	2425	2022	2196	149.6	2.429	2.16	2.308	0.099	11.71	7.003	9.005	1.752
	Flaser/wavy/ lenticular ss	2	2926	2917	2921	n/a	2119	2063	2091	n/a	2.314	2.230	2.272	n/a	15.06	11.91	13.49	n/a
	Planar bedded ss	2	4042	1909	3110	n/a	2874	1318	2223	n/a	2.428	1.840	2.171	n/a	30.33	9.381	18.70	n/a
	Trough cross-bedded ss	5	2521	1533	1963	393.34	1785	1045	1386	297.9	2.184	1.656	1.931	0.201	37.22	16.04	27.03	7.418
	Mud rip-up clasts ss	4	1747	1685	1716	31.80	1275	1136	1206	69.47	2.057	1.946	2.002	0.055	25.98	21.13	23.56	2.435
TIDAL	*Coal*	n/a	2400	1800	2000	200	1200	1200	1200	0	1.2	1.2	1.2	0	n/a	n/a	n/a	n/a
	Carbonaceous shale	9	3985	2667	3117	401.5	2575	2083	2204	183.7	2.925	2.207	2.404	0.217	13.54	3.019	8.061	2.721
	Bioturbated mudstone	8	3709	1929	3235	455.1	2556	2148	2353	318.1	2.445	2.035	2.325	0.103	20.07	6.16	10.13	3.966
	Flaser/wavy/ lenticular ss	9	3147	2320	2645	272.4	1887	1515	1739	243.0	2.318	1.975	2.163	0.126	25.93	10.73	17.79	6.206
	Planar bedded ss	5	4236	1836	2699	940.2	2861	1250	1859	618.4	2.220	1.848	2.049	0.141	30.04	18.02	23.48	4.529
	Trough cross-bedded ss	8	2699	2031	2255	474.4	1929	1178	1546	355.3	2.128	1.765	1.982	0.146	33.17	18.97	26.36	5.347
SHORE-FACE	*Trough cross-bedded ss*	1	2150	2150	2150	n/a	1519	1519	1519	n/a	1.931	1.931	1.931	n/a	27.04	27.04	27.04	n/a
	Structureless ss	1	2031	2031	2031	n/a	1399	1399	1399	n/a	1.892	1.892	1.892	n/a	28.66	28.66	28.66	n/a

TYING ROCK PROPERTIES FROM CORE TO SEISMIC REFLECTIVITY IN THE KAIPAROWITS PLATEAU, UT, USA

Abstract

Fluvial-shoreline transitional deposits are becoming increasingly important to understand due to the large number of global hydrocarbon reserves held in such deposits. As the resolution of seismic reflectivity profiles increases, concepts of sequence stratigraphy offer insight into reservoir quality through interpretation of seismic reflection profiles in these transitional successions. The Cretaceous John Henry Member (JHM), located in the Kaiparowits Plateau of southern Utah, reveals numerous exposures of a transition zone which captures fluvial and tidally influenced paralic deposits capped by prograding fluvial deposits, and offers an excellent opportunity to improve our understanding of imaging similar deposits in the subsurface. Previous work along the plateau has been focused on outcrops along the edge, as well as 4 dispersed cores.

Fluvial-shoreline transitional deposits are typically associated with coal; however, coal geobody mapping can be particularly problematic in these depositional environments due to its exiguous nature. Four supplementary density logs from cores in the JHM were utilized to map coal and gain a more accurate understanding of the coal thickness, distribution, and frequency, as well as their impact on the seismic reflectivity responses.

In this study, we link a newly acquired seismic line to laboratory derived rock

properties from a core (~ 500 meters from the line) and outcrop exposures (~ 1500 m from the line). The goal of this study was to use these new data combined with previous studies to provide insight into reservoir quality interpretation from seismic reflection data in fluvial-shoreline transitional deposits, with particular focus on the interpretation and imaging of coal beds within the tidal sequence.

In order to accurately correlate rock properties to seismic, 60 core plugs were extracted representative of the eight lithofacies exhibited in a single core (EP-25). Bench-top measurements were conducted on the core plugs to obtain compressional-wave velocity, shear-wave velocity, density, permeability, and porosity. Three forward reflectivity models were generated and analyzed using these rock properties derived from the core plugs combined with a detailed core description, 1) simple zone-average properties, 2) simple zone-average properties with coal beds, and 3) complex model capturing representative geobody shapes and sizes. These models provide a template for interpretation of a high resolution seismic line (7 km in the north-south direction, 80 Hz frequency source). Interpreting the difference between environments of deposition between the models and seismic profile were clear due to the difference in averaged impedance contrasts. However, individual architectural elements distinguishing reservoir quality when including architectural elements were not clear due to the overlap in rock properties between these zones.

Introduction

As cheap and easy sources of oil have been exploited, new exploration plays increasingly target more complex reservoirs such as those contained in fluvial-shoreline

transitional environments of deposition. Due to the considerable amount of oil reserves held in transitional deposits and the recognition of their inherent complexity, significant effort has been put into the study of analog outcrops for improved subsurface prediction (O'Bryne and Flint, 1993; Weimar and Posamentier, 1993; Ainsworth and Pattinson, 1994; Tetyukhina et al., 2014). The resulting observations have been used to develop predictive models based on lithofacies and architectural elements at a subseismic scale (Martinius et al., 2001; Essam et al., 2013). Advances in seismic acquisition and processing have also yielded higher quality and better resolution seismic data (Thomas and Anderson, 1994; Kendall, 2006; Duarte, 2014). However, even given higher quality data, informed interpretation of reservoir quality from seismic-reflectivity is a function of the seismic rock properties of the reservoir and non-reservoir facies. Insights into the interpretation of these heterolithic depositional environments can be garnered from forward seismic models of 3-dimensional deterministic interpolations derived from core and log observations coupled tightly with nearby outcrop studies.

Early rock property measurements in the laboratory focused on effects of clay content and porosity on compressional-wave velocity (*Vp*) and shear-wave velocity (*Vs*) as a function of pressure and found a decrease in velocity with an increase in porosity and a decrease in pressure and clay content (Han, 1986; Eberhart-Phillips et al., 1989). These types of laboratory-derived empirical relationships can be used as models to aid in reservoir quality predictions from subsurface seismic reflectivity data.

Before acquiring subsurface data, forward model studies of outcrop exposures can lend insight into the anticipated subsurface seismic expression of geobodies. One of the first seismic forward models used large-scale carbonate basin profiles with acoustic

measurements from a single core plug in each depositional environment (Biddle et al., 1992). Seismic forward modeling studies of outcrops have been conducted in deep water channel systems (Campion et al., 2000; Sullivan et al., 2004; Schwab et al., 2007; Falivene et al., 2010; Stright et al., 2014), and large-scale shallow marine nearshore and shallow marine depositional environments (Hodgetts and Howell, 2000; Tetyukhina et al., 2010; Tetyukhina et al., 2014). Many of these studies have relied on rock properties from local wireline log data or laboratory measurements of core plugs from areas of similar depositional environment to populate seismic properties in models. However, few studies have focused on direct rock property measurements applied to small scale (m) architectural element geobody distribution in a coal-rich transition zone to generate forward synthetic seismic models (Christensen and Szymanski, 1991; Marion et al., 1992; Vernik and Nur, 1992; Hodgetts and Howell, 2000; Schwab et al., 2007; Falivene et al., 2010; Tetyukhina et al., 2010; Stright et al., 2014).

The fluvial-shoreline transition zone is particularly problematic to forward model because the seismic rock properties are not only poorly understood, but they are highly variable. In particular coal deposits, which are prolific in these depositional environments, vary significantly in both rank and distribution. Coal characterization is a key indicator of depositional environment, and therefore, a critical component to predicting and interpreting the seismic expression of nearshore successions (Van Riel, 1965; Ruter and Schepers, 1978; Gochioco, 1992, 2000; Morcote et al., 2010).

The focus of this study is in modeling the geobody distribution in a prograding shoreline succession, from shoreface to lagoonal to fluvial depositional environment in the Cretaceous JHM of the Kaiparowits Plateau (Fig. 2.1). Due to the complicated

depositional setting of coal, their geobody distribution are still not well understood. Because the center of the plateau has the thickest coal deposits, it is an ideal setting to gain a more in-depth understanding of coal distribution in a nearshore fluvial-tidal transition zone. Two cores in the center of the plateau, a data-poor region, are leveraged to document the transition from observed outcrop at Left Hand Collet to the highly heterogeneous, coal-rich transition zone. A high resolution seismic reflection survey (7 km), acquired in order to further fill the data gap in the center of the plateau and coupled with 3-dimensional models generated from a few core and laboratory-derived rock properties, is interrogated to better understand reservoir prediction from seismic reflectivity in a highly complex coal-rich depositional setting. The two key questions this research aims to answer are 1) are coal deposits in the fluvial-tidal transition zone mapable geobodies in seismic reflection profiles and 2) what insights into subsurface seismic interpretation can be garnered from a 3-dimensional model of a highly complex depositional system. Three 3-dimensional models are presented varying in complexity, populated by laboratory derived rock properties from core plugs, and compare the results to the field acquired seismic reflection profile.

Geologic Setting

Regional Geology

The Kaiparowits Plateau is located in the southwestern part of the Colorado Plateau province in southern Utah (Fig. 2.1). The Kaiparowits Plateau is an uplifted plateau comprised of upper Cretaceous foreland basin sediments (Peterson, 1969a; Shanley et al., 1992; Hettinger, 1995a). Paleoshorelines were oriented northwest-

southeast (Peterson, 1969a; Shanley and McCabe, 1991; Hettinger, 1995a). Recent detrital zircon analysis reveals sediment transport to the shoreline via an axial channel system sourced from Mongollan Highlands, Sevier fold and thrust belt (STFB), and Cordilleran volcanic arc, as well as sediment transport via longshore drift from the SFTB (Szwarc et al., 2014). Peterson (1969) divided the Straight Cliffs Formation on the plateau into four members: the lower cliff-forming Tibbet Canyon Member, the slope- and ledge-forming Smoky Hollow and JHM, and the upper cliff-forming Drip Tank Member. This study focuses on the Coniacian to Turonian in age (~88 to 83.5 Ma) JHM in the northeastern central plateau where facies preserved are within a fluvial-tidal transition zone (Gallin, 2010) (Fig. 2.2).

Stratigraphy

The northeast-central section of the plateau is comprised of fluvial channels and overbank fines, tidal channels, tidal mudstone, interspersed coal, and shoreface deposits (Shanley et al., 1992; Gallin, 2010; Dooling, 2012). In the southwestern part of the plateau near Kelly Grade, the strata consist primarily of multistory-multilateral, meandering channel belts enclosed in thick intervals of rooted mudstone overbank deposits and limited coal that increase with tidal deposition and depth (Shanley et al., 1992; Gooley, 2010; Pettinga, 2012) (Fig. 2.2). Paleocurrent data show that the rivers generally flowed from the southwest to the northeast (Shanley et al., 1992). The southeastern part of the plateau near Rodger's Canyon exhibits seven shoreface packages interspersed with four major coal zones which tend to thin in the southwesterly direction (Vaninetti, 1979; Hettinger, 1995b; Allen and Johnson, 2010a) (Fig. 2.2). The northern

part of the plateau reflects a compound incised valley that formed through fluvial incision and backfilling by estuarine and tidal deposits (Chentnik, *in press*). The center of the plateau contains the thickest coal deposits in the JHM (Hettinger, 1995b). These thick deposits of coal accumulated on a coastal plain dissected by tidal creeks and estuaries and are in close proximity to the strand plain (Hettinger, 1995a). The clean low-ash nature of the thicker coal deposits indicate that they accumulated in raised mires similar to those described elsewhere in the Straight Cliffs Formation (Shanley et al., 1992).

Outcrop Study

Outcropping deposits at Left Hand Collet (LHC) provides insight into the geobody architecture distribution, thickness, and vertical stacking patterns (Shanley et al., 1992; Dooling, 2012) (Table 2.1). The JHM at LHC is composed of four main depositional environments: wave-dominated and coastal plain deposits of a regressive shoreface, and tide-dominated and lagoonal deposits in a transgressive barrier island setting (Dooling, 2012) (Fig. 2.2). LHC exposes tidal depositional facies of a tidal barrier island system with frequent migratory inlets and multiple shoreface deposits with some tidal ravinement (Dooling, 2012). Geobody geometries observed in outcrop at LHC were coupled with core observations to better map 3-dimensional rock body distributions (Table 2.1).

Core Study

In the 1970s, approximately 23 Utah Power and Light (UP&L) cores were drilled across the northern Kaiparowits Plateau for coal exploration purposes. Six of these cores intersect at least part to all of the JHM. Gallin (2010) logged two of these cores (EP-07

and EP-25) (Fig. 2.1). The cores intersect the JHM, and each is greater than 210 m thick. The cores correlate through a unique shared fossil assemblage and are located in the transition zone between marine and fluvial depositional environments. Eight different lithofacies, defined by grainsize, sedimentary structures, bioturbation, and laminations, were classified and described at 0.5 ft. scale in the core (Gallin, 2010) (Fig. 2.3). Three depositional environments comprised of five architectural elements were identified in the JHM and Drip Tank Member: 1) coastal plain consisting of fluvial channels and overbank fine, 2) tidally influenced deposits consisting of tidal channels and tidal muds, and 3) shoreface deposits consists of shoreface architectural element (Gallin, 2010) (Fig. 2.4).

Coastal Plain: Fluvial Channels

This architectural element consists of lithofacies mud rip-up sandstone, trough cross-bedded sandstone, planar bedded sandstone, and flaser/wavy/lenticular bedded sandstone. The channels are comprised of fine- to coarse-grained sandstone. The channels are represented by fining upward packages. Trace fossils are absent from this element. The channel belts are laterally extensive, and reflect low sinuosity channel belts. The channels vertically amalgamate to form channel belt complexes up to 10 m thick with a vertical increase in channel amalgamation.

Coastal Plain: Overbank Fines

This architectural element consists of the lithofacies bioturbated mudstone. The floodplain mudstone is mud to silt in grainsize and lacks both carbonaceous shale and

coal. They contain some visible laminations and are weakly bioturbated. These beds occur in thin (< 2 m) intervals between fluvial channels. The upper coastal plain of the JHM which includes the fluvial channels and overbank fines constitutes a sheet-like environment between cores EP-25, EP-07 and LHC.

Tidally Influenced Deposits: Tidal Channels

This architectural element consists of lithofacies trough cross-bedded sandstone, planar bedded sandstone, and flaser/wavy/lenticular bedded sandstone. The channels are comprised of very fine- to medium-grained sandstone that often fine upwards. The channels are comprised of finer grained sediment at the base of the depositional environment and coarser grained sediment near the top. The occurrence of the channels also tends to increases upward in the core. Brackish water bivalves and trace fossils indicate tidal conditions are prevalent including *Teredolites, Ophiomorpha, Thalassinoides, Asterosoma, Taenidium, Planolites,* and *Teichichnus.* The channel belts are laterally restricted and highly sinuous. Channel deposition is represented by relatively thick sandstone beds up to 5 m thick and stack to form sheets up to 20 m thick. Scour surfaces up to 9 m thick separate individual channels. The overall trend in this environment exhibits a transition from marine influence with increasing fluvial influence moving up in the core based on the sedimentation and paleontological observations.

Tidally Influenced Deposits: Tidal Mudstone

This architectural element consists of lithofacies bioturbated mudstone, carbonaceous shale, and coal. Grainsizes range from silt to mudstone. The bioturbated

mudstone lithofacies often grades into carbonaceous shale and terrestrial coal. The base of the tidal environment is characterized by more tidal mudstone, while the top of the environment decreases in mudstone frequency. Heavy bioturbation is present with some original sedimentary structures completely obliterated. There is an abundance of tidal environment trace fossils including *Thalassinods* and *Planolites*. These lagoonal and paludal deposits vary in thickness and lateral frequency. The beds range from 5-90 cm and stack to form bedsets between 8-10 m thick. There is a lack of general information about coal body geometries in the Kaiparowits Plateau. This is due to the fact the coal does not exhibit wide sheet-like distribution. The tidal depositional environment, which contains both tidal channels and tidal mudstone in the middle of cores EP-25 and EP-07, pinches out at LHC into multiple shoreface intervals.

Shoreface

This architectural element consists of lithofacies trough cross-bedded sandstone, planar bedded sandstone, and structureless sandstone. The sandstone in this element is fine to coarse grained, well sorted and clean of mud-draping. The sandstone also tends to coarsen upwards. Marine bivalves and hummocky sedimentary structures indicate shoreface succession. The sandstone forms tabular sheets between 5-25 m thick. The shoreface is a single deposit at the bottom of core EP-25 and EP-07 and correlates to the B sandstone in LHC.

Methods

Benchtop Core Plug Measurements

Sixty core plugs were selected from both the JHM and Drip Tank Member of the EP-25 core to statistically represent rock properties for each lithofacies from the three different depositional environments (Fig. 2.4). Due to the friability and absence due to previous sampling of coal, no core plug samples were extracted from this lithofacies. Core plug measurements were conducted for porosity, permeability, density, (*Vp*), and (*Vs*). The core plugs were categorized into a hierarchical framework from lithofacies into architectural elements within the three different depositional environments.

2-Dimensional Correlation Sections

Two 2-dimensional cross-sections were created between cores EP-25 to EP-07, which was based roughly on strike with the paleoshoreline, and from core EP-25 to the outcrop study at LHC, in the approximate dip direction of the shoreline (see Fig. 2.1 for locations). The 2-dimensional depositional cross-sections were used as a foundation for the 3-dimensional model by tying together established data points to create accurate stratigraphic intervals.

3-Dimensional Models

Three different 3-dimensional models were created ranging in detail and complexity from: 1) average rock properties for each environment of deposition, 2) average rock properties for each environment of deposition with explicit representation of coal, and 3) environment of deposition with mapping of geobodies at the architectural

element scale. Correlations from density logs associated with the UP&L boreholes, interpretations from core EP-25, core EP-07, and geometries of geobodies extracted from the LHC outcrop study were used to generate these three interpretive geocellular models.

The area of interest (AOI) for the 3-dimensional models is 16 km x 13 km rotated 40.5° NW (Fig. 2.1). There are seven stratigraphic zones in each model for a total thickness of 250 m. The zones correspond to the EODs in core EP-25 (Fig. 2.4). For model 1, each EOD is represented as a single layer with average rock properties. In model 2, a single layer was used for each EOD with the exception of the dominant tidal deposits in zone 5 whose grid size was 2 m thick. This grid size was selected to capture the average coal bed thickness observed from wireline logs in that section. The UP&L cores and core EP-25 and EP-07 were upscaled to the grid in zone 5 and employed to map the coal geobody distribution by hand contouring. In model 3, the same stratigraphic base as model 1 was used; however, the vertical grid cell sizes were defined differently for zone 2 and zone 5 as a function of the average size of the architectural element in each zone. The interpreted architectural elements in cores EP-25 and EP-07 (Fig. 2.4) were upscaled to the grid and used to guide the interpretation of geobodies away from the well locations. On each grid layer, a deterministic and interpretive model of architectural elements (geobodies) was created constrained by the two cores (Fig. 2.4), architectural element geometries from LHC (Table 2.1), and constrained to interpolated coal layers from model 2. The geobody shapes and sizes were loosely based using modern analog from the Ogeechee River, Georgia, USA (Fig. 2.5).

Coal Distribution and Rock Properties

Coal beds were interpolated using indicator kriging between four UP&L wells with density logs (Fig. 2.1 for locations) based on the low density of coal (< 1.2 g/cm^3) relative to the surrounding rocks. The velocity value employed for coal was 2000 m/s based on laboratory measurements of coal with similar ranking, age, and location (Morcote et al., 2010).

Synthetic Seismic Model

Vp and density were assigned to each model at either the architectural element (geobody) scale or as averages for each depositional environment. In model 1, average *Vp* and density were assigned for coastal plain, tidal, and shoreface depositional environments. Model 2 rock properties are identical to model 1 with the addition of coal *Vp* and density in zone 5. Model 3 employed the same values as model 2 with the exception of zone 2 and zone 5. In the coastal plain zone, there are two values for fluvial channels and overbank fines, and in the tidal zone, there are two values for tidal mudstone and tidal channels. The resulting 3-dimensional *Ip* model was convolved with 80 Hz Ricker wavelet using 1-D convolution. This wavelet was selected to not only capture the most realistic amount of heterogeneity in the section, but is a comparable wavelet that was also used for the seismic acquisition profile.

Seismic Acquisition, Processing, and Interpretation

The seismic profile is approximately 7 km in length, oriented oblique to the shoreline. The profile was shot in between core EP-25 and EP-07. The profile captures up

to 500 m depth incorporating the entirety of the JHM. The high resolution reflection seismic data were acquired using dense wide aperture geometry with 5 m spacing (Bruno, 2009; Bruno et al., 2010) (Fig. 2.6). The acquisition was carried out over 2-dimensional profiles using a geophonic array of 12 geodes, 240 vertical 40 Hz geophones, and a high resolution vibrating source (IVI Minivib). The acquisition used three sweeps of 40-250 Hz for 15 seconds. The CDP fold has a maximum of ~200 traces with an average fold of 120-130. The refractor depth model statics were corrected and smoothed to a final datum of 2130 m above sea level. The profile was interpreted by projecting cores EP-25 and EP-07 and following the reflectors to correlate between the cores at the different environments of depositions.

Results

Rock Properties

Based on the core plug measurements, the resulting range of porosity values from the porosimeter was 3-37%. The ultrasonic acoustic velocimeter measured velocity with resulting *Vp* ranges from 2500-4500 m/s and *Vs* from 1200-2800 m/s. The measured densities ranged from 1.8-3.2 g/cm^3 (Fig. 2.3).

To visualize the relationship between the rock properties in seismic reflectivity profiles and lithofacies, architectural elements and EODs, values of *Vp/Vs* are cross plotted against *Ip* (Fig. 2.7). The lithofacies plot points to a separation between sandier lithofacies and finer grained ones. The lithofacies were divided into architectural elements; the sandstone lithofacies comprise the channels (both fluvial and tidal) and shoreface elements, while the finer grained lithofacies comprise the overbank fines and

tidal mudstone. Although there is significant overlap, the architectural elements plot demonstrates a slight offset between low *Ip* fluvial channels, tidal channels, and shoreface and a slight offset between the high *Ip* overbank fines and tidal mudstone. However, there is a significant contrast between the sandstone elements and the tidal mudstone and overbank fines. The plots are also differentiated by environment of deposition. The tidal environment tends to have higher *Ip* overall as well as higher *Vp/Vs*, whereas shoreface and coastal plain have relatively lower *Ip* and *Vp/Vs*.

The resulting seismic rock properties were used to populate the three forward models (Table 2.2). Model 1 *Ip* from the rock properties in all depositional zones were averaged; coastal plain *Ip* was 3880 Ns/m^3, the tidal 6530 Ns/m^3, and shoreface 4125 Ns/m^3. These values are the represent the differences in properties in the environment of deposition rock plot. In model 2, the same rock properties were employed as model 1 with the addition of the coal which was populated using *Ip* of 2400 Ns/m^3. Model 3 used the rock properties averages in each individual depositional zone with the exception of zone 2 and zone 5. Zone 2 used impedance from overbank fines: 7475 Ns/m^3 and fluvial channels: 5035 Ns/m^3. In zone 5, the impedance values employed were from tidal mudstone: 8100 Ns/m^3 tidal channels: 5000 Ns/m^{3}and coal: 2400 Ns/m^3.

3-Dimensional Model Construction

The 1-dimensional cores utilized the lithofacies, architectural elements, and environments of deposition of both cores EP-07 and EP-25 (Fig. 2.4). The cores were used to build the 3-dimensional models through the 2-dimensional cross-section correlations based on the correlated environments of deposition (Fig. 2.8). The cross-

section between cores EP-25 to EP-07 consists of an upper coastal plain package, a thick dominant tidal environment with a small coastal plain channel in the middle and shoreface at the base of EP-07. EP-25 is approximately 25 m deeper than EP-07 and exhibits a second small tidal package at the base below the shoreface environment. The cross-section between core EP-25 and outcrop at LHC reveals an upper coastal plain package and the transition between tidal and proximal shoreface in the middle JHM. The B sandstone shoreface package at the bottom of core EP-25 correlates to the B sandstone at LHC. The coal cross-section is in the N-S direction along strike with the shoreline. The density logs are known points of coal locations at specific depths in the JHM (Fig. 2.8). Using the low density assumption, the logs reveal the coal vertical frequency and thickness along strike with the coastline. The architectural elements 3-dimensional model was built using LHC geometries, pertinent analogies, sinuosity, and fluvial paleocurrent direction from southern Kaiparowits Plateau (Gallin, 2010) (Fig. 2.9).

3-Dimensional Synthetic Forward Model

The forward models were used to understand and interpret the acquired seismic profile based on information from the rocks property trends, depositional environments, geobody geometries, and fluvial sinuosity based on Fig. 2.4, 2.8, 2.9, and Table 2.1. The 2-dimensional forward models were extracted from the 3-dimensional models at the location in the northeastern section of that plateau between EP-25 and EP-07 oblique to the paleoshoreline at the same location of the acquired seismic profile (Fig. 2.6). The location of the three 3-dimensional models extracted as a 2-dimensional trace is illustrated in Fig. 2.9. The three 2-dimensional models are ordered by increasing detail

(Fig. 2.10). Table 2.3 catalogues the impedance contrast and seismic response of the three different models. Model 1, the basic environment of deposition, shows a positive reflector in high *Ip* coastal plain and shoreface, and a negative reflector in the tidal zone. Model 2, the EOD forward model with coal, has relatively dim reflectors in areas with thin coal beds and more distinct negative reflector in the thicker coal zones. In the depositional environment with coal, the reflectors do not exhibit definitively clear locations and dimensions of the coal bodies. Model 3, the environment of deposition with architectural elements, demonstrates the same reflectors as model 2 with the addition of architectural elements (Fig. 2.11). In zone 2 between the overbank fines and fluvial channels is a large impedance contrast that is characterized as bright flat reflectors. In zone 5, where the channels are thicker and there are fewer tidal mudstone, the reflectors are dimmer and less distinctive. However, at the base of the tidal zone, the channels are thin and there is a high degree of frequency between thick packages of tidal mudstone and coal; the larger impedance contrast is characterized with bright reflectors.

The result of the seismic responses listed in Table 2.3 is employed as a template for interpretation of the acquired seismic profile. The rock properties assist in recognizing the *Ip* contrasts that are expected between the environments of deposition as well as between the architectural elements in the seismic profile. The LHC geometries in Table 2.1 aid in identifying the geobodies that are expected in the profile. The resulting acquired seismic profile depicts several interesting features (Fig. 2.12). The first is that channels can be mapped in the coastal plain and tidal depositional environments. Second is the washed out zone in the middle of the profile. The third feature is the negative reflector on the right-hand side of the profile that trends upward. Lastly, the profile does

not appear to illustrate any particular area where coal bodies can be easily mapped.

Discussion

Rock Properties

The clustering of the rock properties in the plots helps to visualize the relationship from the lithofacies based core plug measurements to the upscaled environments of deposition and architectural elements. The trends in the plots substantiate the usage of average seismic rock property values to populate the 3-dimensional models (Table 2.2). The trends can be further employed to understand the reflection behavior in both the forward models and the acquired seismic profile (Table 2.3). In the lithofacies plot, the distinction between the sandstone elements or between the tidal mudstone and overbank fines is not clear; however, the distinction between the high *Ip* fine grained elements and the low *Ip* sandstone elements is unmistakably discernable and can be linked to the architectural elements plot. The distinction allows for the juxtaposed architectural elements to be distinguished in their respective environments of deposition.

In model 1, the rock properties were averaged over each depositional environment. The averages are effectively the average of each environment as seen in the EOD plot. The averages revealed the highest *Ip* in the tidal environment and the lowest in the coastal plain. This is due to the exceptionally low impedance values exhibited in the coastal plain channels and the relatively low impedance values of the overbank fines (Fig. 2.13). The coastal plain is a strong peak, the tidal a strong trough, and shoreface a weak peak. Model 2 has the same average impedance values in each depositional zone as model 1 with the addition of coals. The coals are relatively weak reflectors in the tidal

zone 5. The implication of the forward models is that they illustrate the key reflections that are distinguishable are between the coastal plain environment and the tidal environment, while the coal reflections are relatively dim.

Model 3 reveals the closest alignment with the architectural element plot and the most accurate portrayal of detailed *Ip*. As depicted in the architectural element plot, the fine grained elements such as the tidal mudstone and overbank fines have significantly higher *Ip* values than the sandier channel elements. In the tidal zone, the coal impedance is fairly close to the tidal channel impedance and thus is not very distinguished. The tidal mudstone is the main impedance contrast to both the tidal channels and coal bodies, producing strong peaks and troughs where they are juxtaposed. The ability to differentiate architectural elements within the depositional environments offers a notably improved ability to interpret seismic profiles in fluvial-shoreline transitional zones.

The role the coal plays in the interpretation is relatively low. The coal is evident when placed in the high *Ip* tidal environment of model 2; however, when the architectural elements are separated out in model 3, the coal become increasingly difficult to distinguish. Table 2.3 aids in possibly differentiating the elements. The tidal mudstone has the highest impedance and the coal is the lowest impedance with tidal channels exhibiting only slightly higher impedance than coal. Therefore, the brightest reflectors are associated with the juxtaposition of the tidal mudstone and coal, slightly less bright reflectors associated with the juxtaposition of the tidal mudstone and tidal channels, while the juxtaposition of the tidal channels and coal would display a very weak reflector if any.

The variability of the impedance value is based on how the core plugs are

averaged, either by EOD, EOD by zone, or by architectural element, highlights to difficulty in interpreting the seismic behavior in transitional deposits. Although the architectural element scale produces the most accurate representation of the three models, the importance of being able to separate out at least individual depositional environments with the *Ip* information is essential to being able to correctly characterize the seismic response in transitional depositional environments.

Seismic Acquisition Challenges

The seismic profile was acquired in a relatively remote location; therefore, some issues occurred that would have been difficult to predict and may have affected the resulting profile. The twelve-day acquisition itself also took place during an unfortunate weather pattern that ranged from hail to constant drizzle for the entirety of the acquisition. Although the direct link between the noise created on the geophones is not clear, there are likely some repercussions from the noise in the resulting profile. There were also multiple cattle guards and a sharp bend in the road in the middle of the profile that resulted in the minivib skipping large stretches of road in between sweeps. In terms of the processing, the water table depth was also unknown and therefore could not be taken into consideration. However, it is likely that this also may have affected the resulting profile. Although problematic, the profile does lend itself to some interpretations using the three forward models.

Seismic Profile

The acquired seismic profile captured several noteworthy features (Fig. 2.12). Firstly, there are several mapable channels in both the coastal plain and tidal depositional environments. The main geometries observed in outcrop that can be seen in the profile are the channel complexes based on the size of complexes from LHC (Table 2.2). The individual channels and the individual overbank fine beds as seen at LHC are not discernable due to the thickness that the seismic resolution captures.

Secondly, the coal geometries are also difficult to distinguish. Possible explanations are because the beds are too thin to be captured by the resolution or the discontinuous nature of the coal geobodies. Although the profile has a washed out zone in the tidal environment that may be associated with coal deposits, it is not obvious if that is the case. A few possible causes of the washed out zone are geophysical illumination from the processing or a geological attribute, such as a thick homogenous package of high *Ip* tidal mudstone which points to a long period of lagoonal setting or low *Ip* packages such as tidal channels juxtaposed with coal.

Thirdly, there is a distinguishable trough reflector on the right-hand side of the profile that trends at a depth of 300 m and 5200 m upward. On the right-side of this particular reflector, the profile is again washed out. Some possible explanations for this reflector are the transition to the shoreface deposit or it could be related to the incised valleys that are observed in the northern part of the plateau. Fourthly, the profile highlights some small structural features that are not evident from outcrop. Although the structural features are relatively small, they could have a significant impact on processing and interpretation of the seismic profile in the highly heterogeneous tidal transition zone.

Comparison of the Forward Model and the Seismic Acquisition Profile

Comparing the forward model results to the seismic acquisition survey illuminates some interesting similarities and highlights the difficulty in creating an accurate model in a highly heterogeneous depositional environment (Fig. 2.13). Model 1 illustrates that the overall *Ip* contrast between the different depositional environments is the same between the forward model and acquired profile. The impedance difference is largest between the tidal and coastal plain environments. The reflector between these two environments is brighter than between the shoreface and tidal which has less impedance contrast. Similar reflector intensities are also seen in the acquired profile. Model 2 illustrates that the low *Ip* coal is illuminated in the relatively high *Ip* tidal zone 5 which is not clearly similar to the acquired profile. However, the weak trough reflector character of the shoreface is similar to the shoreface reflector in the acquired profile.

Model 3 with architectural elements is the most realistic comparison to the acquired seismic data. The forward model displays the reflections of channels in both the tidal and fluvial zones due to the low *Ip* contrast against the high *Ip* contrast of the tidal mudstone which is also visible in the acquired seismic profile. In the coastal plain depositional zone 2, the acquired profile has flat bright reflectors that likely indicate differentiation between the high *Ip* overbank fines and the low *Ip* fluvial channels which are evident in the models and acquired profile. In both the forward models and the acquired profile, the coal geobodies are not very distinguishable. Because the coal and tidal channels have relatively similar low impedance elements, it is the juxtaposition of the tidal mudstone that may predict the coal and/or channels. One striking difference between the models and the acquired profile is the negative reflector on the right-hand

side of the acquired profile, and a similar shape peak reflector on the forward model that indicated the *Ip* contrast between the tidal and the shoreface environments.

The most notable difference between the acquired profile and the forward model is that the forward model does not capture the same amount of detail. Although heterogeneity is captured in both the acquired profile and the forward models of the tidal zone, the models do not appear to be straightforward interpretation of the acquired profile. There are two possible causes for the dissimilarities between the models and the acquired seismic profile: model error and data error.

The difficulty in tying the seismic to field data in the transitional zone is inextricably linked to the fact that this depositional environment is highly heterogeneous and the field data which are being applied to the interpretation are from data points that are far from the acquired seismic profile. The closest information, both seismic rock properties and geological, is derived from core EP-25 which is 500 m from the profile and the outcrop data being used at LHC is approximately 10 km away. This study highlights the complexity of interpreting fluvial-shoreline transitional deposits. The use of multiple cores and outcrop studies (a robust dataset by industry standards) still does a poor job of capturing the amount of detail that is necessary in order to fully model the complex transition zone. As for the possible errors in data, the culmination of misfortunes including acquisition taking place during poor weather, winding roads with cliffs, lack of information about the water table all could have contributed to a flawed data profile.

Implications for Interpretation of Reservoir in a Tidal Transition Zone

Table 2.3 can be used as a guideline on how to interpret environments of deposition and architectural elements in seismic profiles. Between environments of deposition, the strongest reflection is between the high impedance tidal and low impedance coastal plain environments, while the weakest is between the tidal and shoreface. When the environments of deposition are segmented into individual depositional zones, the brightest reflector is still between the coastal plain environments and the tidal environments. The reflector between the tidal and shoreface remains a dim reflector in comparison. The addition of ancillary architectural elements to the depositional models illustrates the distinctive reflector characteristics in the tidal and coastal plain environments. In the coastal plain environment, the impedance contrast between the overbank fines and the fluvial channels produces bright flat reflectors. In the tidal environment, the high *Ip* tidal mudstone juxtaposed against the exceptionally low *Ip* produces bright discontinuous reflectors, while the impedance contrast between tidal mudstone and tidal channels is slightly lower and thus generates slightly dimmer reflectors. Although it is not captured in the models, the gradational changes and sharp contacts of the coal of the facies association in the tidal environment (Chapter 1) are likely distinguishing features that would be present in seismic profiles. The shoreface reflector continues to be a moderately bright peak, however not as strong as the architectural elements in the coastal plain and tidal environments.

Although the *Ip* and the seismic expression derived from the core plugs and models provides a template for future interpretation in transitional depositional environments, there is risk of misinterpretation. The risk of misinterpretation significantly

depends on the wavelet used; the risk increases with lower frequency. In model 1 and 2, the reflectors are clear-cut between the environments: strong contrasts between coastal plain and tidal, lower contrast between tidal and shoreface. Model 3 illustrates the complexity of differentiating environments when the architectural elements are incorporated at a smaller scale. The characteristics that separate the elements' reflection characteristics inside the tidal environment and coastal plain are particularly subtle. Parameters that would be useful to know in transitional deposits include bed geometries and bed thickness. Bed geometries would provide an accurate differentiator between the coal, tidal mudstone, and overbank fine architectural elements in the tidal and coastal plain environment. By knowing whether beds are laterally discontinuous or widespread, the ability to distinguish the reflectors in conjunction with bed thickness would be a more straightforward task. Bed thickness combined with bed geometries would also provide the means to understand the differences between tidal and fluvial channels in the depositional environments.

Conclusion

In summary, the rock properties identified differentiation not only between depositional environments, but can be divided even further into the channel and mudstone architectural elements. When the rock properties populated the three models that derived information from core and outcrop studies, a few key features were discerned. The first is that the coal does not have as great of an impact as thin ephemeral beds. Although, overall, there is a significant amount of coal, the fact that they do not appear as thick continuous sheets makes them difficult to distinguish in both the forward

model and the acquired seismic profile. The forward models are useful tools and can accurately predict reflection between depositional environments; however, they do a poor job of distinguishing architectural element geobodies in the seismic profile. Even with the utilization of multiple cores and outcrop studies, the forward model was unable to capture the amount of detail that is necessary in order to fully model the complex transition zone. The architectural element forward model does, however, aid in interpreting the reflection characteristics of juxtaposed elements within the depositional environments. The tidal mudstone is the main impedance contrast to both the tidal channels and coal bodies, producing strong peaks and troughs where they are juxtaposed, and bright reflectors in the coastal plain indicating juxtaposition of overbank fines and fluvial channels.

Forward seismic reflection modeling coupled with direct rock property measurements and predictive facies model framework derived from the core and outcrops leads to invaluable insights for interpreting subsurface data. Integrating core and outcrop data improves multiscale synthesis of heterogeneous deposits, and contributes to a better understanding of how to interpret and map architectural element geobodies in paludal nearshore environments. Rock property analysis is essential for optimizing the value of seismic reservoir characterization results to enable advanced quantitative interpretation. The ability to relate specific rock properties such as *Ip* in precise depositional environments to seismic responses using a calibrated model is invaluable for enhancing the understanding of the hydrocarbon reservoirs.

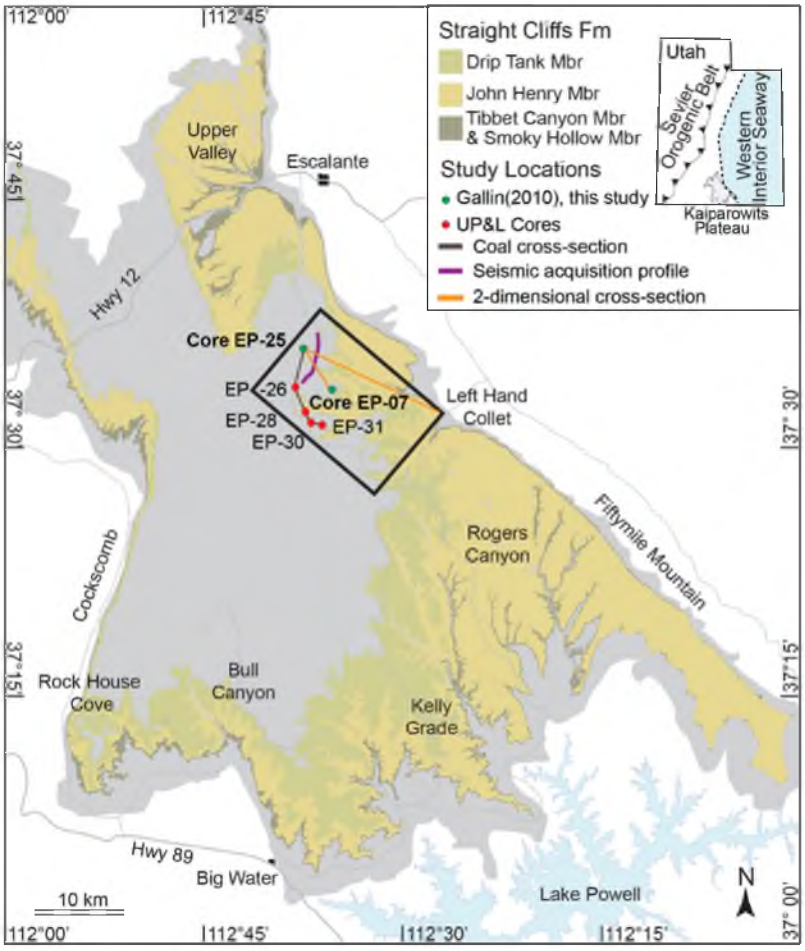

Figure 2.1. Map of Kaiparowits Plateau including study area (modified from Hettinger 1995). The red dots indicate the location of known cores in the northeastern section of the plateau. The green dots represent locations of previously studied core by Gallin (2010). The closest outcrop study to this core is Left Hand Collet (Dooling, 2012). The purple line illustrates the location of the acquired seismic line. For coal cross-section see Figure 2.8; for acquired seismic profile see Figure 2.12.

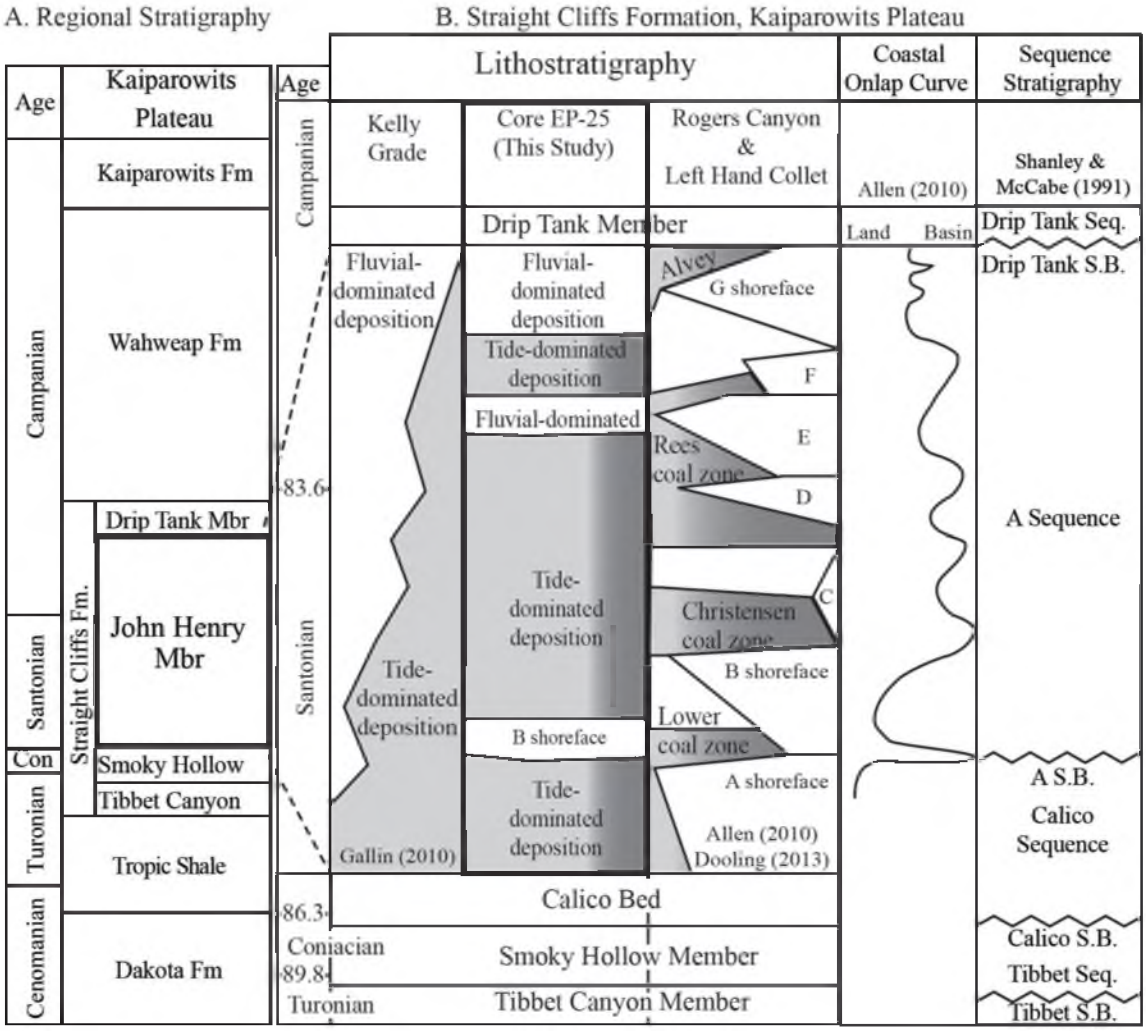

Fig. 2.2 Regional stratigraphy and stratigraphic column of study area (A) Stratigraphic column of the Coniacian to Santonian age deposits throughout the Kaiparowits plateau, and (B) Lithostratigraphy of the John Henry Member for selected locations along the plateau, including the study area. Kelly Grade to Left Hand Collet to EP-25 represents the south to north deposits of the John Henry Member. Seven marine sandstone packages were named "A-G" by Peterson (1969a). The packages pinch out landward into coal zones and coastal plain facies. Core EP-25 intersects the Ree's and Christensen coal zones through the B sandstone. The coastal onlap curve is derived from the Rogers Canyon study on the southwestern part of the plateau (Allen and Johnson, 2011).

	Lithofacies	Description	Number of samples	Interpretation	Core plugs
A	Carbonaceous shale	Dark gray to black colored shale, often laminated but sometimes structureless; abundant organic material; often grades in and out of coal facies	8	Low energy paludal and lagoonal deposits	
B	Bioturbated mudstone	Horizontally laminated mud or mud with no apparent laminations, heavy bioturbation	11	Low energy lagoonal and fluvial overbank muds	
C	Flaser/wavy/lenticular bedded sandstone	Alternating laminations of sandstone and mudstone; sand grain size ranges from very fine to medium sandstone	12	Bi-directional flow associated with tidal deposits	
D	Planar bedded sandstone	Laminations dip at < 5°; grain size ranges from fine to medium sandstone	3	High flow regime, proximal shoreface, tidal and fluvial channels	
E	Trough cross-bedded sandstone	Trough and planar foresets dip between 5-40°; grain size ranges from fine to coarse sandstone	11	Unidirectional flow associated with fluvial and tidal channels	
F	Structureless sandstone	Sedimentary structures are apparent; grain size ranges from very fine to coarse sandstone	7	Rapid deposition from high energy suspension in proximal shoreface deposits	
G	Mud rip-up clast sandstone	Angular to subangular mud rip-up clasts in a sandstone matrix; matrix grain size ranges from very fine to coarse sandstone	4	High energy fluvial channel lag deposits	
H	Coal	Black with dull vitreous reflectance and lacking distinct laminations; coal beds are < 1 m thick	0	Low energy paludal and lagoonal deposits	

Figure 2.3. Lithofacies with core plug photographs and locations. Lithofacies observed in core EP-25 with a representative core plug photograph. The number of core plug samples from each lithofacies is a statistical representation of the proportion of that lithofacies present in the core.

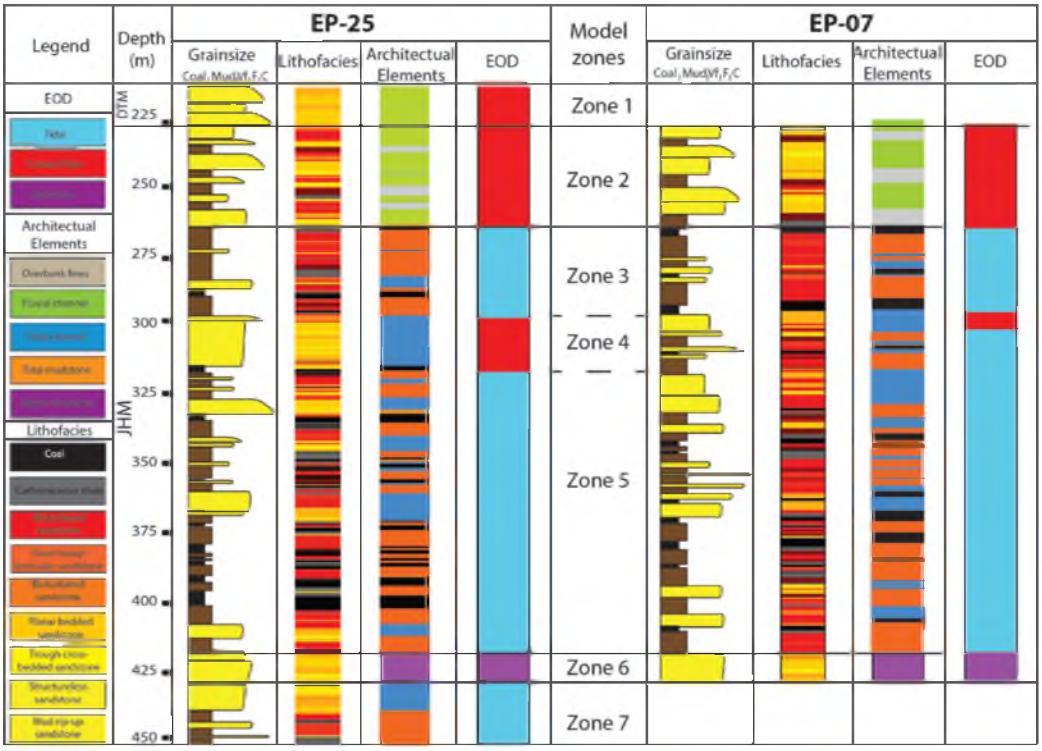

Figure 2.4. Core EP-25 and EP-07 depositional environment, architectural element, and lithofacies logs. Gallin (2010) logged cores EP-25 and EP-07 producing a grainsize log, identifying the three different environments of deposition the architectural elements within each depositional environment and lithofacies. See Fig. 2.1 for location of cores.

Figure 2.5. Modern analogs for building the architectural element 3-dimensional model. Modern analog aerial photo of the Ogeechee River, Georgia. Google maps images (www.google.com/maps).

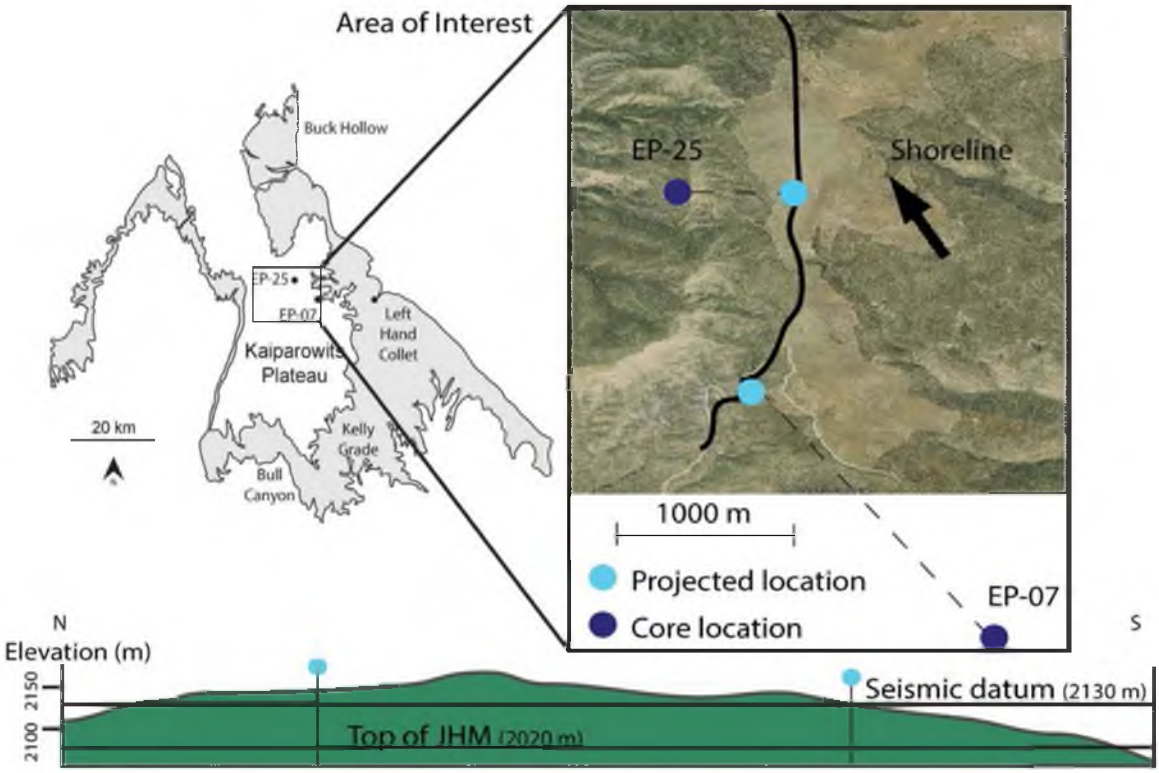

Figure 2.6. Seismic acquisition profile and core locations. The Kaiparowits Plateau highlights the location of seismic acquisition survey. The google image shows original location of cores EP-25 and EP-07 as well as the projection onto the seismic reflection survey. The lower image shows an elevation profile of the seismic survey from north to south as well as the John Henry member elevation and the elevation that the seismic datum was corrected.

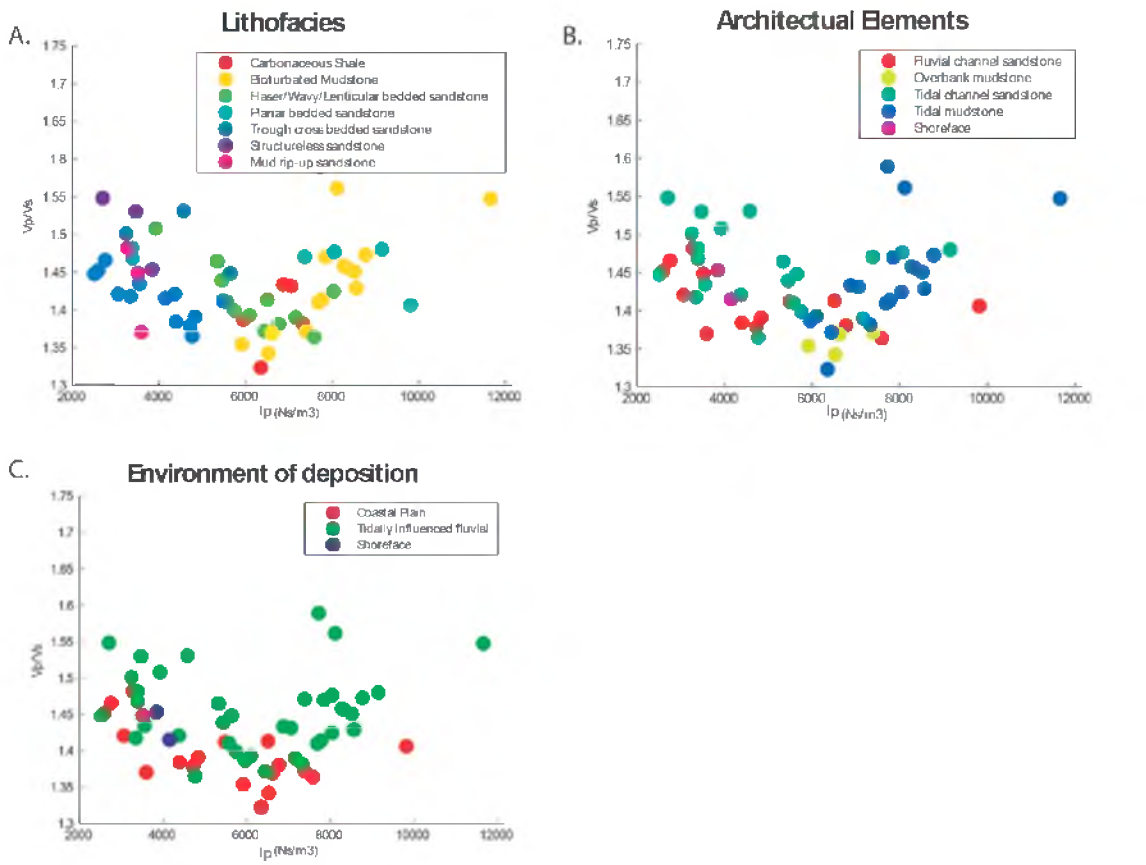

Figure 2.7. Rock plots of depositional environments, architectural elements, and lithofacies. Vp/Vs versus Ip cross plots showing the relationship between measured rock properties and core plug attributes: A) lithofacies, B) architectural elements, C) EOD's.

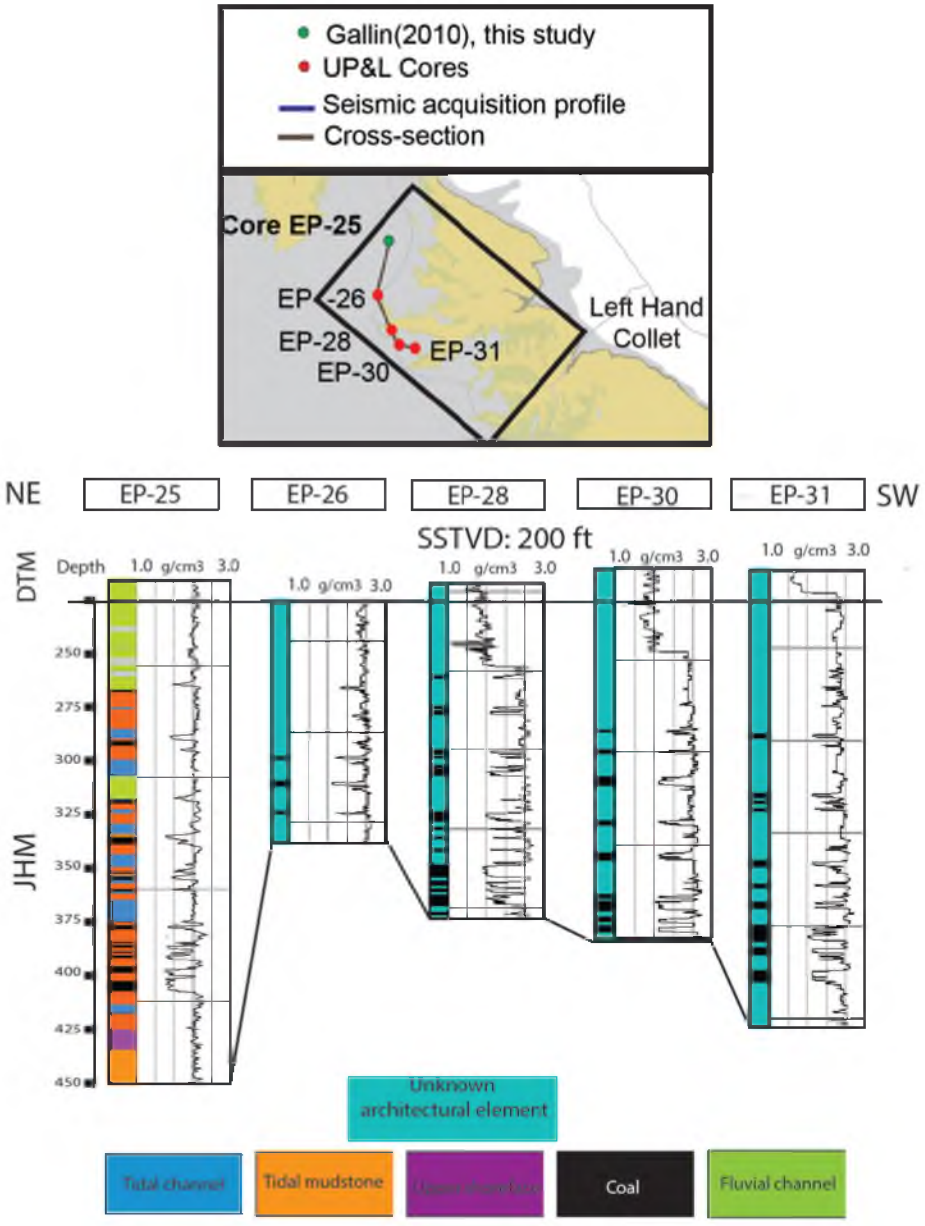

Figure 2.8. 2-dimensional cross-sections between EP-25, EP-07, and Left Hand Collet. In the 3-dimensional model grid, four supplementary density logs from cores were utilized to understand coal distribution. The coal here was located using the assumption that coal has a lower density that the surrounding rocks. The density logs were used as hard data in the 3-dimensional models and assisted in mapping out coal geobodies distribution.

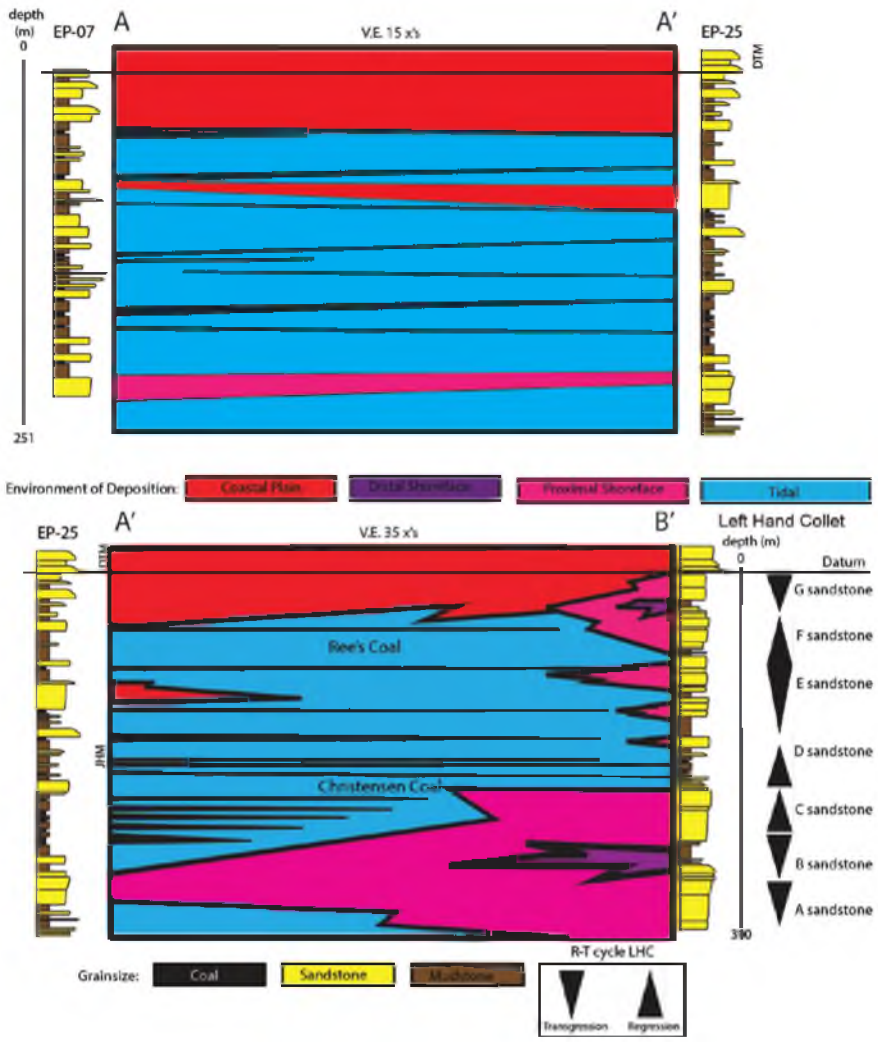

Figure 2.9. Coal geobody cross-section. Correlation of depositional environment between EP-25 and EP-07 (NE to SW; section A-A' on insert map). This cross-section is roughly parallel to the paleoshoreline. The correlation from core EP-25 to Left Hand Collet, indicated on the map from A'-B'. Left Hand Collet information is derived from Dooling (2012). Two main coal zones are identified; Ree's coal zone in the Upper John Henry Member and the Christensen coal zone which is located in the Lower John Henry Member.

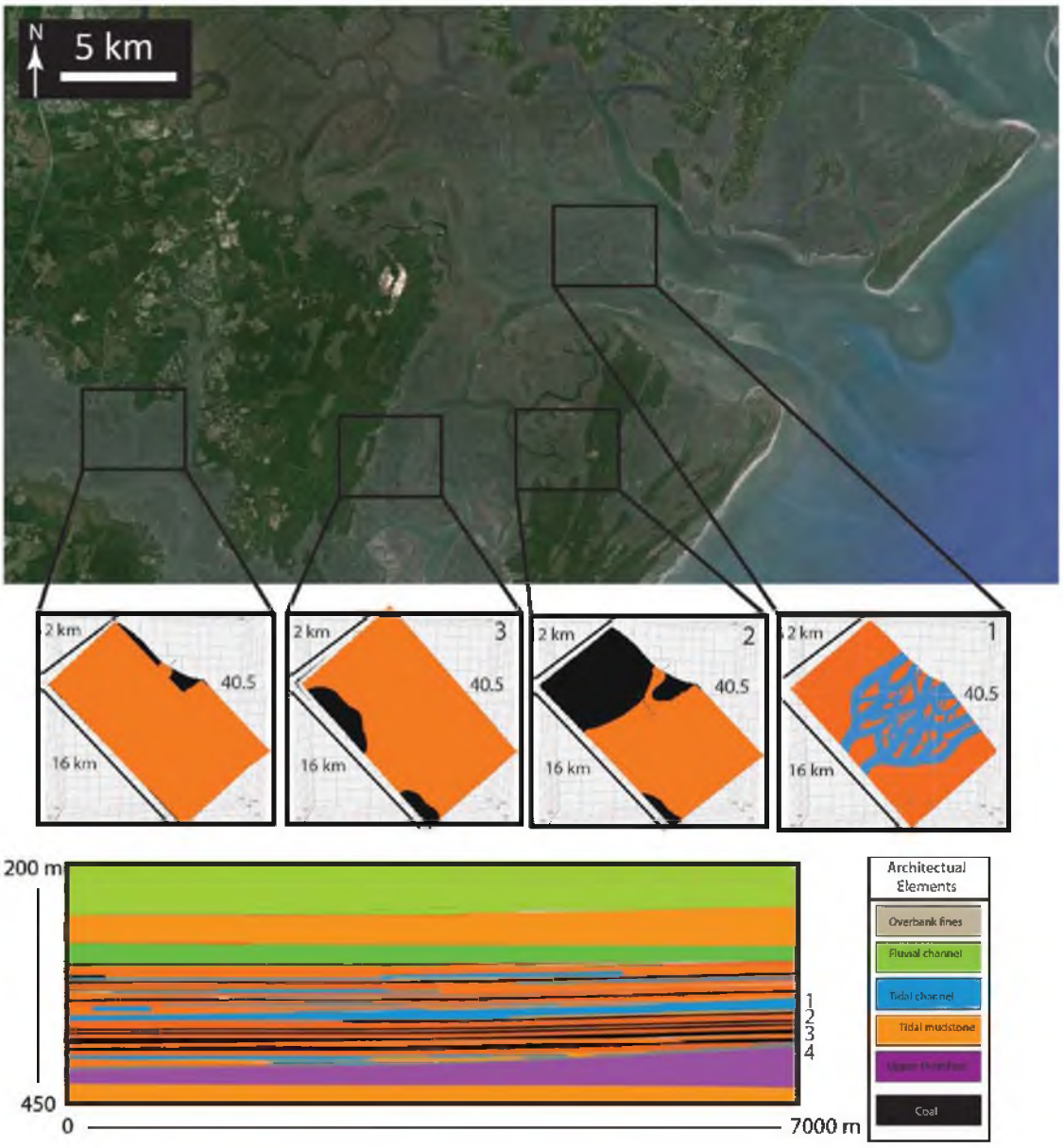

Figure 2.10. Three 3-dimensional models. Analogs from Google maps images were employed to model the geobody distribution of architectural elements in the tidal depositional environment. Each vertical grid the elements were hand contoured using UP&L well logs, core EP-25, EP-07, and LHC geometries

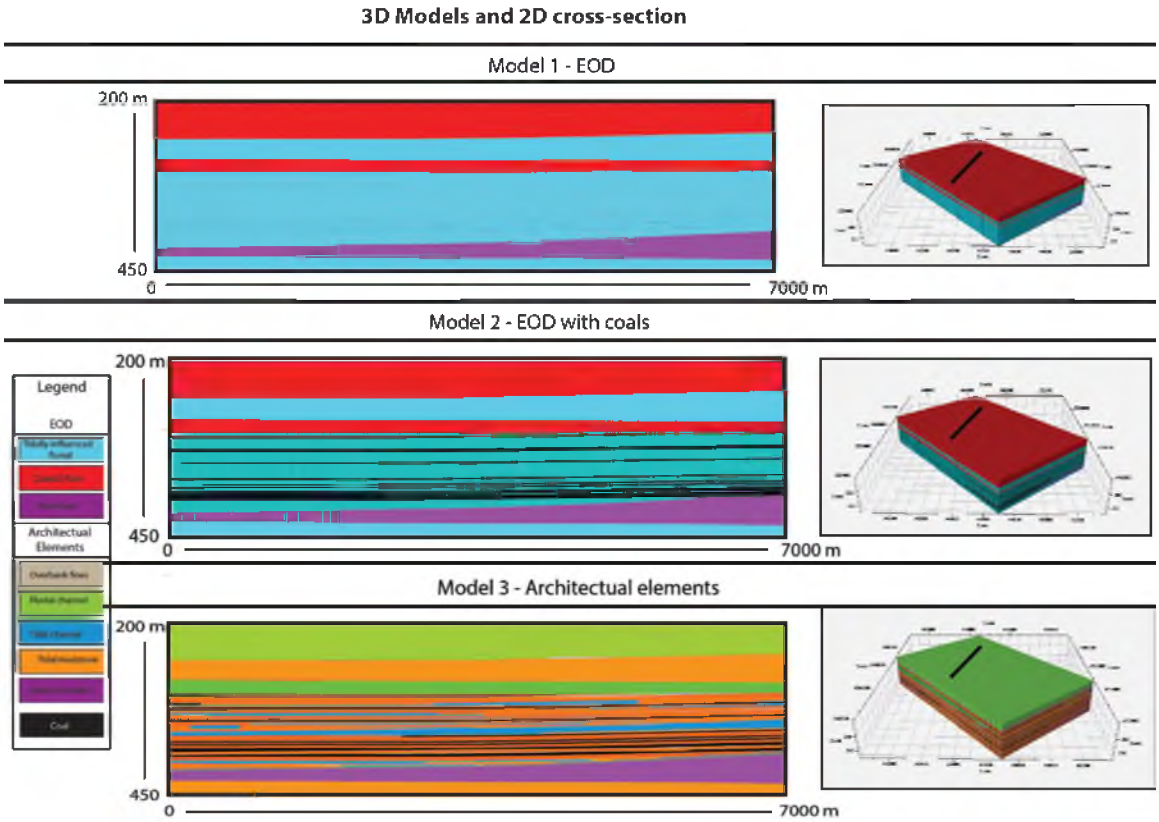

Figure 2.11. Architectural element 3-dimensional model modern analogs. The three 3-dimensional models: model 1-depositional environments, model 2-depositional environments with coal bodies, and model 3-architectural elements. For model 3, each vertical grid slice used the geobody geometry information from LHC and input with the average rock properties from each architectural element in the specific depositional environment zone

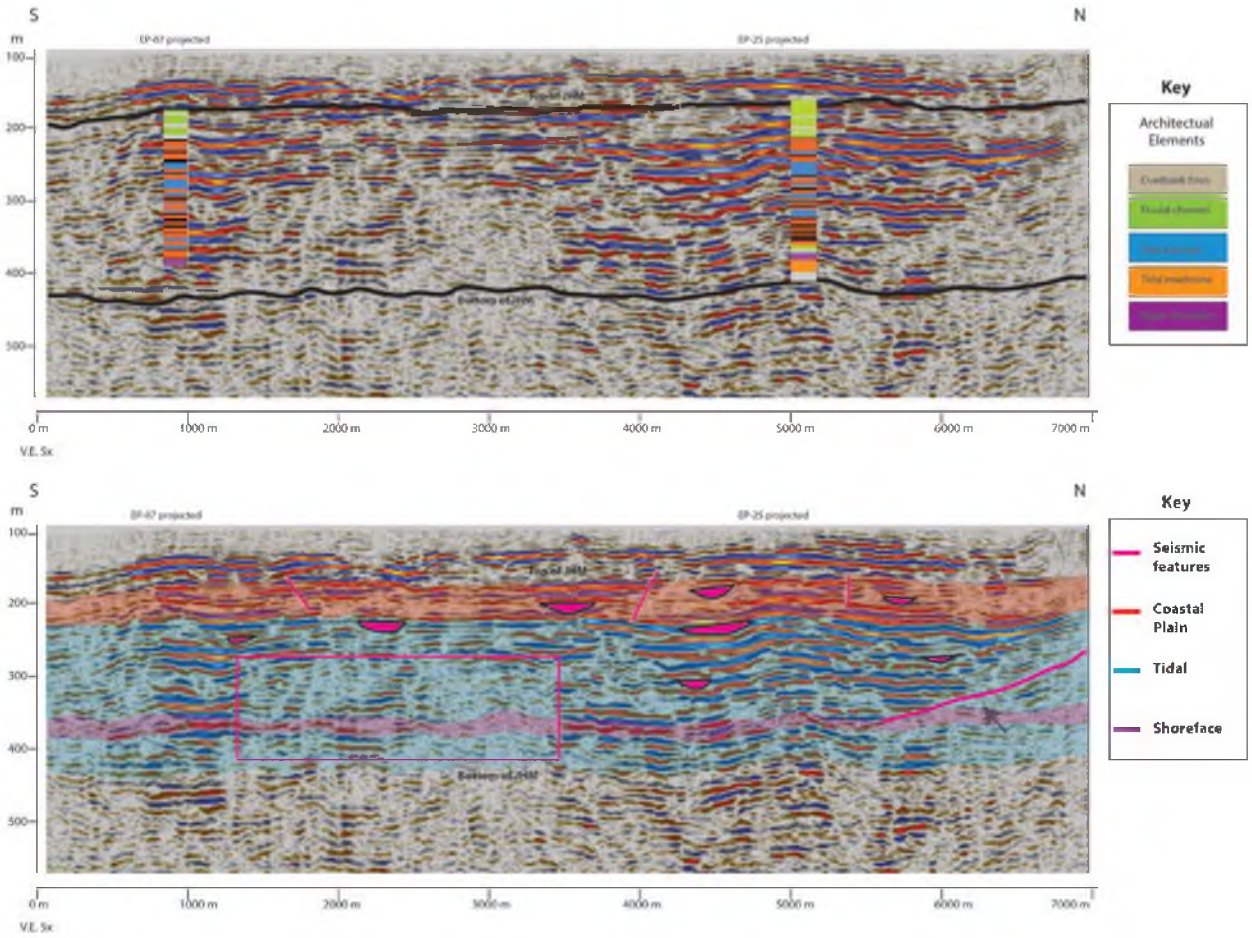

Figure 2.12. Seismic profile and interpreted depositional environments and seismic features. The upper profile is the seismic acquisition profile with the projected architectural element logs from cores EP-25 and EP-07. The black lines indicate the upper and lower portion of the JHM. The lower seismic profile is the interpreted environments of deposition as well as notable seismic features.

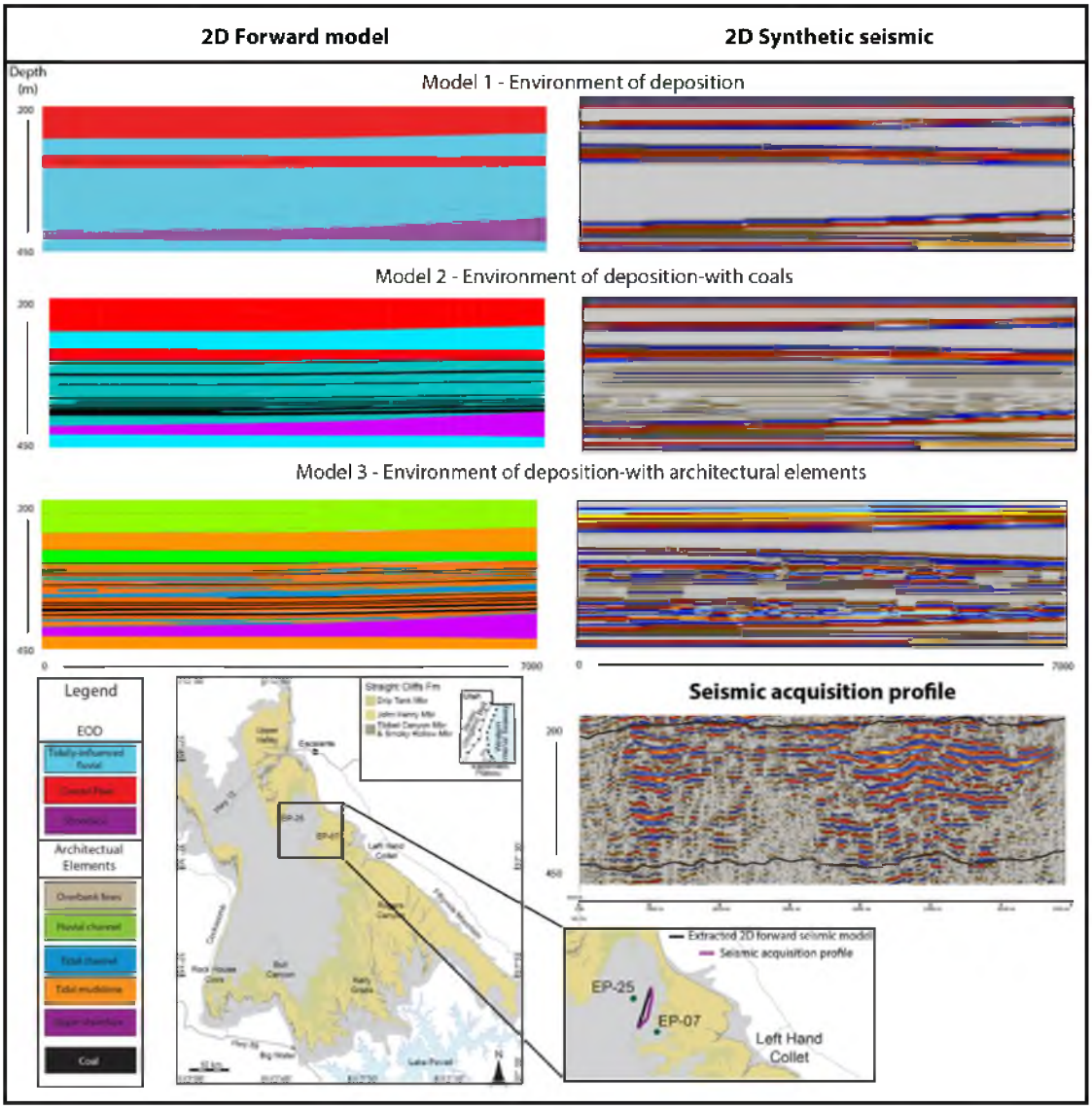

Figure 2.13. Three 2-dimensional seismic forward models at seismic acquisition profile. The 2-dimensional models ranging from model 1 –EOD, model 2 EOD with coal, and model 3- architectural elements and the extracted 2-dimensional slice from each model. The 2-dimensional slice was extracted at the closest location the acquired seismic line.

Table 2.1

Geometries from Left Hand Collet

Depositional environment	**Geometries observed from outcrop**
Coastal plain	Individual channels: 0.5 to 3 m thick Channel complexes: 10 m thick
Tide-dominated fluvial	Individual channels: 1-5 m Channel complexes: 20 m thick Non-channelized sands: 10-16 m thick
Shoreface	Sheet-like sandstone 5-25 m thick

Table 2.2

Acoustic impedance of EOD and architectural elements

Depositional environment	Vertical grid size	Average zone thickness	Architectural elements	Acoustic impedance (Ns/m3)		
				Model 3	Model 2	Model 1
Drip Tank Member	1	10 m	Fluvial channel	8700	8700	3880
JHM - coastal plain 1	1	20 m	Fluvial channel	3130	4675	3880
			Overbank fines	6525		
JHM - tidally influenced 1	1	40 m	Tidal mudstone	7480	7480	6530
JHM - coastal plain 2	1	10 m	Fluvial channel	3090	3090	3880
JHM - tidally influenced 2	50	2 m	Tidal channel	5000	6500	6530
			Tidal mudstone	8100		
			Coal	2400	2400	
JHM - shoreface	1	20 m	Shoreface	4125	4125	4125
JHM - tidally influenced 3	1	20 m	Tidal mudstone	5625	5625	6530

Table 2.3

Impedance contrast and seismic expression of EOD and architectural elements

	Model 1-EOD		Impedance contrast	Seismic expression
	Upper	*Lower*		
	Background	Coastal plain	Lowest	Strong peak
	Coastal plain	Tidally-influenced	Highest	Strong trough
	Tidally-influenced	Shoreface	Medium	peak
	Model 2- EOD with coal		**Impedance contrast**	**Seismic expression**
	Upper	*Lower*		
Zone 5	Coal	Tidal EOD	High	Trough
	Model 3-Architectural elements		**Impedance contrast**	**Seismic expression**
	Upper	*Lower*		
Zone 2	Zone 1	Fluvial channel	Low	Weak peak
	Overbank fines	Fluvial channel	High	Strong peak
	Fluvial channel	Zone 3	High	Strong trough
Zone 5	Zone 4	Tidal mudstone	High	Strong trough
	Zone 4	Tidal channel	Low	Weak trough
	Coal	Tidal mudstone	Highest	Strongest trough
	Coal	Tidal channel	Lowest	Weak trough
	Tidal mudstone	Tidal channel	Medium	Strong peak
	Tidal channel	Zone 6	Low	Weakest peak
	Tidal mudstone	Zone 6	High	Strong peak

FUTURE WORK

This project served as a more in-depth understanding of the transition tidal zone in the Kaiparowits Plateau. In particular, the project produced the first direct measurements of rock properties in the Kaiparowits. Now that the measurements have been taken, the seismic acquisition survey completed, and the 3-dimensional model created, many more opportunities are available to explore with this dataset. Although research opportunities are endless, there are three key areas in which the dataset can be extended for more in-depth research.

The first area involves the rock properties dataset. Although the rock properties have been thoroughly studied in this paper, there are still some explanations that may rely on contributions from mineralogy and clay content. A detailed microscopic study on the mineralogical composition and clay type and content would be an exciting addition to the laboratory measurements in order to more accurately understand the rock plots and seismic reflection in the tidal transition zones.

The second area in which the study could benefit from further research is logging the cores surrounding core EP-25. This would provide a better handle on the 3-dimensional forward model as well as the seismic profile which is directly overlain by core EP-08. Because the tidal transition zone which is the location of this study is highly heterolithic, multiple core logged in a small vicinity would provide invaluable information about the tidal maximum, tidal deposition, paludal sedimentation in an

estuarine environment, and coal geobody distribution. Information from additional logged UP&L cores could be fed into the 3-dimensional model creating a more realistic depositional model that can be used for forward seismic modeling and flow simulations.

Lastly, the third area which this study could be extended is with the AVO modeling. In this study, the AVO modeling does not take into account any types of fluids present in the pore spaces. A more realistic, and industry-related method to make the AVO work more pertinent is to do fluid substitutions using oil, gas, and water.

APPENDIX A

CORE EP-25

This appendix shows the logged core EP-25 and the location and photograph of the core plugs extracted. The information next to the core plugs includes the grainsize, lithofacies, porosity, *Vp, Vs,* and density.

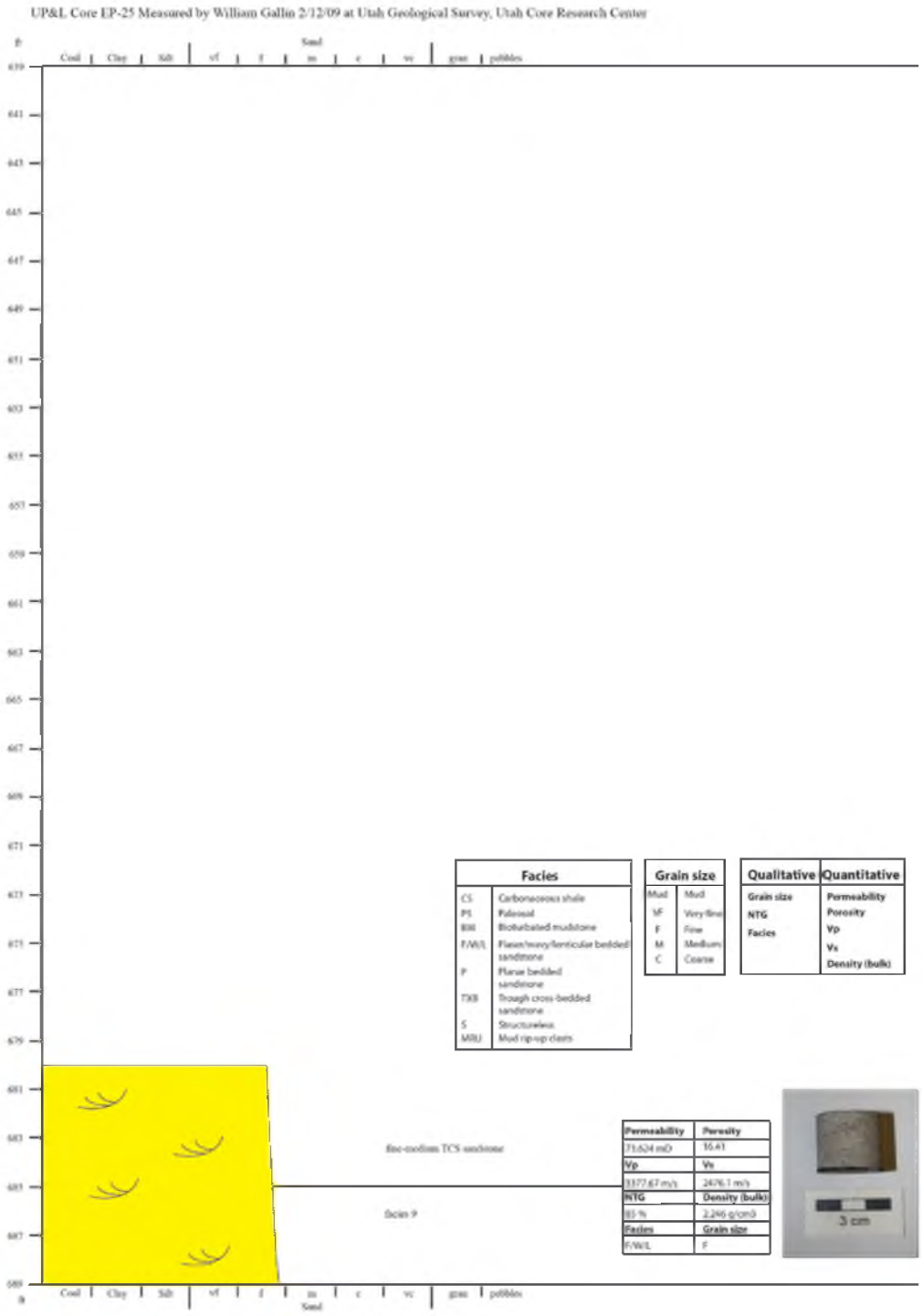
UP&L Core EP-25 Measured by William Gallio 2/12/09 at Utah Geological Survey, Utah Core Research Center
Cond
Clay
Silt
Sand
vf
f
m
c
vc
gran
pebbles
Facies
CS Carbonaceous shale
PS Paleosol
BIOI Bioturbated mudstone
F/W/L Flaser/wavy/lenticular bedded sandstone
P Planar bedded sandstone
TXB Trough cross-bedded sandstone
S Structureless
MRU Mud rip-up clasts
Grain size
Mud Mud
VF Very fine
F Fine
M Medium
C Coarse
Qualitative
Grain size
NTG
Facies
Quantitative
Permeability
Porosity
Vp
Vs
Density (bulk)
fine-coolinm TCS sandstone
facies 9
Permeability
Porosity
71.624 mD
16.41
Vp
Vs
3177.67 m/s
2476.1 m/s
NTG
Density (bulk)
85 %
2.246 g/cm3
Facies
Grain size
F/W/L
F
3 cm

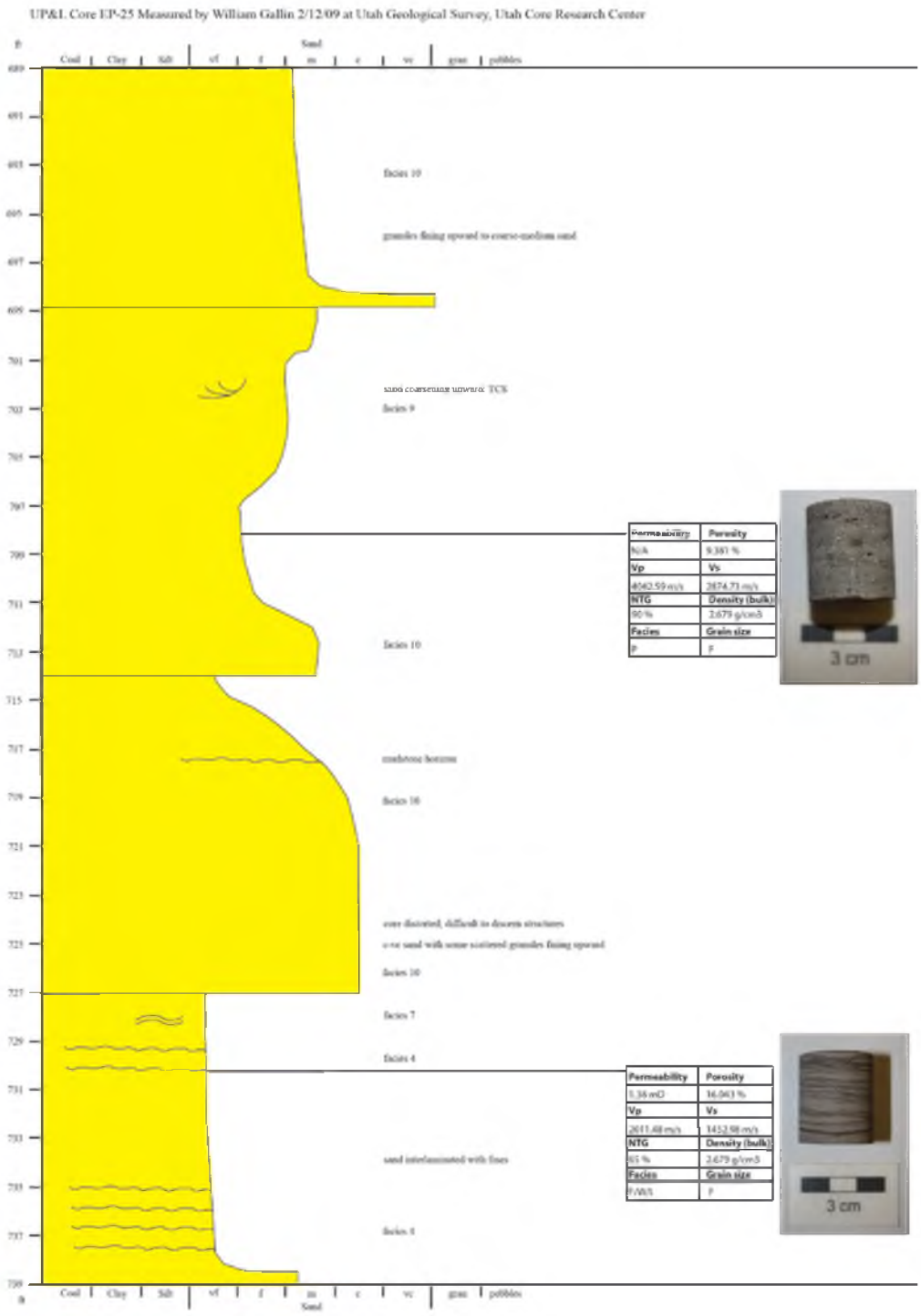
UP&L Core EP-25 Measured by William Gallin 2/12/09 at Utah Geological Survey, Utah Core Research Center
Coal
Clay
Silt
vf
f
m
c
vc
gran
pebbles
Sand
facies 10
granules fining upward to coarse-medium sand
facies 9
facies 10
sandstone horizon
facies 10
facies 10
facies 7
facies 4
sand interlaminated with fines
facies 4
Permeability
Porosity
N/A
9.381 %
Vp
Vs
4042.59 m/s
2674.71 m/s
NTG
Density (bulk)
90 %
2.679 g/cm3
Facies
Grain size
P
F
3 cm
Permeability
Porosity
0.38 mD
16.063 %
Vp
Vs
2011.48 m/s
1452.98 m/s
NTG
Density (bulk)
95 %
2.679 g/cm3
Facies
Grain size
P/M/S
F
3 cm

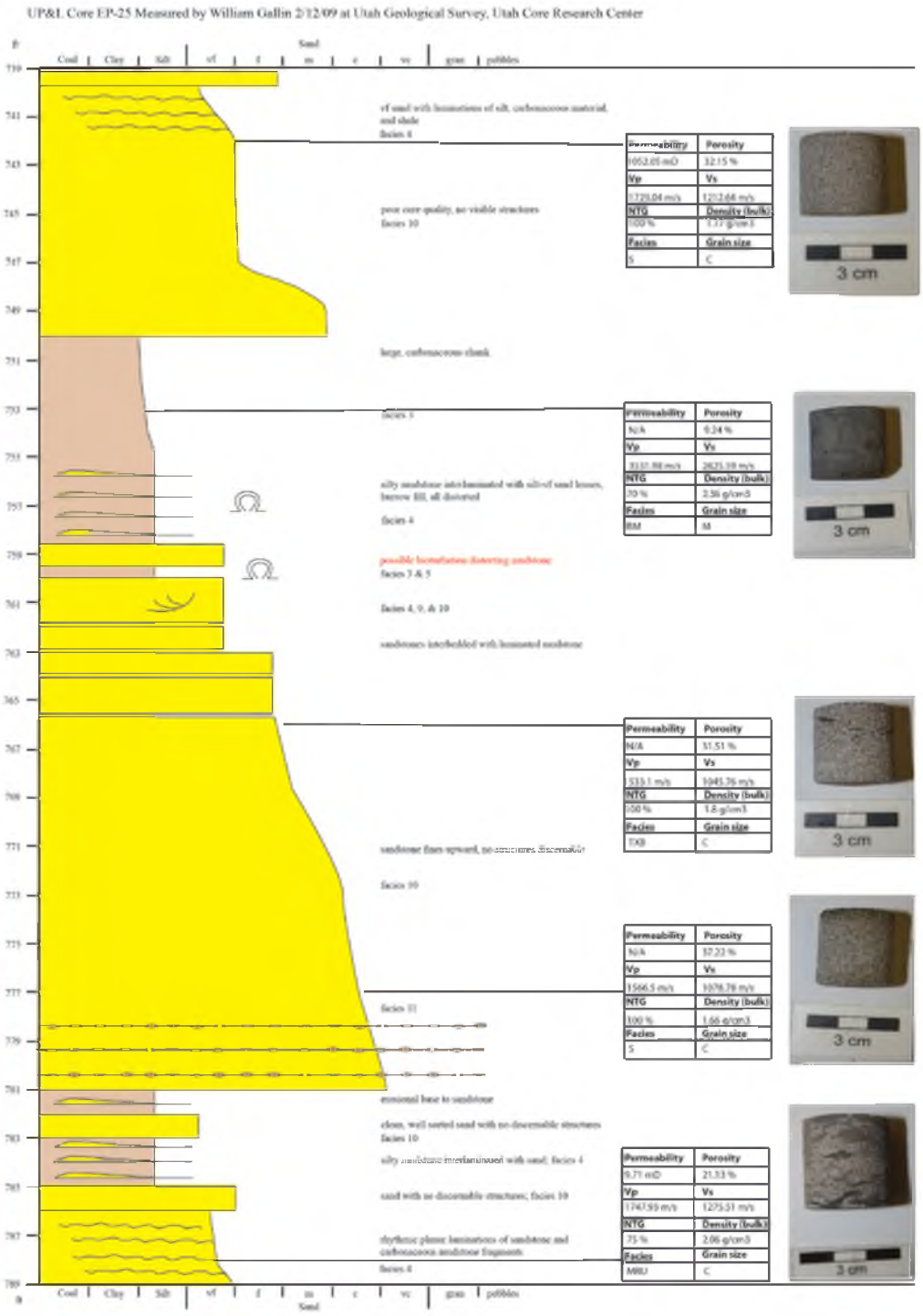
UP&L Core EP-25 Measured by William Gallin 2/12/09 at Utah Geological Survey, Utah Core Research Center
ft
Coal
Clay
Silt
Sand
vf
f
m
c
vc
gran
pebbles
739
741
743
745
747
749
751
753
755
759
761
763
765
767
769
771
773
775
777
779
781
783
785
787
789
vf sand with laminations of silt, carbonaceous material, and shale
facies 6
poor core quality, no visible structures
facies 10
large, carbonaceous clasts
facies 3
silty sandstone interlaminated with silt/vf sand lenses, burrow fill, all distorted
facies 4
possible lenticularious fluvial sandstone
facies 3 & 5
facies 4, 9, & 10
sandstones interbedded with laminated sandstone
sandstone fines upward, no structures discernable
facies 10
facies 11
erosional base to sandstone
clean, well sorted sand with no discernable structures
facies 10
silty sandstone interlaminated with sand; facies 4
sand with no discernable structures; facies 10
rhythmic planar laminations of sandstone and carbonaceous sandstone fragments
facies 6
Permeability
Porosity
Vp
Vs
NTG
Density (bulk)
Facies
Grain size
3 cm

UP&L Core EP-25 Measured by William Gallin 2/12/09 at Utah Geological Survey, Utah Core Research Center

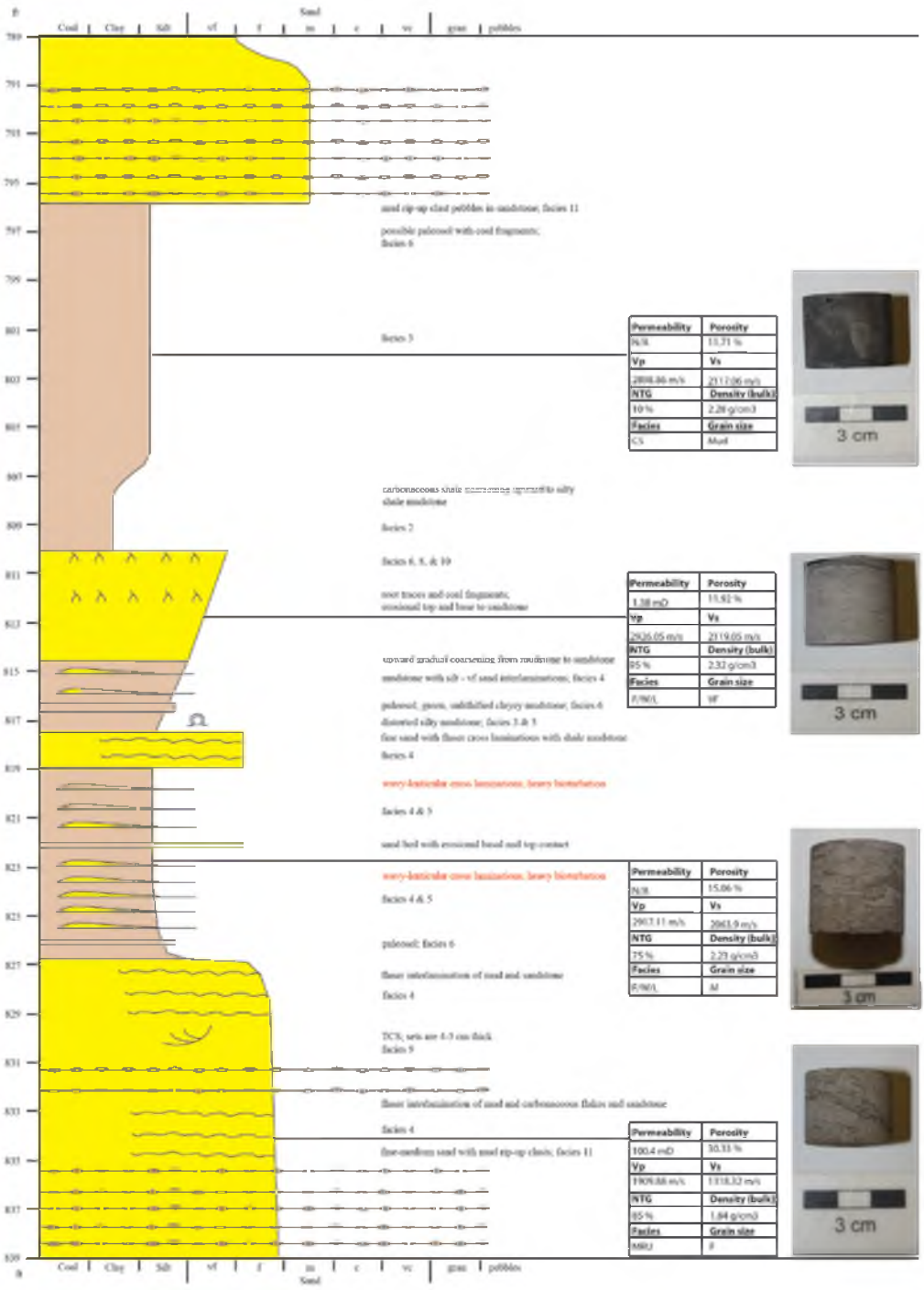

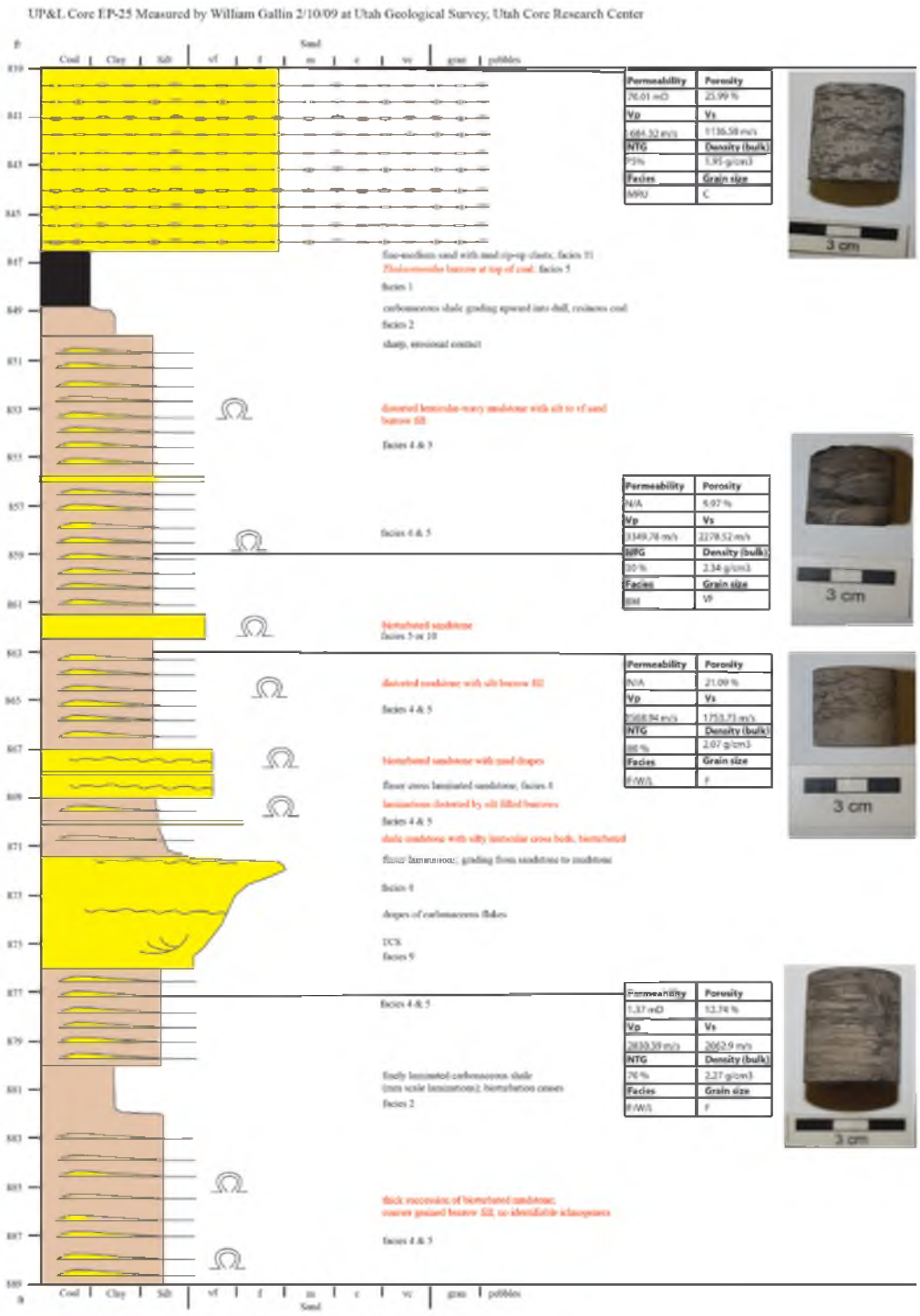
UP&L Core EP-25 Measured by William Gallin 2/10/09 at Utah Geological Survey, Utah Core Research Center
Coal
Clay
Silt
Sand
vf
f
m
c
vc
gran
pebbles
Permeability
Porosity
Vp
Vs
NTG
Density (bulk)
Facies
Grain size
3 cm
fine-medium sand with mud rip-up clasts, facies 11
Thalassinoides burrow at top of coal, facies 5
facies 1
carbonaceous shale grading upward into shale, resistors coal
facies 2
sharp, erosional contact
distorted lenticular-wavy sandstone with silt to vf sand
burrow fill
facies 4 & 3
facies 4 & 5
bioturbated sandstone
facies 3 or 10
distorted sandstone with silt burrow fill
facies 4 & 5
bioturbated sandstone with mud drapes
flaser cross laminated sandstone, facies 4
laminations distorted by silt filled burrows
facies 4 & 5
shale sandstone with silty lenticular cross beds, bioturbated
flaser laminations; grading from sandstone to mudstone
facies 4
drapes of carbonaceous flakes
TCK
facies 9
facies 4 & 5
finely laminated carbonaceous shale
(mm scale laminations); bioturbation ceases
facies 2
thick succession of bioturbated sandstone;
convex grained burrow fill; no identifiable ichnogenera
facies 4 & 5

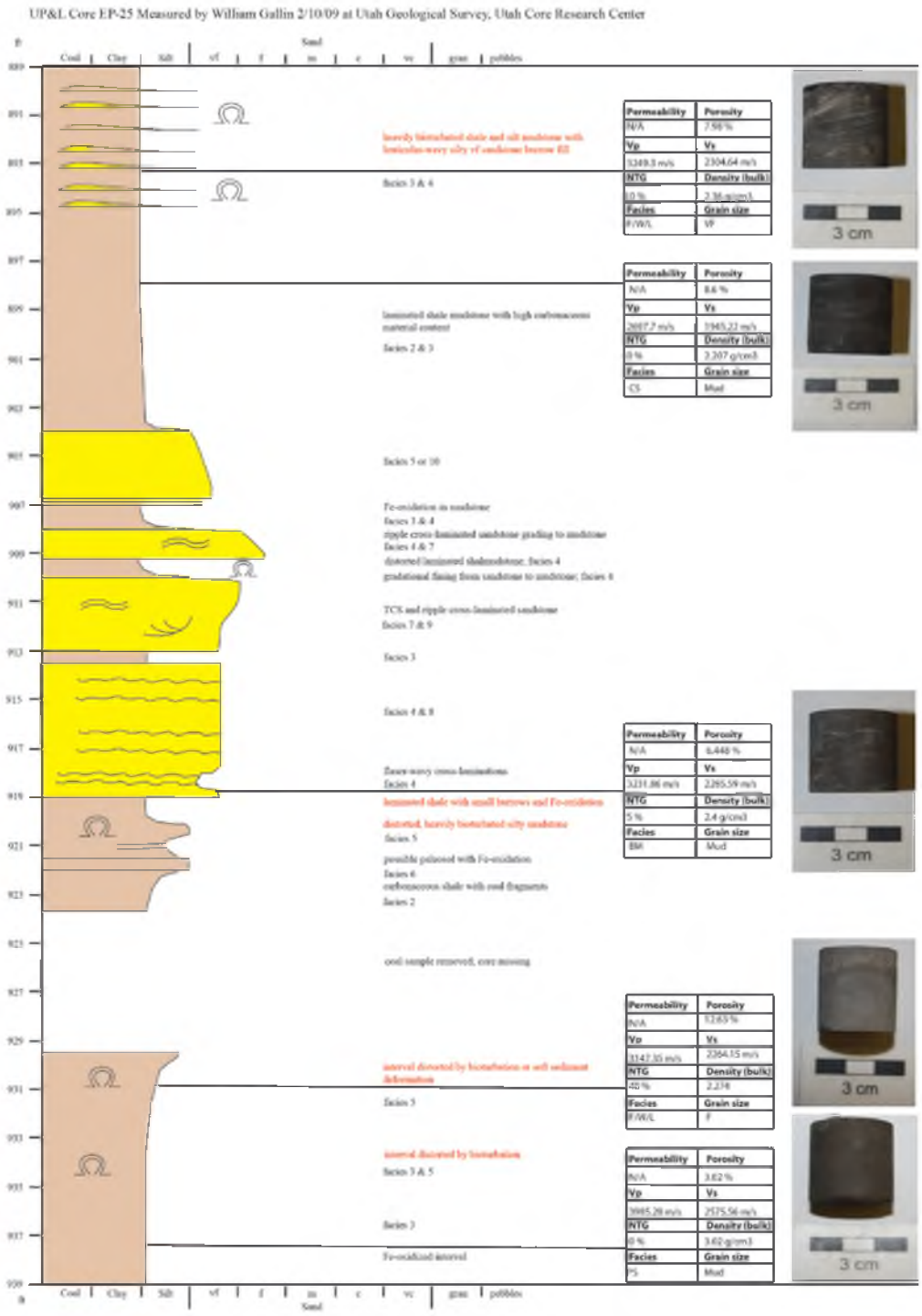
UP&L Core EP-25 Measured by William Gallin 2/10/09 at Utah Geological Survey, Utah Core Research Center
Coal
Clay
Silt
Sand
vf
f
m
c
vc
gran
pebbles
Permeability
Porosity
Vp
Vs
NTG
Density (bulk)
Facies
Grain size
3 cm

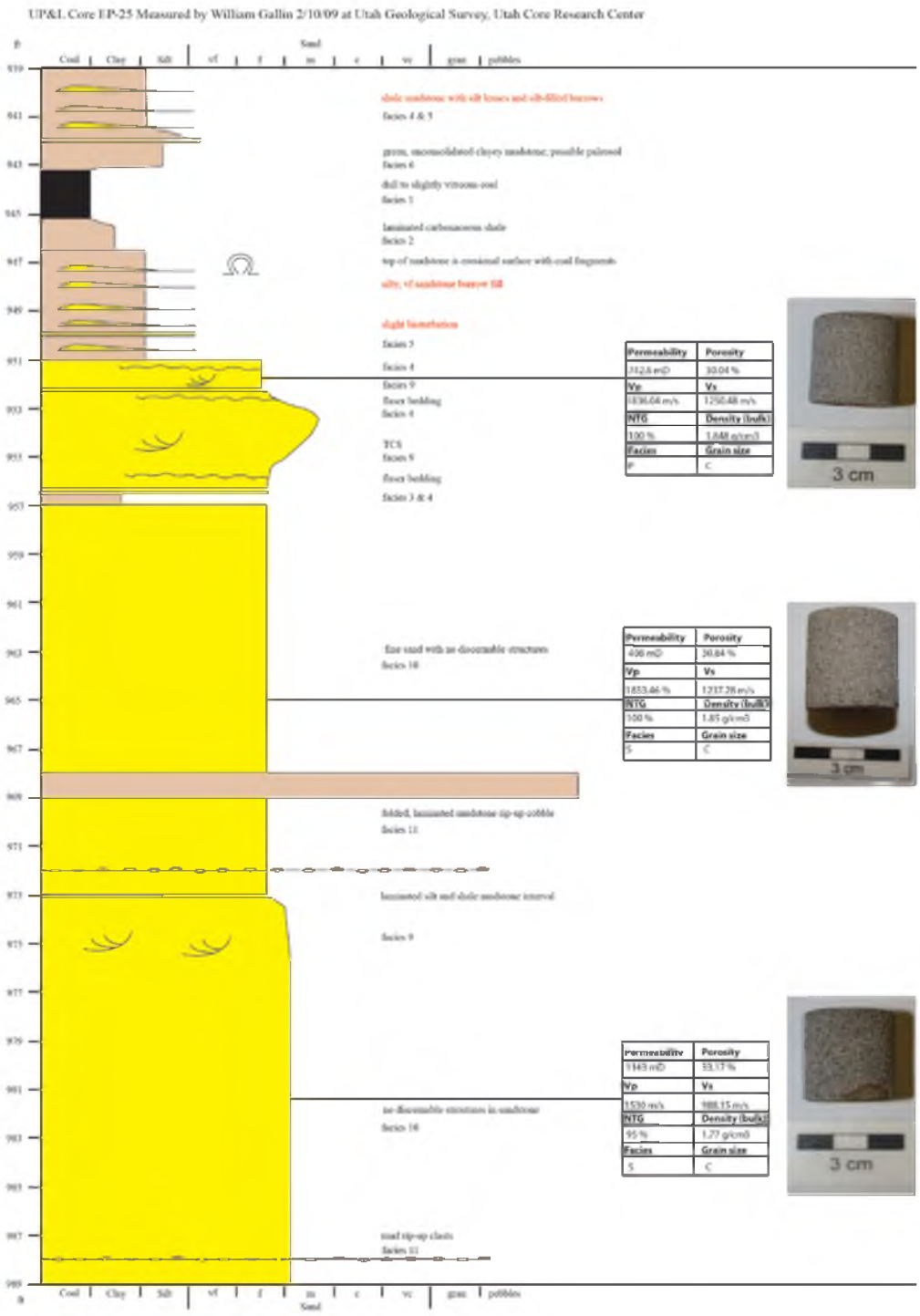
UP&L Core EP-25 Measured by William Gallin 2/10/09 at Utah Geological Survey, Utah Core Research Center
Coal
Clay
Silt
Sand
vf
f
m
c
vc
gran
pebbles
Permeability
Porosity
Vp
Vs
NTG
Density (bulk)
Facies
Grain size
3 cm

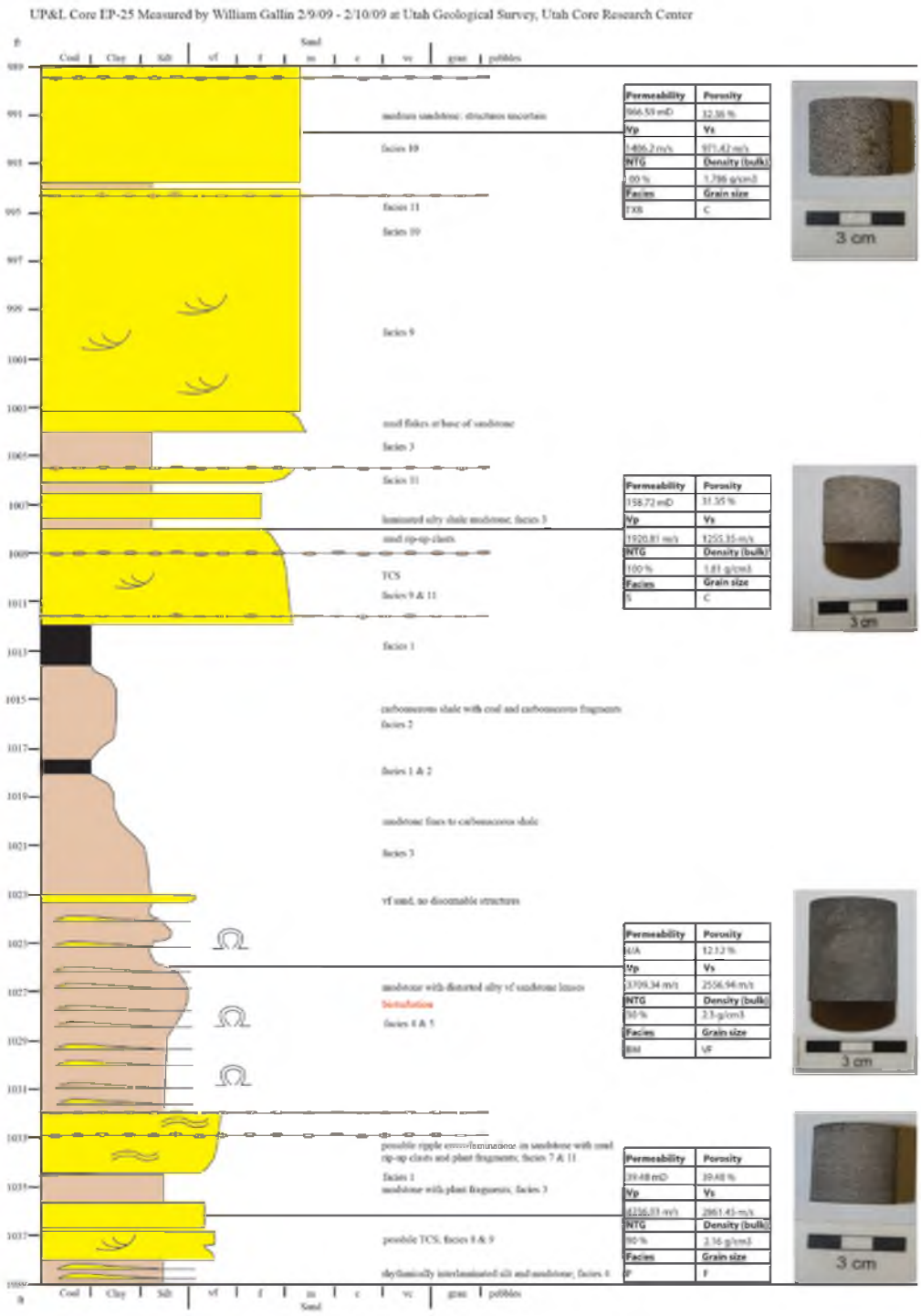
UP&L Core EP-25 Measured by William Gallin 2/9/09 - 2/10/09 at Utah Geological Survey, Utah Core Research Center
Coal
Clay
Silt
vf
f
m
c
vc
gran
pebbles
Sand
Permeability
Porosity
Vp
Vs
NTG
Density (bulk)
Facies
Grain size
3 cm

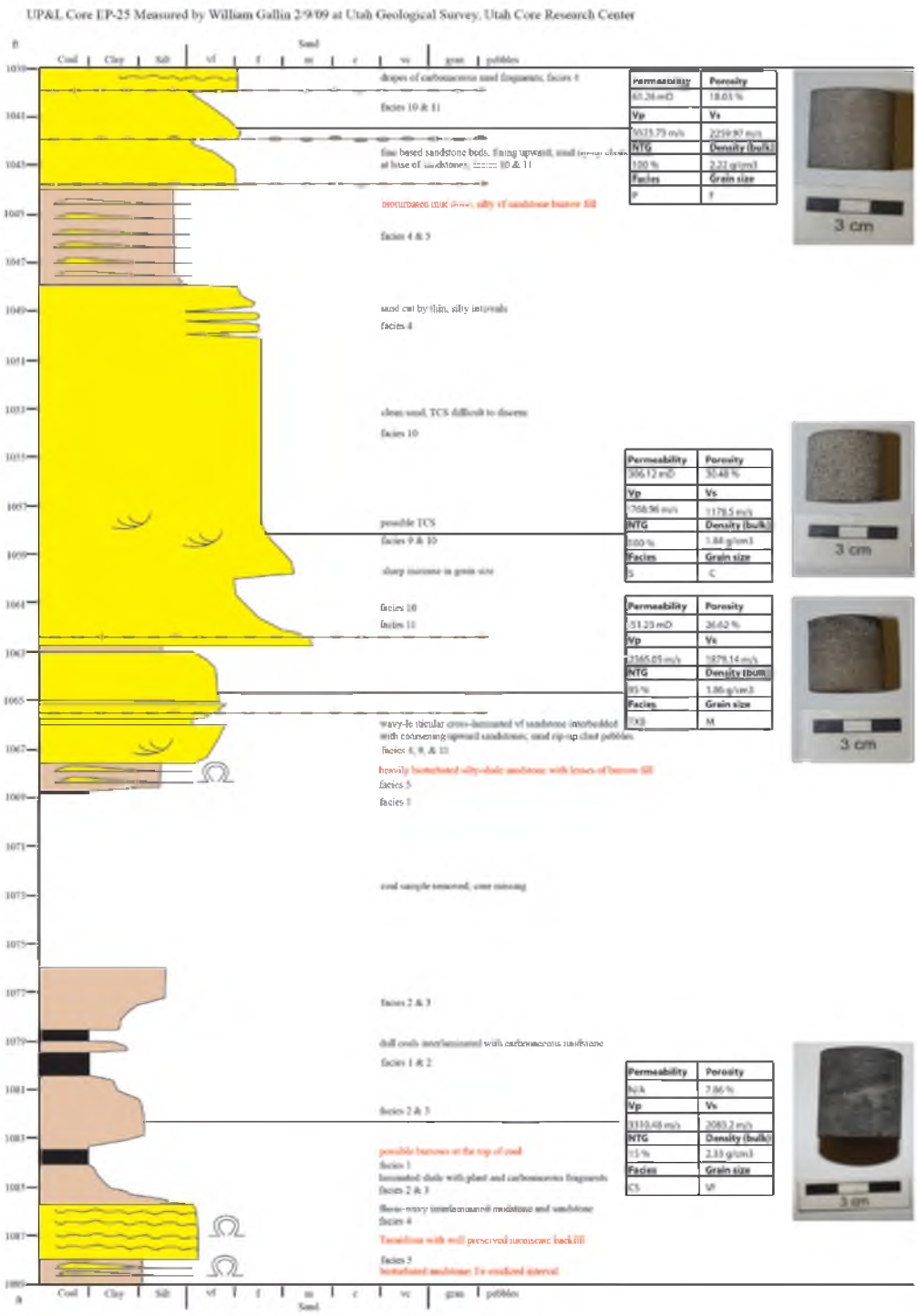
UP&L Core EP-25 Measured by William Gallin 2/9/09 at Utah Geological Survey, Utah Core Research Center
Coal
Clay
Silt
Sand
vf
f
m
c
vc
gran
pebbles
drapes of carbonaceous sand fragments; facies 4
facies 10 & 11
fine based sandstone beds, fining upward, sand layer clasts at base of sandstones; facies 10 & 11
facies 4 & 5
sand cut by thin, silty intervals
facies 4
clean sand, TCS difficult to discern
facies 10
possible TCS
facies 9 & 10
sharp increase in grain size
facies 10
facies 11
wavy-lenticular cross-laminated vf sandstone interbedded with coarsening-upward sandstones; sand rip-up clast pebbles
facies 8, 9, & 10
heavily bioturbated silty-shale sandstone with traces of burrow fill
facies 5
facies 1
coal sample removed, core missing
facies 2 & 3
dull coals interlaminated with carbonaceous mudstone
facies 1 & 2
facies 2 & 3
possible burrows at the top of coal
facies 1
laminated shale with plant and carbonaceous fragments
facies 2 & 3
flaser-wavy interlaminated mudstone and sandstone
facies 4
Teredolites with well preserved suicidesare backfill
facies 5
bioturbated mudstone; Fe-oxidized interval
Permeability
Porosity
61.26 mD
18.03 %
Vp
Vs
3033.79 m/s
2259.97 m/s
NTG
Density (bulk)
100 %
2.22 g/cm3
Facies
Grain size
F
F
3 cm
Permeability
Porosity
306.12 mD
30.48 %
Vp
Vs
1768.96 m/s
1178.5 m/s
NTG
Density (bulk)
100 %
1.84 g/cm3
Facies
Grain size
S
C
3 cm
Permeability
Porosity
51.23 mD
26.62 %
Vp
Vs
2365.05 m/s
1879.14 m/s
NTG
Density (bulk)
93 %
1.86 g/cm3
Facies
Grain size
TCS
M
3 cm
Permeability
Porosity
N/A
7.86 %
Vp
Vs
3310.68 m/s
2080.2 m/s
NTG
Density (bulk)
15 %
2.33 g/cm3
Facies
Grain size
CS
VF
3 cm

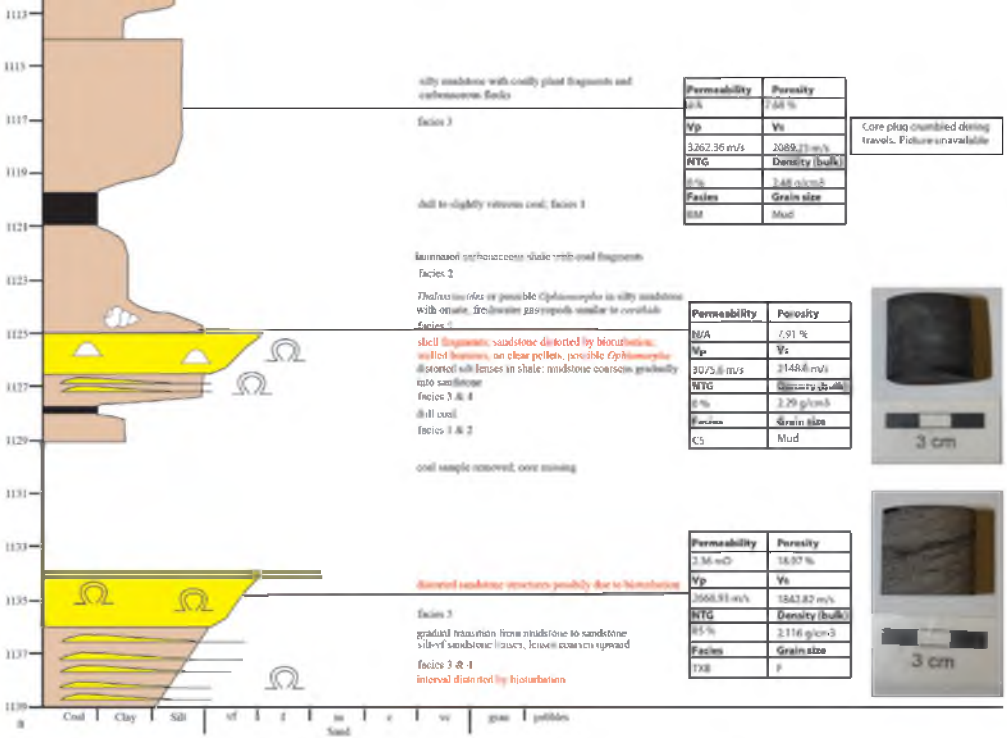
1113
1115
1117
1119
1121
1123
1125
1127
1129
1131
1133
1135
1137
1139
ft
Coal
Clay
Silt
vf
f
m
c
vc
gran
pebbles
Sand
silty mudstone with coalfy plant fragments and carbonaceous flecks
facies 3
dull to slightly vitreous coal; facies 1
laminated carbonaceous shale with coal fragments
facies 2
Thalassinoides or possible Ophiomorpha in silty mudstone with ornate, freshwater gastropods similar to cerithids
facies 5
shell fragments; sandstone distorted by bioturbation; mollusc burrows, no clear pellets, possible Ophiomorpha
distorted silt lenses in shale; mudstone coarsens gradually into sandstone
facies 3 & 4
dull coal
facies 1 & 2
coal sample removed; core missing
distorted sandstone structures possibly due to bioturbation
facies 5
gradual transition from mudstone to sandstone
silt-vf sandstone flasers, lenses coarsen upward
facies 3 & 4
interval disturbed by bioturbation
Permeability
Porosity
mD
7.68 %
Vp
Vs
3,262.36 m/s
2089.71 m/s
NTG
Density (bulk)
85 %
2.68 g/cm3
Facies
Grain size
BM
Mud
Core plug crumbled during travels. Picture unavailable
Permeability
Porosity
N/A
7.91 %
Vp
Vs
3075.8 m/s
2148.6 m/s
NTG
Density (bulk)
85 %
2.29 g/cm3
Facies
Grain size
CS
Mud
3 cm
Permeability
Porosity
2.36 mD
18.97 %
Vp
Vs
2668.93 m/s
1843.82 m/s
NTG
Density (bulk)
85 %
2.116 g/cm3
Facies
Grain size
TSB
F
3 cm

UP&L Core EP-25 Measured by William Gallin 2/5/09 - 2/9/09 at Utah Geological Survey, Utah Core Research Center

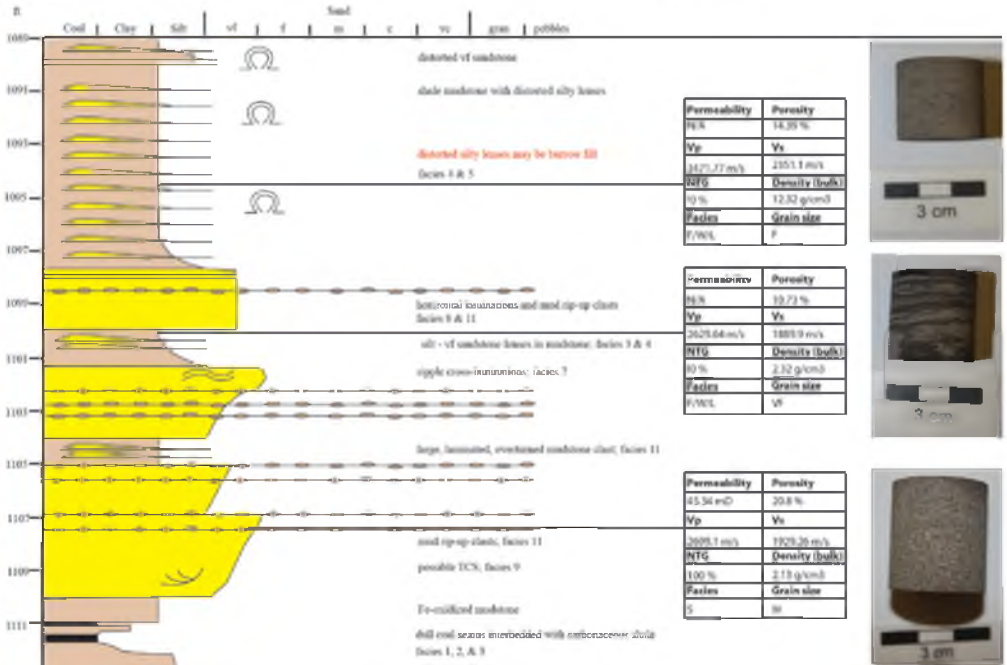

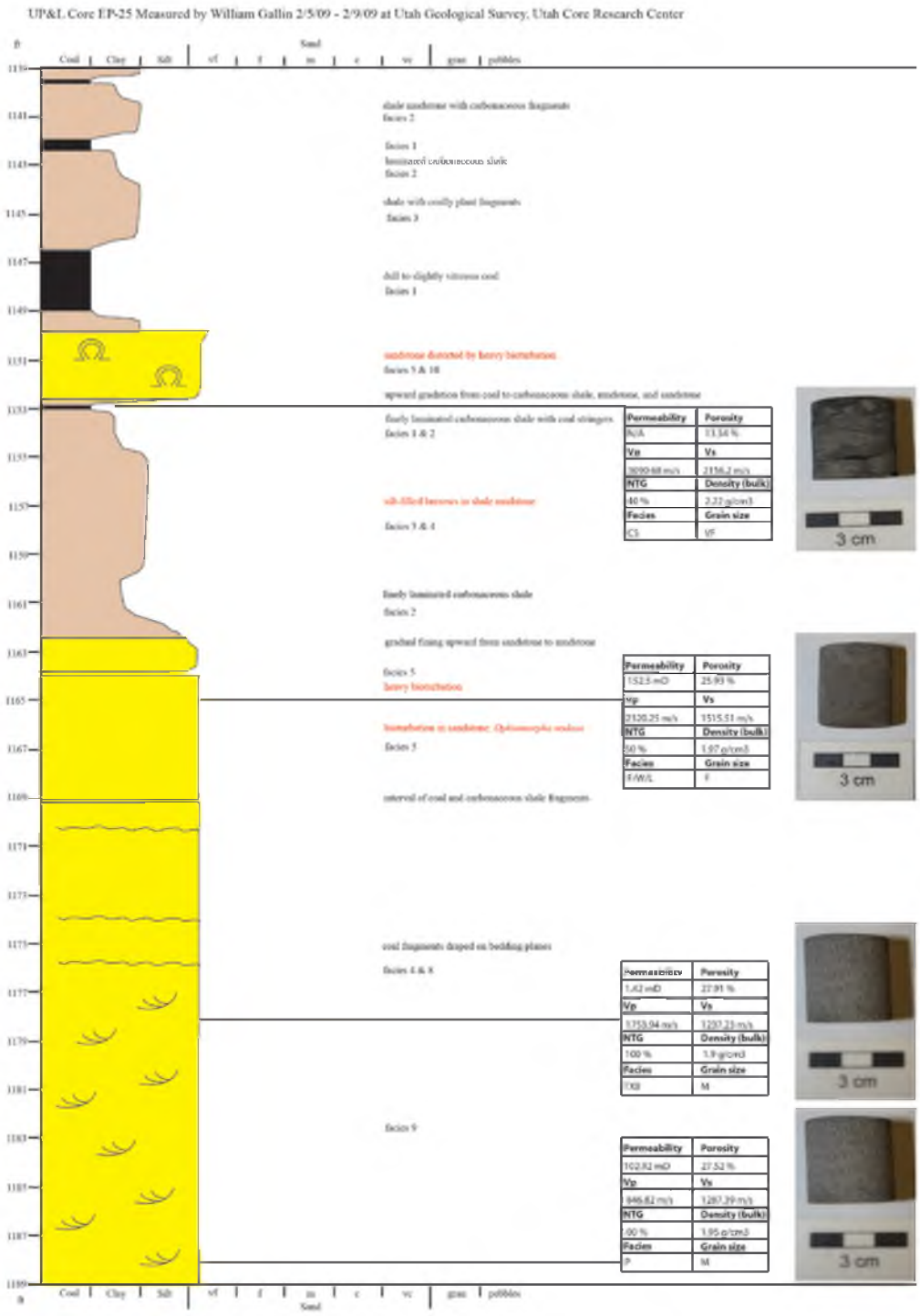
UP&L Core EP-25 Measured by William Gallin 2/5/09 - 2/9/09 at Utah Geological Survey, Utah Core Research Center
ft
Coal
Clay
Silt
Sand
vf
f
m
c
vc
gran
pebbles
1139
1141
1143
1145
1147
1149
1151
1153
1155
1157
1159
1161
1163
1165
1167
1169
1171
1173
1175
1177
1179
1181
1183
1185
1187
1189
shale sandstone with carbonaceous fragments
facies 2
facies 1
laminated carbonaceous shale
facies 2
shale with coally plant fragments
facies 3
dull to slightly vitreous coal
facies 1
sandstone disrupted by heavy bioturbation
facies 9 & 10
upward gradation from coal to carbonaceous shale, sandstone, and sandstone
finely laminated carbonaceous shale with coal stringers
facies 1 & 2
silt-filled burrows in shale sandstone
facies 3 & 4
finely laminated carbonaceous shale
facies 2
gradual fining upward from sandstone to sandstone
facies 5
heavy bioturbation
bioturbation in sandstone: Ophiomorpha nodosa
facies 5
interval of coal and carbonaceous shale fragments
coal fragments draped on bedding planes
facies 4 & 8
facies 9
Permeability
Porosity
N/A
11.34 %
Vp
Vs
3090.68 m/s
2156.2 m/s
NTG
Density (bulk)
40 %
2.22 g/cm3
Facies
Grain size
CS
VF
Permeability
Porosity
152.5 mD
25.93 %
Vp
Vs
2120.25 m/s
1515.51 m/s
NTG
Density (bulk)
50 %
1.97 g/cm3
Facies
Grain size
F/W/L
F
Permeability
Porosity
1.42 mD
27.91 %
Vp
Vs
1753.94 m/s
1207.23 m/s
NTG
Density (bulk)
100 %
1.9 g/cm3
Facies
Grain size
FXB
M
Permeability
Porosity
102.82 mD
27.52 %
Vp
Vs
1846.82 m/s
1287.39 m/s
NTG
Density (bulk)
100 %
1.95 g/cm3
Facies
Grain size
P
M
3 cm
3 cm
3 cm
3 cm

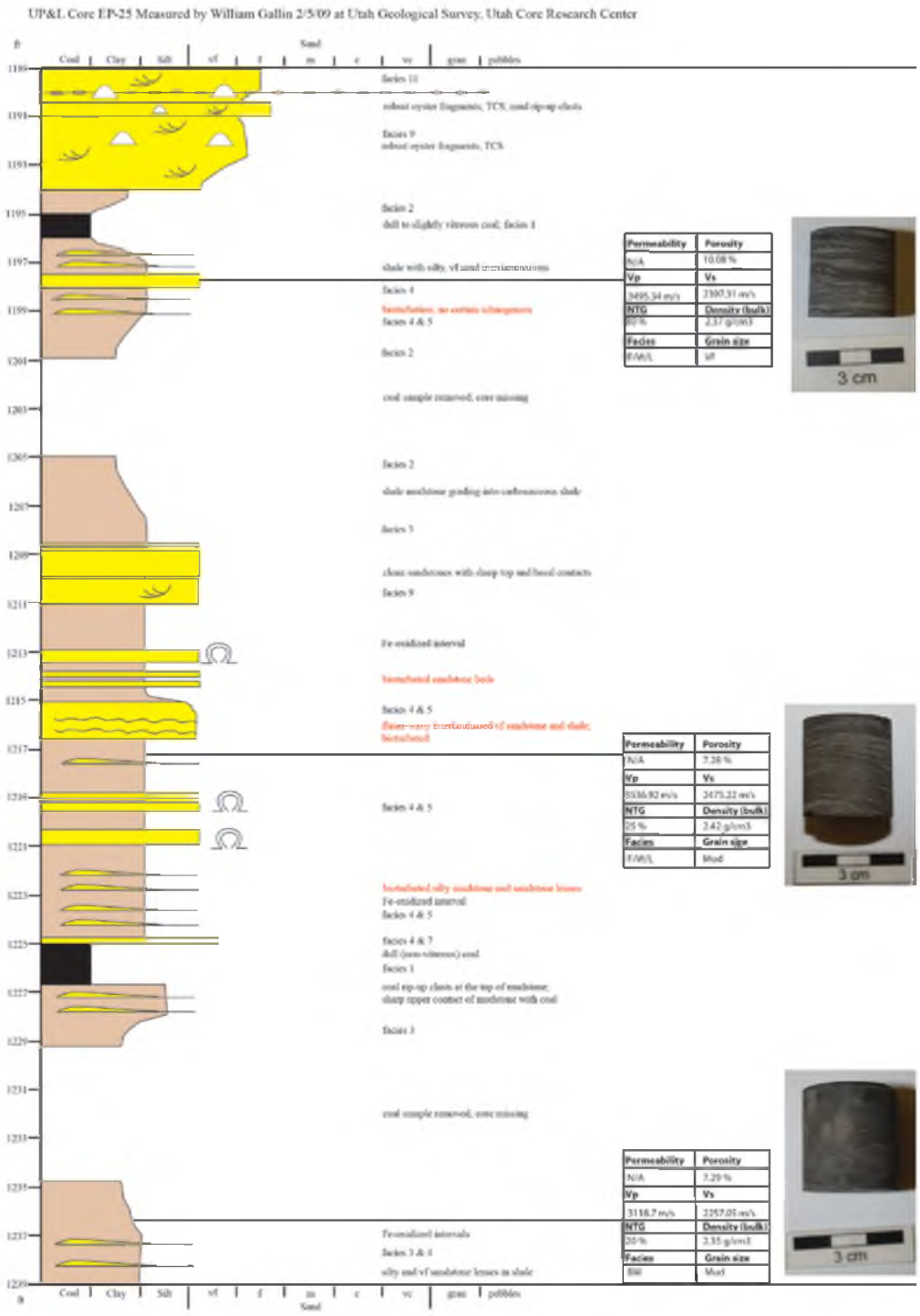
UP&L Core EP-25 Measured by William Gallin 2/5/09 at Utah Geological Survey, Utah Core Research Center
ft
Coal
Clay
Silt
Sand
vf
f
m
c
vc
gran
pebbles
1189
1191
1193
1195
1197
1199
1201
1203
1205
1207
1209
1211
1213
1215
1217
1219
1221
1223
1225
1227
1229
1231
1233
1235
1237
1239
facies 11
robust oyster fragments, TCS, coal rip-up clasts
facies 9
robust oyster fragments, TCS
facies 2
dull to slightly vitreous coal; facies 1
shale with silty, vf sand interlaminations
facies 4
facies 4 & 5
facies 2
coal sample removed, core missing
facies 2
shale mudstone grading into carbonaceous shale
facies 3
clean sandstones with sharp top and basal contacts
facies 9
Fe-oxidized interval
facies 4 & 5
facies 4 & 5
Fe-oxidized interval
facies 4 & 5
facies 4 & 7
dull (non-vitreous) coal
facies 1
coal rip-up clasts at the top of mudstone;
sharp upper contact of mudstone with coal
facies 3
coal sample removed, core missing
Fe-oxidized intervals
facies 3 & 4
silty and vf sandstone lenses in shale
Permeability
Porosity
N/A
10.08 %
Vp
Vs
3495.34 m/s
2300.31 m/s
NTG
Density (bulk)
20 %
2.37 g/cm3
Facies
Grain size
FA6/L
vf
3 cm
Permeability
Porosity
N/A
7.38 %
Vp
Vs
5536.92 m/s
3475.22 m/s
NTG
Density (bulk)
25 %
2.42 g/cm3
Facies
Grain size
FA6/L
Mud
3 cm
Permeability
Porosity
N/A
7.29 %
Vp
Vs
3138.7 m/s
2257.05 m/s
NTG
Density (bulk)
20 %
2.35 g/cm3
Facies
Grain size
FA6
Mud
3 cm

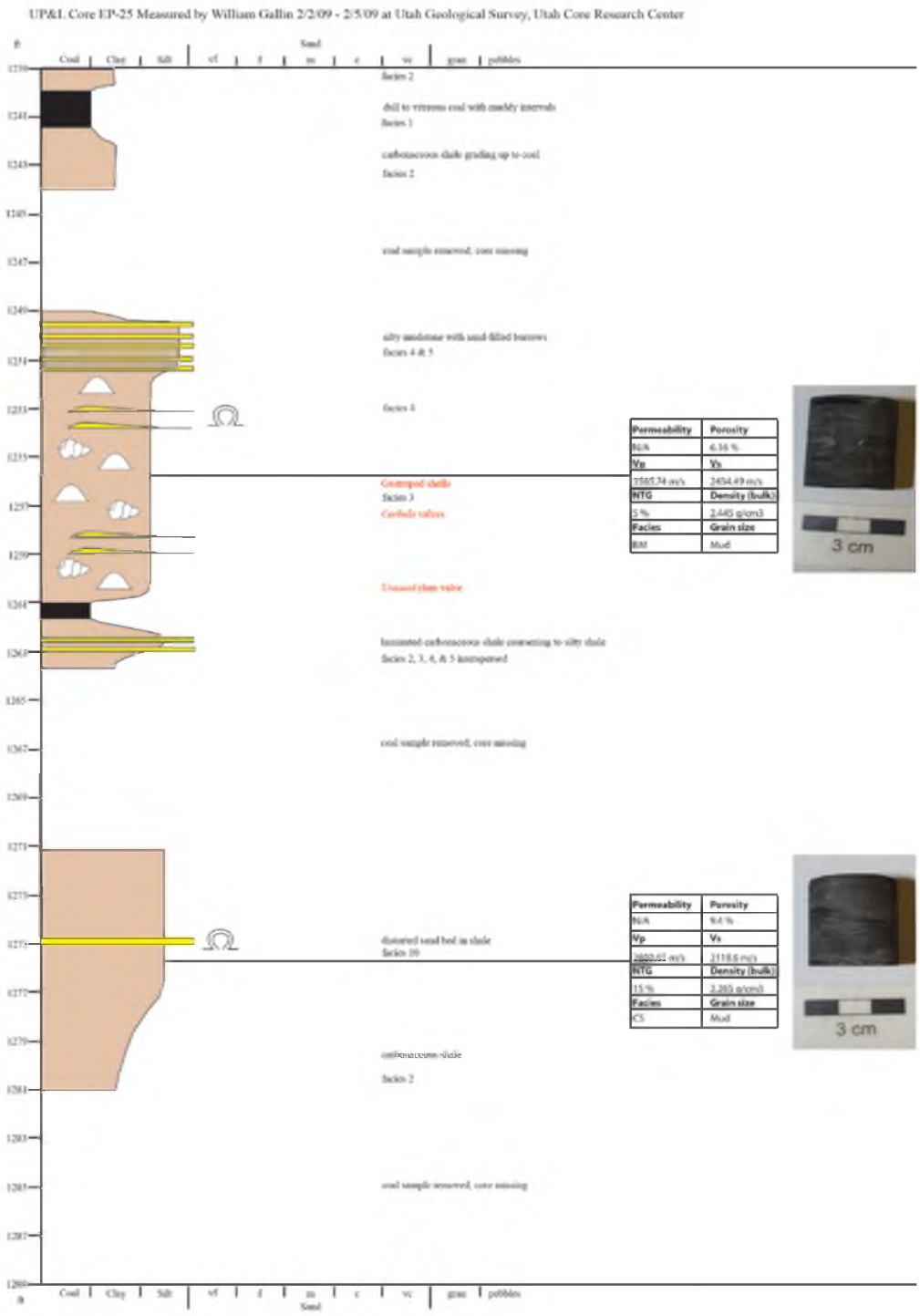
UP&L Core EP-25 Measured by William Gallin 2/2/09 - 2/5/09 at Utah Geological Survey, Utah Core Research Center
ft
Coal
Clay
Silt
Sand
vf
f
m
c
vc
gran
pebbles
facies 2
drill to vitreous coal with muddy intervals
facies 1
carbonaceous shale grading up to coal
facies 2
coal sample removed; core missing
silty sandstone with sand-filled burrows
facies 4 & 5
facies 4
Permeability
Porosity
N/A
6.16 %
Vp
Vs
3585.74 m/s
2404.49 m/s
NTG
Density (bulk)
5 %
2.440 g/cm3
Facies
Grain size
BM
Mud
Gastropod shells
facies 3
Corbula valves
3 cm
Unused plum valve
laminated carbonaceous shale coarsening to silty shale
facies 2, 3, 4, & 5 interspersed
coal sample removed; core missing
Permeability
Porosity
N/A
9.4 %
Vp
Vs
2118.6 m/s
NTG
Density (bulk)
11 %
2.265 g/cm3
Facies
Grain size
C5
Mud
distorted sand bed in shale
facies 10
3 cm
carbonaceous shale
facies 2
coal sample removed; core missing

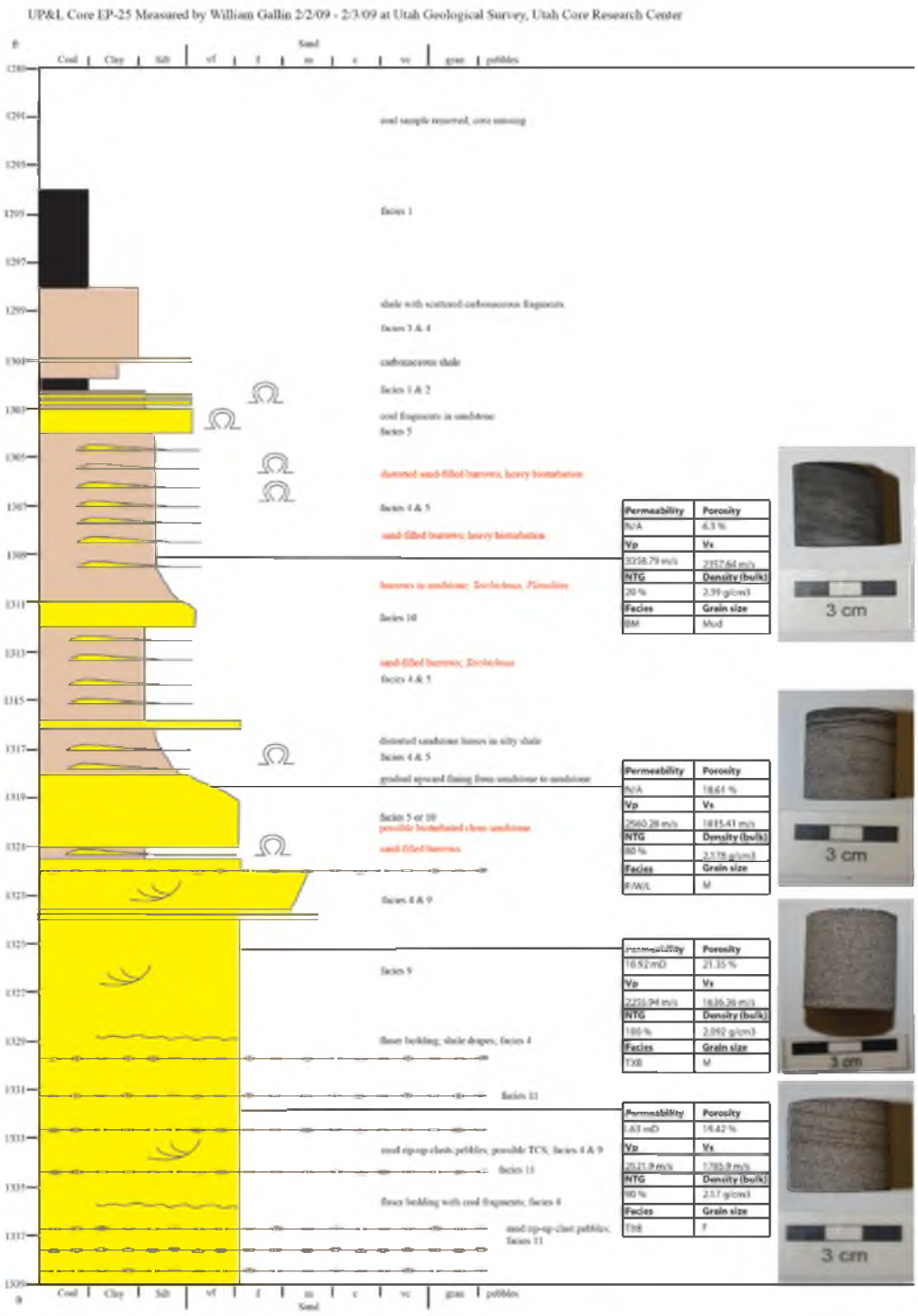
UP&L Core EP-25 Measured by William Gallin 2/2/09 - 2/3/09 at Utah Geological Survey, Utah Core Research Center
Coal
Clay
Silt
Sand
vf
f
m
c
vc
gran
pebbles
1289
1291
1293
1295
1297
1299
1301
1303
1305
1307
1309
1311
1313
1315
1317
1319
1321
1323
1325
1327
1329
1331
1333
1335
1337
1339
coal sample removed, core missing
facies 1
shale with scattered carbonaceous fragments
facies 3 & 4
carbonaceous shale
facies 1 & 2
coal fragments in sandstone
facies 5
distorted sand-filled burrows; heavy bioturbation
facies 4 & 5
sand-filled burrows; heavy bioturbation
burrows in sandstone; Zoophycus, Planolites
facies 10
sand-filled burrows; Zoophycus
facies 4 & 5
distorted sandstone lenses in silty shale
facies 4 & 5
gradual upward fining from sandstone to sandstone
facies 5 or 10
possible bioturbated clean sandstone
sand-filled burrows
facies 4 & 9
facies 9
flaser bedding; shale drapes; facies 4
facies 11
mud rip-up clasts, pebbles; possible TCS; facies 4 & 9
facies 11
flaser bedding with coal fragments; facies 4
mud rip-up clast pebbles; facies 11
Permeability
Porosity
N/A
6.3 %
Vp
Vs
3038.79 m/s
2357.64 m/s
NTG
Density (bulk)
20 %
2.39 g/cm3
Facies
Grain size
BM
Mud
3 cm
Permeability
Porosity
N/A
18.61 %
Vp
Vs
2560.28 m/s
1815.41 m/s
NTG
Density (bulk)
80 %
2.178 g/cm3
Facies
Grain size
F/W/L
M
3 cm
Permeability
Porosity
10.52 mD
21.35 %
Vp
Vs
2220.94 m/s
1636.36 m/s
NTG
Density (bulk)
100 %
2.092 g/cm3
Facies
Grain size
TXB
M
3 cm
Permeability
Porosity
.63 mD
14.42 %
Vp
Vs
2021.9 m/s
1785.9 m/s
NTG
Density (bulk)
80 %
2.37 g/cm3
Facies
Grain size
TXB
F
3 cm

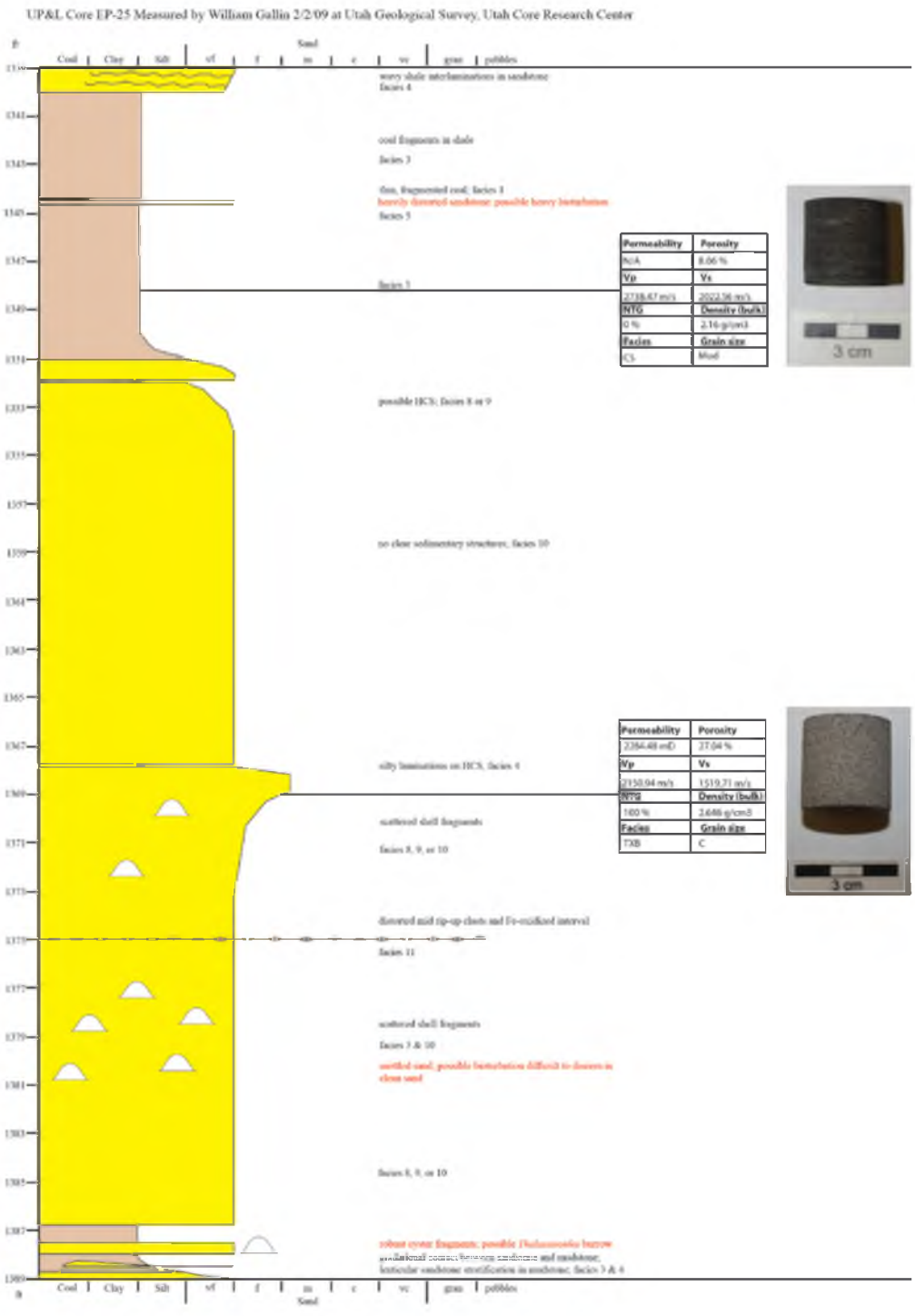
UP&L Core EP-25 Measured by William Gallio 2/2/09 at Utah Geological Survey, Utah Core Research Center
Cool
Clay
Silt
vf
f
m
c
vc
gran
pebbles
Sand
wavy shale interlaminations in sandstone
facies 4
coal fragments in shale
facies 3
thin, fragmented coal; facies 1
heavily distorted sandstone; possible heavy bioturbation
facies 5
Permeability
Porosity
N/A
8.66 %
Vp
Vs
4738.47 m/s
2022.58 m/s
NTG
Density (bulk)
0 %
2.16 g/cm3
Facies
Grain size
CS
Mud
3 cm
facies 3
possible HCS; facies 8 or 9
no clear sedimentary structures; facies 10
Permeability
Porosity
2364.48 mD
27.04 %
Vp
Vs
2150.94 m/s
1519.71 m/s
NTG
Density (bulk)
100 %
2.648 g/cm3
Facies
Grain size
TXB
C
3 cm
silty laminations on HCS; facies 4
scattered shell fragments
facies 8, 9, or 10
distorted mid rip-up clasts and Fe-oxidized interval
facies 11
scattered shell fragments
facies 3 & 10
mottled sand; possible bioturbation difficult to discern in clean sand
facies 8, 9, or 10
robust oyster fragments; possible Thalassinoides burrow
sandstone; lenticular sandstone stratification in mudstone; facies 3 & 4

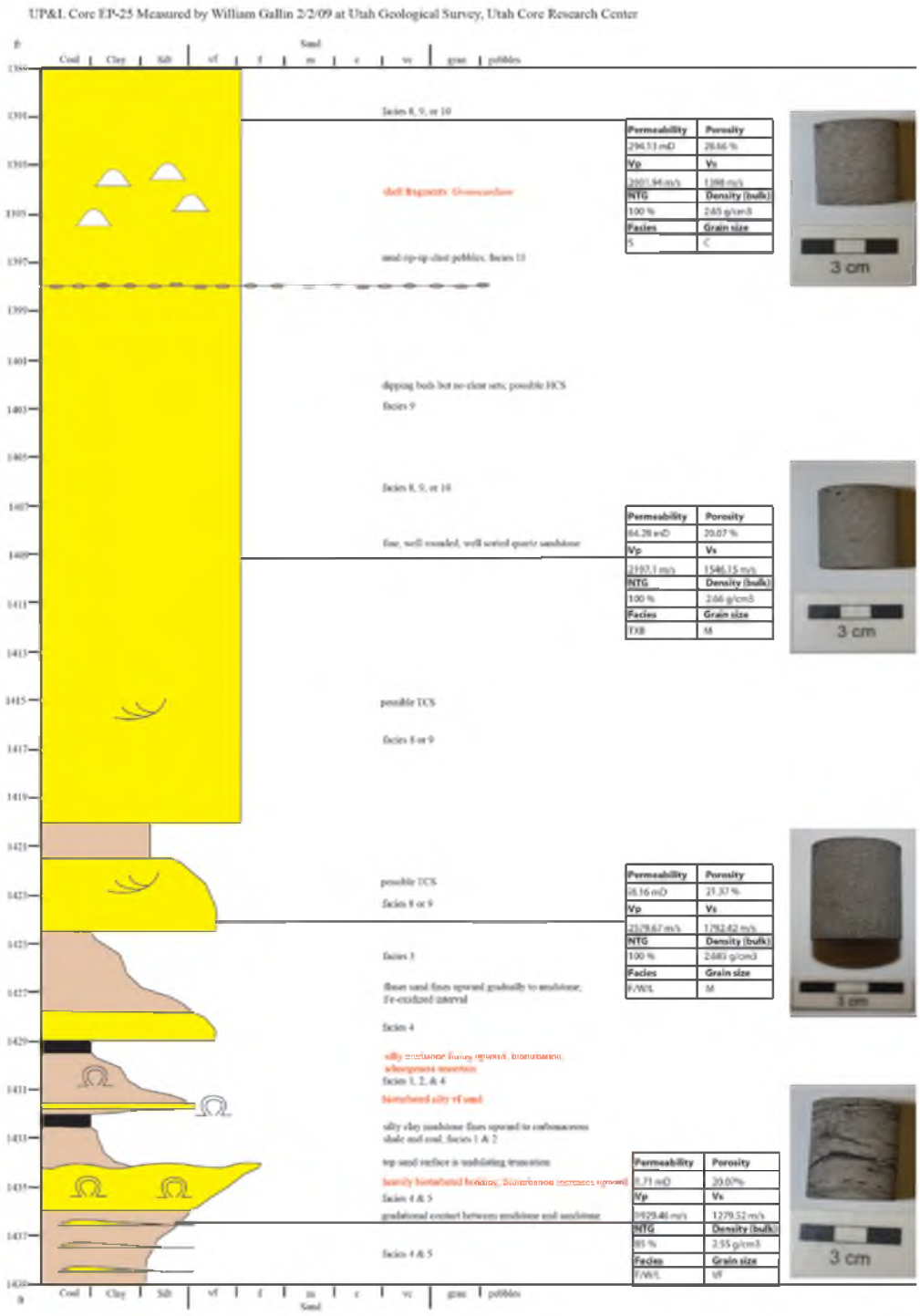
UP&L Core EP-25 Measured by William Gallin 2/2/09 at Utah Geological Survey, Utah Core Research Center
Coal
Clay
Silt
vf
f
m
c
vc
gran
pebbles
Sand
facies 8, 9, or 10
shell fragments: Grossecardium
mud rip-up clast pebbles, facies 11
dipping beds but no clear sets; possible HCS
facies 9
facies 8, 9, or 10
fine, well rounded, well sorted quartz sandstone
possible TCS
facies 8 or 9
possible TCS
facies 8 or 9
facies 3
fluser sand fines upward gradually to mudstone; Fe-oxidized interval
facies 4
silty mudstone fining upward, bioturbation, wherigenous resorbtion
facies 3, 2, & 4
bioturbated silty vf sand
silty clay mudstone fines upward to carbonaceous shale and coal, facies 1 & 2
top sand surface is undulating truncation
heavily bioturbated bedding, bioturbation increases upward
facies 4 & 5
gradational contact between mudstone and sandstone
facies 4 & 5
Permeability
Porosity
Vp
Vs
NTG
Density (bulk)
Facies
Grain size
3 cm

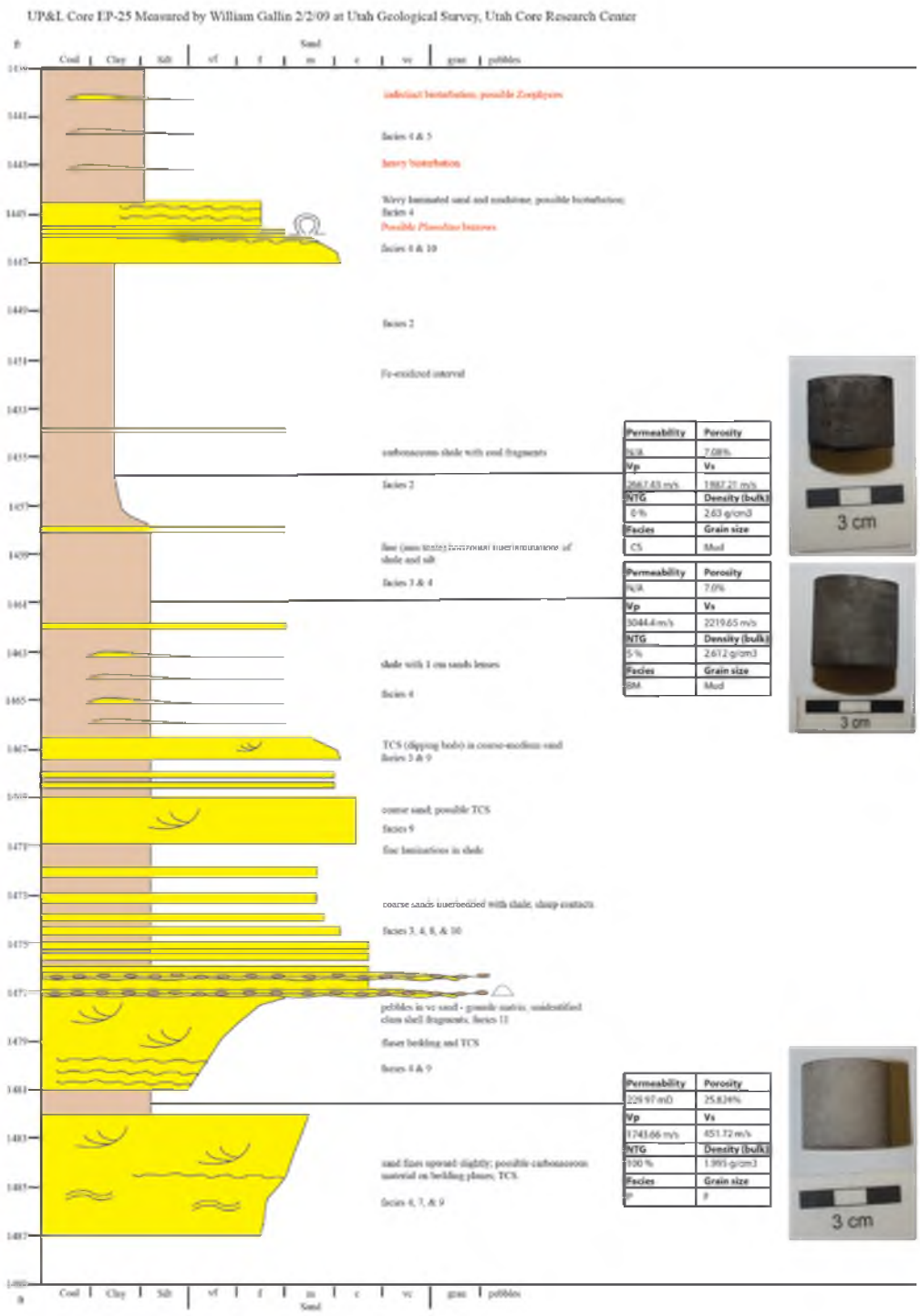
UP&L Core EP-25 Measured by William Gallin 2/2/09 at Utah Geological Survey, Utah Core Research Center
Coal
Clay
Silt
Sand
vf
f
m
c
vc
gran
pebbles
individual bioturbation, possible Zoophycos
facies 4 & 5
heavy bioturbation
Silty laminated sand and sandstone, possible bioturbation;
facies 4
Possible Planolites burrows
facies 4 & 10
facies 2
Fe-oxidized interval
carbonaceous shale with coal fragments
facies 2
fine (pass to) interbedded interlaminations of
shale and silt
facies 3 & 4
shale with 1 cm sands lenses
facies 4
TCS (dipping beds) in coarse-medium sand
facies 3 & 9
coarse sand; possible TCS
facies 9
fine laminations in shale
coarse sands interbedded with shale, sharp contacts
facies 3, 4, 8, & 10
pebbles in vc sand - granule matrix, unidentified
clam shell fragments, facies 11
flaser bedding and TCS
facies 4 & 9
sand fines upward slightly; possible carbonaceous
material on bedding planes; TCS.
facies 4, 7, & 9
Permeability
Porosity
n/a
7.08%
Vp
Vs
266.7.63 m/s
1887.27 m/s
NTG
Density (bulk)
0 %
2.63 g/cm3
Facies
Grain size
CS
Mud
Permeability
Porosity
n/a
7.0%
Vp
Vs
3044.4 m/s
2219.65 m/s
NTG
Density (bulk)
5 %
2.612 g/cm3
Facies
Grain size
SM
Mud
Permeability
Porosity
229.97 mD
25.824%
Vp
Vs
1743.66 m/s
651.72 m/s
NTG
Density (bulk)
100 %
1.395 g/cm3
Facies
Grain size
3 cm
3 cm
3 cm

APPENDIX B

RAW CORE PLUG LABORATORY DATA

Sample #	depth(m)	Facies type	Grain rho (g/cm3)	Porosity	Bulk rho (g/cm3)	Vp (m/s)	Vs (m/s)	Ip (Ns/m3)
1	208.788	9	2.687	16.41	2.246	3377.67	2476.1	7586.247
2	215.1888	10	2.679	9.381	2.428	4042.59	2874.73	9815.409
3	222.6564	4	2.602	16.043	2.184	2011.48	1452.98	4393.072
4	226.1616	10	2.62	32.155	1.777	1723.04	1212.64	3061.842
5	229.5144	3	2.6	9.242	2.359	3531.98	2425.59	8331.941
6	233.4768	10	2.627	31.511	1.799	1533.1	1045.76	2758.047
7	236.8296	10	2.637	37.219	1.656	1566.5	1078.78	2594.124
8	240.3348	10	2.609	21.128	2.057	1747.93	1275.51	3595.492
9	244.602	3	2.586	11.712	2.283	2898.86	2117.06	6618.097
10	247.4976	6	2.626	11.913	2.314	2926.39	2119.05	6771.666
11	250.8504	5	2.625	15.064	2.23	2917.11	2063.91	6505.155
12	254.2032	9	2.642	30.332	1.84	1909.88	1318.32	3514.179
13	255.4224	11	2.629	25.998	1.946	1684.32	1136.58	3277.687
14	261.8232	4	2.602	9.973	2.343	3349.78	2278.52	7848.535
15	263.1948	5	2.632	21.09	2.077	2568.94	1753.75	5335.688
16	267.462	4	2.608	12.74	2.275	2830.39	2062.99	6439.137
17	272.6436	4	2.57	7.978	2.365	3249.3	2304.64	7684.595
18	273.7104	2	2.414	8.608	2.207	2697.7	1945.22	5953.824
19	279.8064	4	2.571	6.448	2.405	3231.86	2285.59	7772.623
20	283.7688	5	2.603	12.626	2.274	3147.35	2264.15	7157.074
21	285.75	3	3.016	3.019	2.925	3985.28	2575.56	11656.94
22	290.1696	9	2.641	30.041	1.848	1836.04	1250.48	3393.002
23	294.132	10	2.654	30.837	1.848	1833.46	1237.28	3388.234
24	299.3136	9	2.642	33.173	1.765	1530	988.15	2700.45
25	302.0568	10	2.64	32.355	1.786	1406.19	971.42	2511.455
26	307.2384	9	2.633	31.352	1.807	1920.81	1255.35	3470.904
28	312.7248	4	2.612	12.115	2.295	3709.34	2556.94	8512.935
29	315.7728	11	2.717	20.489	2.16	4236.03	2861.45	9149.825
30	317.6016	10	2.708	18.026	2.22	3323.73	2259.97	7378.681
31	322.4784	10	2.64	30.484	1.835	1768.96	1178.5	3246.042

32	324.612	9	2.531	26.619	1.858	2565.05	1879.14	4765.863
33	330.0984	2	2.53	7.861	2.331	3310.48	2083.2	7716.729
34	333.4512	4	2.71	14.389	2.319	3471.77	2351.1	8051.035
35	335.28	4	2.597	10.733	2.318	2629.64	1887.91	6095.506
36	337.4136	11	2.687	20.806	2.128	2699.08	1929.26	5743.642
37	340.3092	2	2.695	7.698	2.487	3262.36	2089.23	8113.489
38	342.9	3	2.492	7.911	2.295	3075.6	2148.66	7058.502
39	345.6432	10	2.612	18.972	2.116	2668.93	1842.82	5647.456
40	351.4344	2	2.572	13.537	2.224	3090.68	2156.2	6873.672
41	355.2444	5	2.662	25.931	1.972	2320.25	1515.51	4575.533
42	359.0544	8	2.645	27.91	1.907	1753.94	1237.23	3344.764
43	362.1024	9	2.654	27.516	1.924	1846.82	1287.39	3553.282
44	365.1504	4	2.632	10.079	2.367	3495.34	2397.31	8273.47
45	371.094	4	2.613	7.384	2.42	3536.92	2475.22	8559.346
46	377.0376	3	2.532	7.287	2.348	3118.7	2257.05	7322.708
47	382.8288	4	2.606	6.16	2.445	3585.74	2434.49	8767.134
48	388.62	2	2.501	9.403	2.265	2803.65	2118.6	6350.267
49	398.9832	4	2.554	6.299	2.393	3358.79	2357.64	8037.584
50	401.7264	5	2.676	18.608	2.178	2560.28	1815.41	5576.29
51	403.86	9	2.66	21.349	2.092	2255.94	1636.36	4719.426
52	405.9936	11	2.696	19.422	2.172	2521.92	1785.9	5477.61
53	410.8704	3	2.349	8.065	2.16	2738.47	2022.56	5915.095
54	417.2712	10	2.646	27.042	1.931	2150.94	1519.71	4153.465
55	423.9768	11	2.652	28.66	1.892	2031.94	1398	3844.43
56	429.6156	9	2.664	25.257	1.991	2197.064	1546.15	4374.355
57	434.0352	9	2.685	21.357	2.112	2579.67	1792.42	5448.263
58	437.6928	4	2.546	20.069	2.035	1929.46	1279.52	3926.451
59	443.7888	2	2.633	7.082	2.447	2667.43	1987.21	6527.201
60	445.3128	3	2.612	7.003	2.429	3044.4	2219.65	7394.848

APPENDIX C

ROCK PROPERTIES LABORATORY MEASUREMENTS METHODOLOGY

All laboratory work was done courtesy of the Stanford Rock Physics Laboratory and the coring done by the Utah Geological Society. The core samples were drilled vertically, perpendicular to the bedding. Once extracted, the end faces were ground flat and parallel to ensure precise measurement and good contact with laboratory equipment. A caliper tool (0.001 mm accuracy) was used to measure length and diameter of each sample. The average diameter and length of the samples is 25.4 mm and 26.9 mm, respectively. The plugs were stored for one month at 70° and dried in an oven at 80° for 24 hours before taking measurements. The mass of the plugs was measured using a balance with 0.1% accuracy. As a result, we were able to calculate bulk density with the following equation.

$$\rho_{bulk} = \frac{Mass_{dry}}{Volume_{bulk}} \tag{1}$$

The laboratory tests were conducted as followed: porosity, permeability, acoustic measurement (Vp and Vs). Porosity was calculated using a porosimeter which measures porosity based on Boyle's Law with Helium.

$$\varphi = Volume_{sample} - B + \frac{P_{of}}{P_f} * \frac{B}{\frac{P_{ob}}{P_b} - \frac{P_{ob}}{P_f}} - \frac{Pos}{P_s} * \frac{B}{\frac{P_{ob}}{P_b} - \frac{P_{ob}}{P_f}} \tag{2}$$

B is the size of billets removed to accommodate the sample size. P_{of} is the recorded

initial equilibrated pressure with all the billets. P_f is the recoded reference pressure with the billets. P_{ob} and P_b are pressure value used for calibration. These measurements are taken and recalibrated based on the length of the sample and how many billets were removed to accommodate the sample size. Pos and P_s record the initial and subsequent pressure of each sample when the He is charged and discharged. The range of porosity values is 3-37%. The permeameter measures permeability using Darcy's law with Nitrogen. The equation takes into account the Klinkenberg effect, which is the gas slippage between the sample and the equipment.

$$k = \frac{a*L}{A*t} * Ln * \frac{h_o}{h_t} \quad (3)$$

K is the permeability coefficient, a is area of tube, L length of sample, A is area of sample, t is time, h_o is head at beginning, and h_t is head at end of time. Resulting permeability ranges are 1.3-1134 mD. Ultrasonic acoustic velocimeter uses a high voltage electric pulse into the core plug to measure velocity. Two sets of piezoelectric crystals are used to generate either P- or S-waves. After initial calibration, molasses is applied to each sample for suitable coupling and transducers are positioned in direct contact on both sides on the core plug. The P-wave is picked at the first arrival of the resulting waveform, and the S-wave is picked at the first peak. *Vp* ranges from 2500-4500 m/s and *Vs* is 1200-2800 m/s.

REFERENCES

Ahmad, S. R., Ghazi, S., Sharif, S., Khan, M. S., and Mehmood, S. A., 2012, Cyclicity and lithofacies modelling by application of Markov Chain Analysis to the Warchha Sandstone, Salt Range, Pakistan: Pakistan Journal of Science, v. 64, no. 3, p. 232-241.

Ainsworth, B. R., and Pattinson, S. A. J., 1994, Where have all the lowstands gone? Evidence for attached lowstand systems tracts in the Western Interior of North America: Geology, v. 22, p. 415-418.

Allen, J. L., and Johnson, C., 2010a, Sedimentary facies, paleoenvironments, and relative sea level changes in the John Henry Member, Cretaceous Straight Cliffs Formation, southern Utah, USA, *in* Carney, S., Carney, D. E., and Johnson, C., eds., Geology of South-Central Utah, Volume 39, Utah Geological Association Publication.

Allen, J. L., and Johnson, C. L., 2010b, Facies control on sandstone composition (and influence of statistical methods on interpretations) in the John Henry Member, Straight Cliffs Formation, Southern Utah, USA: Sedimentary Geology, v. 230, no. 1-2, p. 60-76.

Biddle, K. T., Schlager, W., Rudolph, K. W., and Bush, T. L., 1992, Seismic model of a progradational carbonate platform, Picco di Vallandro, the Dolomites, northern Italy: AAPG Bulletin, v. 76, no. 1, p. 14-30.

Bruno, P. P., 2009, High-resolution onshore seismic imaging of complex volcanic structures: An example from Vulcano Island, Italy: Journal of Geophysical Reserach.

Bruno, P. P., Castiello, A., and Improta, L., 2010, Ultrasonic seismic imaging of the caustive fault of the 1980, M6.9, southern Italy earthquake by pre-stack depth migration of dense wide-aperture data: Geophysical Research Letters.

Campion, K., Sprague, A., Sullivan, M. D., Mohrig, D., Ardill, J., Lovell, R., and Drezewiecki, P., 2000, Outcrop expression of confined complexes, Gulf Coast Section SEPM Foundation 20th Annual Research Conference Deepwater Reservoirs of the World.

Castanga, J. P., 1992, Offset-dependence refelctivity: Theory and practice of avo analysis, p. 3-36.

Chakrabarti, A., 2005, Sedimnetary structures of tidal flats: a journey from coast to inner estuarine region of Eastern India: Journal of Earth System Science, v. 114, no. 3, p. 353-368.

Chentnik, B. M., Johnson, C., Mulhern, J., and Stright, L., 2014, Valleys, estuaries, and lagoons: Paleoenvironments and regressive-transgressive architecture of the upper Cretaceous Stright Cliffs Formation [M.S. Geology M.S.]: University of Utah, p. 65.

Christensen, N. I., and Szymanski, D. L., 1991, Seismic properties and the origin of reflectivity from a classic Paleozoic sedimentary sequence, Valley and Ridge province, southern Appalachians: Geological Society American Bulletin, v. 103, p. 277-289.

Dooling, P., 2012, Tidal facies, stratigraphic architecture, and along-strike variability of a high energy, transgressive shoreline, late Cretaceous, Kaiparowits Plateau, southern Utah [MS Geology: University of Utah, p. 148.

Droser, M. L., and Bottjer, D. J., 1988, Trends in depth and extent of bioturbation in Cambrian carbonate marine environments, western United States: Geology, v. 16, p. 558-569.

Duarte, L. T., 2014, Seismic signal processing: some recent advances, IEEE international conference on acoustics, speech and signal processing: Florence, IEEE, p. 2363-2366.

Eaton, J. G., and Nations, J. D., 1991, Introduction; tectonic setting along the margin of the Cretaceous Western Interior Seaway, southern Utah and northern Arizona, *in* Nations, J. D., and Eaton, J. G., eds., Stratigraphy, depositional environments, and sedimentary tectonics of the western margin, Cretaceous Western Interior Seaway: Geological Society of America Special Paper, Volume 260, p. 2-8.

Eberhart-Phillips, D., Han, D., and Zoback, M. D., 1989, Empirical relationships among seismic velocity, effective pressure, porosity, and clay content in sandstone: Geophysics, v. 54, no. 1, p. 82-89.

Essam, M., El-Sayed, A., Benyamin, M., and El-Batal, A., 2013, A sedimentological and integrated case study towards more understanding of the depositional regimes in complex structures: SPE International, v. 164742, p. 1-14.

Falivene, O., Arbues, J., Ledo, J., Benjumea, B., Munoz, J. A., Fernandez, O., and Martinez, S., 2010, Synthetic seismic models from outcrop-derived three-dimensional facies models: The Eocene Ainsa turbidite system (southern Pyrenees): AAPG Bulletin, v. 94, no. 3, p. 317-343.

Feldman, H. R., Fabijanic, J. M., Faulkner, B. L., and Rudolph, K. W., 2014, Lithofacies, parasequence stacking, and depositional architecture of wave- To tide-dominated shorelines in the Frontier Formation, Western Wyoming, U.S.A: Journal of Sedimentary Research, v. 84, no. 8, p. 694-717.

Fenies, H., Faugeres, J., Porter, B. E., and Stracke, A., 1998, Facies and geometry of tidal channel-fill deposits (Arcachon Lagoon, SW France): Marine Geology, v. 18, p. 131-148.

Finzel, E. S., Ridgway, K. D., Reifenstuhl, R. R., Blodgett, R. B., White, J. M., and Decker, P. L., 2009, Stratigraphic framwork and estuarine depositional environmnets of the Miocene Bear Lake Formation, Bristol Bay Basin, Alaska: onshore equivalents to potential reservoir strat in a frontier gas-rich basin: AAPG Bulletin, v. 93, no. 3, p. 379-405.

Gallin, W., 2010, Fluvial stratigraphic architecture of the John Henry Member of the Straight Cliffs Formation, Kauparowits Plateau, Utah, USA [MS Geology MS]: University of Utah.

Gochioco, L. M., 1992, Modeling studies of interference refelctions in thin-layered media bounded by coal seams: Geophysics, v. 57, no. 9, p. 1209-1216.

-, 2000, High-resolution 3-D seismic survey over a coal mine reserve area in the USA case study: Geophysics, v. 65, no. 3, p. 712-718.

Gooley, J., 2010, Alluvial architecture and predictive modeling of the late Cretaceous John Henry Member, Straight Cliffs Formation, southern Utah [Geology MS]: University of Utah, p. 1-280.

Han, D., 1986, Effects of porosity and clay content on acoustic properties of sandstones and unconsolidated sediments [PhD: Stanford University, p. 1-255.

Hettinger, R. D., 1995a, Sedimentological descriptions and depositional interpretations, in sequence stratigraphic context, of two 300-meter cores from the Upper Cretaceous Straight Cliffs Formation, Kaiparowits Plateau, Kane Country, Utah: U.S. Geological Survey Bulletin v. 2115-A, p. 1-38.

-, 1995b, A Summary of Coal Distribution and Geology in the Kaiparowits Plateau, Utah, *in* Kirschbaum, M. A., Roberts, L. N. R., and Biewick, L. R. H., eds., Geologic Assessment of Coal in the Colorado Plateau: Arizona, Colorado, New Mexico, and Utah: Denver, CO, U. S. Geological Survey.

Hodgetts, D., and Howell, J. A., 2000, Synthetic seismic modelling of a large-scale geological cross-section from the Book Cliffs, Utah, USA: Petroleum Geoscience, v. 6, p. 221-229.

Howell, J. A., Martinius, A. W., and Good, T. R., 2014, The application of outcrop analogues in geological modelling: a review, present status and future outlook: Geological Society, London, Special Publications, v. 387, no. 1, p. 1-25.

Kauffman, E. G., and Caldwell, W. G. E., 1993, The Western Interior Basin in space and time, Geological Association of Canada Special Paper, Evolution of the Western Interior Basin.

Kendall, R., 2006, Advances in land multicomponent seismic: acquisition, processing and interpretation: CSEG recorder, v. 75.

Longhitano, S. G., Mellere, D., STeel, R. J., and Ainsworth, B. R., 2012, Tidal depositional systems in the rock record: A review and new insights: Sedimentary Geology, v. 279, p. 2-22.

Marion, D., Nur, A., Yin, H., and Han, D., 1992, Compressional velocity and porosity in sand-clay mixtures: Geophysics, v. 57, p. 554-563.

Martinius, A. W., and Gowland, S., 2011, Tide-influenced fluvial bedforms and tidal bore deposits (Late Jurassic Lourinhã Formation, Lusitanian Basin, Western Portugal): Sedimentology, v. 58, no. 1, p. 285-324.

Martinius, A. W., Kaas, I., Naess, A., Helgesen, G., Kjaerefjord, J. M., and Leith, D. A., 2001, Tidal Sedimentology of the heterolithic and tide-dominated Tilje Formation (Early Jurassic, Halten Terrace offshore mid-Norway), *in* Martinsen, O. J., and Dreyer, T., eds., Sedimentary Environmnets Offshore Norway - Paleozoic to Recent, Volume 10: Amsterdam, Elsevier Science, p. 103-144.

Morcote, A., Mavko, G., and Prasad, M., 2010, Dynamic elastic properties of coal: Geophysics, v. 75, no. 6, p. 227-234.

Nordahl, K., Ringrose, P. S., and Wen, R., 2005, Petrophysical characterization of a heterolithic tidal reservoir interval using a process-based modelling tool: Geoscience, v. 11, p. 17-28.

O'Bryne, C. J., and Flint, S. S., 1993, High-resolution sequence stratigraphy of Cretaceous shallow marine sandstones, Book Cliffs outcrops, Utah, U.S.A. - Applications to reservoir modeling: First Break, v. 11, p. 445-459.

Peterson, F., 1969a, Four New Members of the Upper Cretaceous Straight Cliffs Formation in the Southeastern Kaiparowits Region Kane County, Utah: GEOLOGICAL SURVEY BULLETIN, v. 1274-J.

Pettinga, L., 2012, Tectonic controls on alluvial architecture in the upper Cretaceous John Henry Member, Straight Cliffs Formation, southern Utah [MS Geology MS]: University of Utah, 1-280 p.

Powers, D. W., and Easterling, R. G., 1982, Improved methodology for using embedded Markov chains to describe cyclical sediments: Journal of Sedimentary Petrology, v. 52, p. 913-923.

Ruter, H., and Schepers, R., 1978, Investigation of the seismic response of cyclically layered caboniferous rock by means of synthetic seismograms: Geophysics, v. 26, p. 29-47.

Schwab, A. M., Cronin, B. T., and Ferreira, H., 2007, Seismic expression of channel outcrops: Offset stacked versus amalgamated channel systems: Marine and Petroleum Geology, v. 24, no. 6-9, p. 504-514.

Shanley, K. W., and McCabe, P. J., 1991, Predicting facies architecture through sequence stratigraphy—An example from the Kaiparowits Plateau, Utah: Geology, v. 19, p. 742-745.

Shanley, K. W., McCabe, P. J., and Hettinger, R. D., 1992, Tidal influence in Cretaceous fluvial strata from Utah, USA: a key to sequence stratigraphic interpretation: Sedimentology, v. 39, p. 905-930.

Shanmugam, G., Spalding, T. D., and Rofheart, D. H., 1993, Process sedimentology and reservoir quality of deep-marine bottom-current reworked sands (Sandy Contourites): An example from the Gulf of Mexico: AAPG Bulletin, v. 77, no. 7, p. 1241-1259.

Stright, L., Stewart, J., Campion, K., and Graham, S., 2014, Geologic and seismic modeling of a coarse-grained deep-water channel reservoir analog (Black's Beach, La Jolla, California): AAPG Bulletin, v. 98, no. 4, p. 695-728.

Sullivan, M. D., Foreman, J. L., Jennette, D. C., Stern, D., Jensen, G. N., and Goulding, F. J., 2004, An integrated approach to characterization and modeling of deepwater reservoirs, Diana field, western Gulf of Mexico: Integration of outcrop and modern analogs in reservoir modeling: AAPG Memoir, v. 80, p. 215-234.

Szwarc, T., Johnson, C., Stright, L., and McFarlane, C., 2014, Interactions between axial and transverse drainage systems in the Late Cretaceous Cordilleran foreland basin: Evidence from detrital zircons in the Straight Cliffs Formation, southern Utah, USA: GSA Bulletin.

Tanavsuu-Milkeviciene, K., and Plink-Bjorklund, P., 2009, Recognizing tide-dominated versus tide-influenced deltas: Middle-Devonian strata of the Baltic Basin: Journal of Sedimentary Research, v. 59, p. 887-905.

Tetyukhina, D., J., V. L., Luthi, S., and Wapenaar, C., 2010, High-resolution reservoir characterization by an acoustic impedance inversion of a Tertiary deltaoic clinoform system, in the North Sea: Geophysics, v. 75, no. 6, p. 57-67.

Tetyukhina, D., Luthi, S., and Gisolf, A., 2014, Acoustic nonlinear full-waveform inversion on an outcrop-based detailed geological and petrophysical model (Book Cliffs, Utah): AAPG Bulletin, v. 98, no. 1, p. 119-134.

Thomas, M. A., and Anderson, J. B., 1994, Sea-level controls on the facies architecture of the Trinity/Sabine incised valley systems, Texas Continental Shelf, *in* Dalrymple, R. W., Boyd, R., and Zaitlin, B. A., eds., Incised Valley systems: origin and sedimentary sequences, Volume 51, SEPM Special Publications, p. 63-82.

Van Riel, W. J., 1965, Synthetic seismograms applied to the seismic investigation of a coal basin: Geophysics, v. 13, p. 105-121.

Vaninetti, G. E., 1979, Coal stratigraphy of the John Henry Member of the Straight Cliffs Formation, Kaiparowits Plateau, Utah [Geology MS]: University of Utah.

Vernik, L., and Nur, A., 1992, Ultrasonic velocity and anisotrophy of hydrocarbon source rocks: Geophysics, v. 57, no. 5, p. 727-735.

Weimar, P., and Posamentier, H. W., 1993, Siliciclastic sequence stratigraphy: Recent developments and applications: AAPG.

Wen, R., Martinius, A. W., Naess, A., and Ringrose, P. S., 3D simulations of small-scale heterogeneity in tidal deposits - a process-based stichastic simulation method, *in* Proceedings IAMG, Naples, Italy, 1998.

Yoshida, S., Jackson, M. D., Johnson, H. D., Muggeridge, A. H., and Martinius, A. W., 2001, Outcrop studies of tidal sandstones for reservoir characterization (Lower Cretaceous Vectis Formation, Isle of Wight, southern England), *in* Martinsen, O. J., and Dreyer, T., eds., Sedimentary Environments Offshore Norway - Paleozoic to Recent, Volume 10: Amsterdam, Elsevier Science, p. 233-257.

Yoshida, S., Johnson, H. D., Johnson, M. D., and Martinius, A. W., 1999, Quantification of heterogeneities within tidal sandstone outcrops: analogue study for subsurface reservoir characterization *in* Lippard, S. J., Naess, A., R., and Sinding-Larsen, eds., Proceedings of IAMG 99: Trondheim, Norway, p. 677-682.

Zoeppritz, K., 1919, On the refelction and propagation of seismic waves: ErdbebenwellenVIIIB, Gottinger Nachrichten, v. 66.